Aus dem

Department für Augenheilkunde Tübingen

Universitäts-Augenklinik

How Innate Immunity affects CRISPR/Cas9 Gene Editing

Inaugural-Dissertation
zur Erlangung des Doktorgrades
der Medizin

der Medizinischen Fakultät
der Eberhard Karls Universität
zu Tübingen

vorgelegt von

Pfromm, Julia Katherine

2022

Dekan:	Professor Dr. B. Pichler
1. Berichterstatter	Professor Dr. M. D. Fischer
2. Berichterstatter:	Professorin Dr. M. Avci-Adali

Tag der Disputation: 04.11.2022

TABLE OF CONTENTS

ABBREVIATIONS

AAV: adeno-associated virus

ABM: Applied Biological Material

ACAID: anterior chamber-associated immune deviation

AD: Alzheimer's dementia

ADA: adenosine deaminase

AIM: absent in melanoma

AMD: age related macular degeneration

APCs: antigen presenting cells

ARL: aim2-like receptor

ATP adenosine triphosphate

AdV: adenovirus

BFP: blue fluorescent protein

bp: base pairs

BRB: blood-retinal barrier

CDS: cytosolic DNA Sensors

cGAS: cyclic-GMP-AMP synthase

CIP: calf intestinal alkaline phosphatase

CjCas9: *C. jejuni* Cas9

CLRs: C-type lecithin receptors

CMV: cytomegalovirus

CNS: central nervous system

CRISPR/Cas: clustered regularly interspaced short palindromic repeat/CRISPR associated protein nucleases

crRNA: crispr RNA

DAMPs: damage-associated molecular patterns

DC: dendritic cells

DMD: Duchenne muscular dystrophy

DNA: deoxyribonucleic acid

DSB: double-stranded breaks

dsDNA: double-stranded DNA

dsRNA: double-stranded RNA

EAU: autoimmune uveitis

ELISA: enzyme-linked immunoabsorbent assay

FDA: Federal Drug Administration

GFP: green fluorescent protein

gRNA: guide RNA

HEK: human embryonic kidney

HIV: human immunodeficiency virus

HSPs: heat-shock proteins

ICC: immunocytochemistry

IFN: interferon

IL: interleukin

IMhu: immortalized human microglia SV40 cell line

IRD: inherited retinal diseases

IRF3: interferon regulatory factor 3

ITAFs: immunoreceptor tyrosine-based activation motifs

ITIMs: immunoreceptor tyrosine-based inhibitory motifs

LCA: Leber congenital amaurosis

LPS: lipopolysaccharide

LRR: leucine-rich repeats

MAPK: mitogen-activated protein kinase

MHC: major histocompatibility complex

MS: multiple sclerosis

mTOR: mechanistic target of rapamycin

NAB: neutralizing antibodies

NHP: non-human primate

NK: natural killer

NLRs: nucleotide-binding oligomerization domain-like receptors

NOD: nucleotide-binding oligomerization domain

NTN: neuroturin

OD: optical density

PAM: protospacer adjacent motif

PAMPs: pathogen-associated-molecular-patterns

PBMCs: peripheral blood mononuclear cells

PCR: polymerase chain reaction

PFA: paraformaldehyde

PGN: peptidoglycans

PMA: phorbol 12-myristate 13-acetate

PR: photoreceptor

PRRs: pattern-recognition receptors

RLRs: retinoic acid-inducible gene-I-like receptors

RNA: ribonucleic acid

RNPs: ribonucleoproteins

RPE: retinal pigment epithelium

RP: Retinitis pigmentosa

SaCas9: *S. aureus* Cas9

SpCas9: *S. pyogenes* Cas9

SCID: severe combined immune deficiency

SEAP: secreted embryonic alkaline phosphatase

STING: stimulator of interferon genes

TALE: transcription activator-like effector

TALENs: transcription activator like effector nucleases

TGF: transforming growth factor

TLR: Toll-like receptor

TNF: tumor necrosis factor

TRIF: TIR-domain-containing adapter-inducing interferon-β

WB: wash buffer

ZFN: zinc finger nucleases

FIGURES

TABLES

1. INTRODUCTION

1.1 MOTIVATION

Even with the advent of modern gene therapies, the notion of actively modifying the human genome still feels, to many, fantastically impossible. However, gene-editing technologies remain no longer tantalizingly out of reach; they are already being applied in clinical trials [1–3]. The applications of gene editing are virtually limitless, though some organs seemingly permit extraneous modification more readily than others. The eye, due to its immune privilege, as evidenced by the successes seen in corneal transplantation, is an attractive target for gene therapies [4]. Genetically inherited diseases affecting the retina, especially those caused by categorized mutations, serve as appealing targets for initial ocular gene therapies. This appeal is demonstrated by the existence of gene therapies already on the market targeting inherited retinal diseases (IRD), such as Leber congenital amaurosis (LCA). Developments in the field of gene therapy, including clustered regularly interspaced short palindromic repeat/CRISPR associated protein nucleases (CRISPR/Cas), are being rapidly advanced and promise to deliver groundbreaking treatments for long under-treated diseases.

Factors such as the immune response to gene therapy may challenge the efficacy and safety of future therapies, however. Immune responses to gene therapy trials have, in extreme cases, led to fatalities in human subjects [5]. This demonstrates the need to assess potential immune responses to gene therapies. The immune response-mediated inactivation of gene therapies, or the destruction of modified cells, pose additional challenges to future gene therapies; both phenomena have been recorded [6,7]. Even the eye, with its immune privileged status, may be affected by innate or adaptive immune responses to gene therapies, responses potentially executed by ocular immune competent cells including the macrophages of the central nervous system (CNS) like microglia, perivascular macrophages, or meningeal macrophages [8]. To ensure the safety and longevity of future gene therapies, immune responses initiated by CRISPR/Cas systems must be evaluated.

To assess these immune responses, the innate immune responses of cell line models of systemic and CNS macrophages were characterized using commercially available

immune stimuli, to determine their immune capacities and their similarities to primary cells. Subsequently, these cell lines were transfected with plasmids containing Cas9, and the innate immune response was assessed through analysis of cytokine production. This work aims to improve the safety and efficacy of ocular CRISPR/Cas gene therapies by assessing the innate immune response of CNS macrophages to CRISPR/Cas plasmid transfection and expression.

1.2 Inherited Retinal Diseases

Vision is a vital sensory function, and blindness is a debilitating disability with profound personal, societal, and economic impact. In 2015 it was estimated that 36 million people worldwide were blind and 216.6 million more had moderate to severe visual impairment [9]. In Germany alone, blindness is estimated to cost €49.6 billion annually [10].

The leading causes of blindness internationally are uncorrected refractive error, cataract, glaucoma, and diabetic retinopathy [11]. In comparison, the absolute numbers of patients affected by IRD may seem minor. It is estimated that 1 in every 3000 people, or over 2 million people worldwide, are affected by IRD [12]. IRD, though, tend to affect patients at an earlier age than other causes of blindness, and are the leading cause of blindness in patients between 15 and 45 years of age [13]. IRD are a heterogeneous group of degenerative diseases including Retinitis pigmentosa (RP), LCA, Choroideremia, and Achromatopsia. Most forms of IRD affect the photoreceptors (PR), though the retinal pigment epithelium (RPE) and other retinal layers can also be affected. More than 300 genes have been implicated in causing IRD [14]. Development of therapies targeting IRD remains challenging, with a lack of causative treatments leading to most patients becoming legally blind by the age of 40 [15].

Rapid strides are being made toward developing treatments for IRD, with over 50 ongoing clinical trials ranging from gene amplification via Adeno-associated virus (AAV) vectors to gene modification with transcription activator like effector nucleases (TALENs) or CRISPR/Cas [16]. Luxturna (Voretigene Neparovovec), an AAV-mediated therapy for biallelic *RPE65*-caused IRD, delivers a healthy copy of the *RPE65* gene to diseased RPE cells via subretinal injection, and was approved by the Federal Drug Administration (FDA) in the U.S. in 2017, making it the first causative therapy for an

IRD on the market [17]. This approach to gene therapy can be referred to as gene supplementation. Luxturna's market approval was an exciting development and has opened the doors for further gene therapy treatments for IRD. However, the safety and longevity of potential gene therapies must be further assessed to maximize their efficacy and therapeutic potential.

1.3. THE IMMUNE SYSTEM

The human immune system is composed of various mechanisms, which the body employs to defend against infection and pathogens. It can be divided into three categories: anatomical and physiological barriers, innate immunity, and adaptive immunity [18]. Anatomical and physiological barriers include the skin, sclera, and mucosal membranes, which serve as the first line of defense against invasion.

1.3.1 THE INNATE IMMUNE SYSTEM

The innate immune system is hereditary and immediately active upon birth. All multi-cellular organisms have developed some form of an innate immune system, which constitutes the initial immune response to invading pathogens. Cellular components of the innate immune system include phagocytes (neutrophils, macrophages, and monocytes), dendritic cells (DC), fibroblasts, and epithelial cells. These cells identify pathogens via a limited number of germline-encoded pattern-recognition receptors (PRRs), in contrast to the large number of heterogeneous recombined receptors found in the adaptive immune system [19]. Humoral components of the innate immune response include C-reactive protein, lipopolysaccharide (LPS)-binding proteins, antimicrobial proteins, and the complement system [20]. The innate immune system includes three distinctly activated complement pathways: the classical complement pathway, the alternative complement pathway, and the lectin pathway. The activation of these pathways triggers phagocytosis, inflammation, and the activation of the membrane attack complex. As this work evaluates the effects of gene editing therapies on the innate immune response, various effectors of the innate immune response are elucidated to summarize possible sources of an immune response to CRISPR/Cas-mediated gene therapies.

1.3.1.1 PRRs

PRRs are main effectors of the cellular innate immune response and therefore facilitate the potential initial immune response to gene therapies. PRRs are constitutively expressed and can initiate an immune response within minutes of pathogen binding. PRRs identify pathogen-associated-molecular-patterns (PAMPs) and consequently activate specific signaling pathways. PAMPs are broadly found on pathogens (e.g. LPS, peptidoglycan (PGN), or porins), and generally not found in host cells, allowing the innate immune system to rapidly differentiate between self- and non-self [21]. PRRs are also capable of recognizing damage-associated molecular patterns (DAMPs) derived from damaged cells [e.g. adenosine triphosphate (ATP), heat-shock proteins (HSPs), deoxyribonucleic acid (DNA), and ribonucleic acid (RNA)]; these also activate signaling pathways [22]. The activation of PRRs leads to the production of cytokines and is an integral component of the induction of the innate immune response. Presently described PRRs include Toll-like receptors (TLRs), nucleotide-binding oligomerization domain (NOD)-like receptors (NLRs), and retinoic acid-inducible gene-I-like receptors (RLRs) [23].

1.3.1.1.1 TLRs

TLRs were the first class of PRRs to be identified and are therefore the best-characterized family of PRRs. Ten TLRs (TLR1-TLR10) have been identified in humans and are localized either intra- or extra-cellularly. TLR1, 2, 4, 5, 6, and 10 are located on the cell surface [24]. Intracellular TLRs include TLR3, 7, 8, and 9, which are found on endoplasmic reticulum, endosomes, and lysosomes [25,26]. TLRs are type I transmembrane proteins with extracellular leucine-rich repeats (LRR) which recognize PAMPs, DAMPS, transmembrane domains, and intracellular Toll or interleukin (IL)-1 receptor domains before activating downstream signaling pathways [27]. TLRs are expressed on all innate immune cells, including macrophages and monocytes, as well as on non-immune cells including fibroblast and epithelial cells [28].

1.3.1.1.1.1 TLR Activation

The discovery of *lps* mice, which lack a systemic response to LPS due to a loss-of-function mutation in the TLR4 gene, established TLR4 as an integral LPS sensor [29]. TLR3 is implicated in the recognition of double-stranded RNA (dsRNA) [30]. TLR5 recognizes bacterial flagellin [31]. TLR9 receptors are activated in response to bacterial CpG-ODN as

well as viral DNA sequences [32]. Imidazoquinolines, small anti-viral immune response modifiers made of single-stranded RNA, activate the TLR7 and TLR8 receptors [33]. TLRs also respond to endogenous factors, including factors like HSPs produced by damaged cells [34].

The activation of TLRs leads to the production and secretion of multiple pro-inflammatory cytokines and chemokines, dependent on the TLR activated and the host cell type [35,36]. Activation of TLR signaling through PAMPs and DAMPs involves the MyD88 pathway and the TIR-domain-containing adapter-inducing interferon-β (TRIF) pathway [28]. The MyD88-dependent pathway is utilized by all TLRs and leads to the production of inflammatory cytokines and type I interferon (IFN) through nuclearization of NF-κB and the activation of the mitogen-activated protein kinase (MAPK) pathway [28,37]. The TRIF-dependent pathway is additionally recruited to TLR3 and TLR4 and leads to the activation of interferon regulatory factor 3 (IRF3), NF-κB, and MAPKs, inducing the production of IFN type I and inflammatory cytokines [25]. Pathological activation of TLRs has been implicated in various diseases including: lupus erythematous [38], cancer [39], type one diabetes [40], and rheumatoid arthritis [41].

1.3.1.1.2 NLRs

NLRs serve as PAMP recognition sites within the cytosol. At least 23 NLR proteins have been identified in humans, the best researched of these being NOD1 and NOD2 [42]. While NOD1 is ubiquitously expressed, NOD2 expression is limited to monocytes, macrophages, DCs, and Paneth cells [43]. Both NOD1 and 2 induce NF-κB nuclearization and subsequent proinflammatory cytokine production [44]. NOD1 and 2 activation can also induce MAPK activation, leading to proinflammatory cytokine production [45]. NOD1 specifically recognizes gamma-d-Glutamyl-meso-diaminopimelic acid, found in all gram negative as well as in some gram positive bacteria [46]. Muramyl dipeptide, which is present in all gram negative and gram positive bacteria, activates NOD2 [47].

1.3.1.1.2.1 The Inflammasome

NLRs also play a key role in the formation and activation of the inflammasome, a signaling construct whose triggering initiates the activation of caspase-1. Caspase-1 cleaves Pro-IL-1β to IL-1β as well as maturing IL-18. NLRC4, NLRP1, and NLRP3 have all been identified as playing a part in inflammasome formation [48]. NLRC4 is stimulated

by bacterial flagellin [49]. NLRP1 can be triggered by *Bacillus anthrax* lethal toxin [50]. The NLRP3 inflammasome can be activated by various PAMPs, including LPS, dsRNA, PGN, and extracellular ATP [51]. Some PAMPs can stimulate the activation of the inflammasome on their own, but the addition of extracellular ATP often enhances this activation [52]. In general, the NLRP3 inflammasome is activated by markers of cellular stress; NLRP3 serves as a sensor for cell stress or death [42].

In addition, the absent in melanoma (AIM) 2-like receptor (ARL) plays a key role in identifying cytosolic DNA and activating the AIM2 inflammasome, which also leads to caspase-1 dependent IL-1β activation [53]. The ability to identify double-stranded DNA (dsDNA) makes the AIM2 inflammasome indispensable in response to viral infection, as well as in response cellular stress, and implicates it as a possible effector of immune responses to Cas9 plasmids.

1.3.1.1.3 C-type lecithin receptors

C-type lecithin receptors (CLRs) are a heterogeneous family of receptors that contain carbohydrate-recognition domains able to Ca^{2+}-dependently recognize glycans [54]. CLRs on macrophages and DCs serve as PRRs vital for the recognition and binding of pathogens. The fate of a pathogen bound by a CLR is dependent on the individual CLR and the host cell type. The CLR DC-SIGN binds and internalizes enveloped viruses [e.g. coronavirus, human immunodeficiency virus (HIV)] after recognizing their envelopes' mannose and fructose structures, and leads to their degradation via lysosomes [55]. Other CLRs, which contain immunoreceptor tyrosine-based activation motifs (ITAFs) or immunoreceptor tyrosine-based inhibitory motifs (ITIMs), are capable of modulating the production and secretion of IFNα and IFNβ, components of the main anti-viral cytokine response [56]. CLRs can also induce NF-κB activation, leading to the production of proinflammatory cytokines [57].

1.3.1.1.4 RLRs

The RLRs RIG-I, MDA5, and LGP2 initiate an immune response to RNA viruses [58]. They sense intracellular dsRNA, a marker of viral infection. RLRs are expressed on a variety of cells, and their expression levels rise when cells have been exposed to IFN, as is often the case in viral infections [59]. RIG-I and MDA5 induce the production of IFN as well as other components of the antiviral response.

1.3.1.1.5 Cytosolic DNA sensors

Physiologically, free DNA has no place in the cytosol of the eukaryotic cell. In the scenario of infection by DNA or RNA viruses, or in potential gene therapies involving Cas9 plasmids, though, it may be pathologically introduced there. Multiple molecular pathways identify and destroy such non-physiological DNA in the cytosol. It has been proven that the main effectors of the cytosolic DNA response are the cyclic-GMP-AMP synthase (cGAS) and stimulator of interferon genes (STING) [60]. cGAS activation can be initiated by contact with microbial or endogenous DNA, including chromatin that has been extranuclearized due to cellular stress [61]. Once activated, cGAS-STING induces the production of IFN type I.

1.3.1.2 Cytokines

This work measured cytokine production to assess the activity of PRRs in response to Cas9 plasmids, as PRRs induce the production of cytokines in response to stimulation. Cytokine production is therefore a key measurement of the activation of the innate immune system. Plasmid-mediated CRISPR/Cas therapies can potentially stimulate a variety of PRRs to produce cytokines, as they are initially present in the cell as plasmid DNA; and their expression may lead to the production of RNAs and proteins. Additionally, further elements of plasmid-mediated CRISPR/Cas therapies including crispr RNA (crRNA) may induce their own immune responses. Cytokines are secretory proteins that can affect a variety of cellular responses through paracrine, autocrine, or endocrine signaling. The broad, heterogeneous family of cytokines includes IFN, lymphokines, IL, chemokines, and tumor necrosis factors (TNF). Cytokines are produced by a variety of cells including macrophages, mast cells, and B- and T-lymphocytes. Cytokines modulate immune responses and inflammation, and are directly implicated in a multitude of disease processes including Asthma bronchiale, chronic obstructive pulmonary disease, HIV, multiple sclerosis (MS), and Alzheimer's dementia (AD) [62]. In short, they affect nearly every biological process, from embryonic development to degenerative aging.

To organize the multitudinous known cytokines, functional classes were developed, with cytokines organized by primary properties. The most important of these classes include Th1 and Th2 cytokines, which affect Th1 and Th2 responses, pro- and anti-

inflammatory cytokines, and type I and II IFN [63]. Pro-inflammatory cytokines are primarily secreted by macrophages and serve to induce an inflammatory response to PAMPs and DAMPs. In contrast, anti-inflammatory cytokines inhibit the inflammatory response, primarily by inhibiting the synthesis of pro-inflammatory cytokines. In non-pathogenic immune responses, pro- and anti-inflammatory cytokine responses must remain balanced to avoid over-inflammation or infection due to immunosuppression. Type I IFN are characterized by their ability to induce direct antiviral responses within infected and neighboring cells, as well as activating natural killer (NK) cells [64]. Type II interferons, or IFNγ, are produced by NK cells during infection and function to coordinate the innate and adaptive immune responses to viral infections, as well as modulating the innate immune response to viruses [65,66]

1.3.2 THE ADAPTIVE IMMUNE SYSTEM

The adaptive immune system produces a specialized, targeted immune response to pathogens and is capable of creating an immunological memory in response to an encounter with a pathogen. This memory allows the adaptive immune system to respond to further pathogen encounters in a rapid, focused fashion. This highly specific immune response can provide enduring protection against pathogens and forms the basis for the practice of immunization.

The main effectors of the adaptive immune system are the lymphocytes, primarily B and T cells. B cells drive the humoral immune response. They produce and secrete antibodies, which bind antigens on pathogens. Memory B cells retain the ability to produce antibodies in response to activation and are key to long-lasting immunity. Somatic hypermutation and V(D)J recombination allow cells to use a small number of genes to produce a large variety of antibodies and antigen receptors specific for pathogens the immune system encounters [67].

T cells lead the cell-mediated immune response, neutralizing damaged or infected cells. Three types of T cells: cytotoxic, helper, and suppressor, all play varying roles. Cytotoxic CD8+ T cells directly destroy infected or damaged cells. CD4+ Helper T cells activate antibody and cell-mediated immune responses by stimulating B cells to secrete cytokines, while suppressor T cells deactivate other lymphocytes when necessary. Antigen presenting cells (APCs) including DCs phagocytize antigens and present them

on major histocompatibility complex (MHC) class I or II molecules [68]. The adaptive immune response to gene therapies is also highly relevant to their effectivity and longevity; however, it was unable to be assessed in this thesis, leaving further avenues of research open.

1.4. THE OCULAR IMMUNE RESPONSE

1.4.1 OCULAR IMMUNE PRIVILEGE

The ocular immune system is fundamental in the production of immune responses to ocular CRISPR/Cas-mediated gene therapies. To better understand the immune milieu in the eye, the state of knowledge regarding ocular immunology relevant to this work is discussed below.

Due to the sensitivity of the retina and cornea to swelling and immune reactions as evidenced by the loss of PR function after macular edema in retinal vein occlusion, for example [69], the eye evolved mechanisms designed to minimize tissue damage caused by infection. These mechanisms are also collectively referred to as ocular immune privilege. The ease of corneal transplantation is an elegant example of ocular immune privilege. 90% of corneal allografts survive without tissue matching or immunosuppression [4]. The eye is shielded from a systemic or inappropriate immune response by three key features (Fig. 1): the blood-retinal barrier (BRB), the inhibitory ocular microenvironment, and the active regulation of systemic immune responses [70].

The BRB is an essential component in sustaining ocular immune privilege. It consists of the non-fenestrated capillaries of retinal circulation, and the tight junctions between RPE cells. Pathological changes in the BRB are implicated in diseases including age-related macular degeneration and diabetic retinopathy [71].

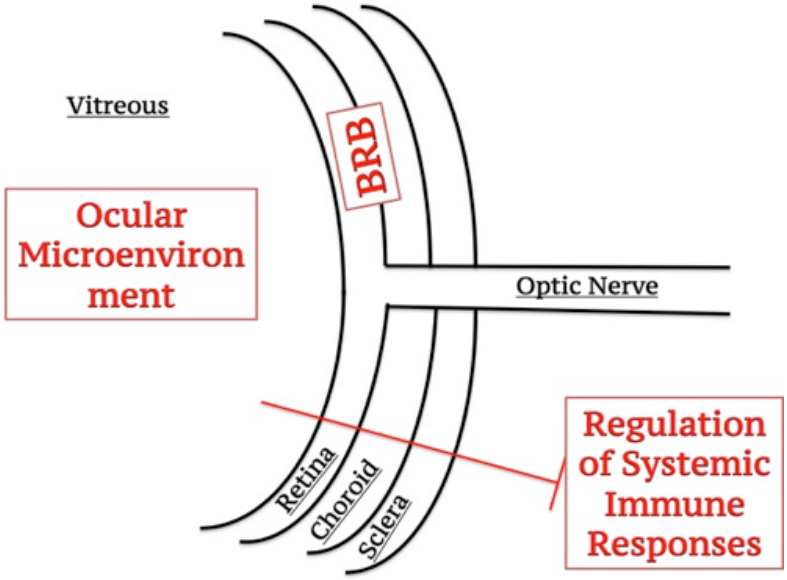

Figure 1**: Components of the Ocular Immune Privilege.**

BRB: blood-retinal barrier

The ocular microenvironment has evolved to avoid and repress inflammation. For example, the RPE can inhibit T cells and induce them to become T regulatory cells [72]. Soluble factors in the vitreous such as transforming growth factor (TGF)-β, α-Melanocyte stimulating hormone, somatostatin, and vasoactive intestinal peptide inhibit the activity of immunocompetent cells [70]. Immunosuppressive neuropeptides in the aqueous humor also serve to suppress the activation of Th1 cells while inducing the activation of CD28+ and CD4+ T regulatory cells [73].

Active regulation of systemic immune responses is the final component of the ocular immune privilege, of which anterior chamber-associated immune deviation (ACAID) is the classic example. Pathogens introduced into the anterior chamber of the eye activate F4/80+ APCs, which migrate through the trabecular meshwork and eventually to the thymus and spleen [70]. These APCs induce the generation of natural killer T cells, which induce the production of splenic suppressor cells. In the marginal zone of the spleen, immunomodulatory cells including CD4+ and CD8+ T regulatory cells are generated. As a result, T cells are inhibited from transformation into inflammatory Th1 effector cells,

and proinflammatory cytokine production and delayed-type hypersensitivity is suppressed [74]. The Th2-mediated inflammatory response is also suppressed.

1.4.2 Components of the Ocular Immune Response

The eye does, however, possess immunologic mechanisms that allow it to counteract foreign or pathogenic material. The conjunctiva is capable of undergoing lymphoid hyperplasia and plays a key role in the immune response of the external eye [75]. The tear film coating the surface of the conjunctiva contains various active proteins including IgG, IgM, and IgA.

Cellular components of the ocular immune response include lymphocytes, macrophages, RPE cells, mast cells, and APCs. The retinal immune response is directed by the RPE, with macrophages playing a key role. The RPE initiates innate and adaptive immune responses using TLRs and MHC class I and II molecules [76]. RPE cells can also inhibit unwarranted immune responses, for example through the production of anti-inflammatory cytokines [76].

The human retina contains three glial cell types: Müller cells, astrocytes, and microglia [77]. Müller cells and astrocytes serve to support retinal neurons by modulating metabolic and trophic factors [78]. Microglia serve a unique role in retinal immune regulation, and respond to pathologic conditions including oxidative stress or genetically induced neurodegeneration by proliferating and migrating to sites of injury [79]. Microglia are highly sensitive to environmental fluctuations and are kept in check in large part by immunosuppression from the RPE [80]. Microglia become active in IRD, and these activated microglia secrete IL-1β IL-6, and TNFα in mouse models of Goldmann-Favre syndrome, for example [81].

This capacity to secrete cytokines in response to pathological retinal states indicates that microglia may be key players in potential ocular immune responses to gene therapy with CRISPR/Cas, which is the focus of this work.

1.5. Macrophage-like Cells

The effectivity of ocular gene therapies is directly impacted by possible macrophage-driven immune responses. Macrophages play a key role in mediating innate immune

responses. They are present in the bloodstream as well as a wide variety of tissues, including the eye. Microglia are a subset of macrophages found in the eye and CNS.

Microglia are yolk-sac derived long-living tissue-resident mononuclear phagocytes [82]. Microglia have two key functions, maintaining CNS homeostasis and mediating innate immune responses [83]. In the healthy retina microglia are localized to the plexiform layers [80]. Microglial activation has been implicated in a variety of ocular and CNS diseases, making them suspect in mediating immune reactions to gene therapies in the eye. Microglia migrate to the outer retina in RP, which can accelerate PR degradation, possibly due to phagocytosis of PR proteins [84]. Activation of the innate immune system is also implicated in age related macular degeneration (AMD), with macrophage activation postulated to play a key role [85]. Retinal resident microglia have also been proven to be key effectors driving the development and maintenance of autoimmune uveitis (EAU), microglial ablation was shown to completely inhibit development of EAU [86]. In the broader CNS, microglial activation is also implicated in the development of AD and Parkinson's disease, making microglia attractive targets for gene therapy [87]. Additionally, microglial activation in a variety of pathological states involving retinal inflammation implicates the likelihood of their involvement in the ocular immune response to CRISPR/Cas therapies, making the investigation of their innate immune responses to CRISPR/Cas highly relevant in elucidating the ocular immune response to genetic therapies.

1.5.1 Gene Therapy in Microglia

To maximize the effectivity of genetic therapies in the CNS, the innate immune response of microglia to CRISPR/Cas is of interest. CRISPR/Cas systems may potentially be utilized to modify microglia to minimize harmful over-inflammatory effects or pathological processes. Additionally, microglia could be key effectors of the innate immune response to genetically modified PRs, which may hinder gene therapy attempts. Therefore, microglial interaction with gene therapies must be evaluated.

Currently, there exist a multitude of studies involving modifying microglia or systemic macrophages. For example, in cancer therapy there are attempts to "arm" macrophages with cytochrome P4502B6 to specifically target tumor cells [88]. In HIV therapy, there are efforts to utilize CRISPR/Cas9 to disrupt the latently integrated viral

genome found in macrophages and monocytes, which serve as a reservoir for the virus [89]. Microglia are also being specifically targeted as cellular vehicles for gene therapy in Parkinson's disease, as they are often recruited to sites of neurodegeneration or inflammation. In a murine model of Parkinson's disease, microglia were transduced with neuroturin (NTN), which promotes neuronal survival, which they then transported to sites of neuronal degradation [90]. In AD treatment, microglia were transduced with *S. aureus* Cas9 (SaCas9) and a guide RNA (gRNA) specific to the glia maturation factor, which is up-regulated in AD brains, though low transduction efficiencies proved problematic [91].

Challenges involving microglial gene therapies remain to be overcome. These include gaining access to the CNS, though this may be mitigated in the eye with the established practice of subretinal injections [92]. Subretinal injection is additionally made more attractive in the treatment of IRD by the knowledge that microglia replenish from local pools, making indirect CNS application (e.g. through lumbar puncture) of modified microglia insufficient [93]. Microglial interactions with the CNS milieu also appear to be influential, and long-term modulations of the CNS immune system may prove to be complicated by interactions with other immune cells [94]. In addition, microglial-mediated immune responses to gene therapies have yet to be satisfactorily elucidated.

1.5.2 THP-1 CELLS

To assess the innate immune response to CRISPR/Cas in macrophage-like cells, immortalized human cell lines were utilized. This is due to the fact that primary human CNS cells are particularly problematic to procure, and peripheral blood mononuclear cell (PBMC)-derived macrophages are challenging to isolate and maintain in culture. Immortalized human cell lines are an invaluable tool in the study of microglia and macrophages in vitro. There exist some well-known and highly characterized immortalized macrophage-like cell lines, such as THP-1 cells. These cells are some of the best-characterized and studied macrophage-like cells and serve as one possible model for microglia in the CNS. Therefore, they lend themselves to the initial study of immune responses to gene therapy in macrophage-like cells.

THP-1 cells were derived from the peripheral blood of a child with acute monocytic leukemia in 1980, and are a spontaneously immortalized monocyte-like cell line [95]. In culture THP-1 cells are suspension cells with a monocyte-like phenotype. To induce

monocyte-like THP-1 cells to differentiate into a macrophage-like phenotype, they must be differentiated using phorbol 12-myristate 13-acetate (PMA). Unfortunately, there is no widespread standard for the protocols surrounding PMA differentiation, and varying protocols have been shown to produce differing immune responses to stimuli [96]. These findings mean that it is vital to identify the best PMA concentration for differentiation for each individual experiment, especially as it has been shown that lower PMA concentrations can lead to a more robust immune response to stimuli [97]. THP-1 cells have been proven to express DC-SIGN [98] as well as producing similar cytokine responses to pathogens as primary human monocyte derived macrophages [99]. THP-1 derived macrophages are capable of producing TNFα, IL-1β, IL-6, and IL-10 [100] among many cytokines. These immunological capacities are another indicator that THP-1 cells serve as an appropriate model of macrophage-like human cells.

1.5.3 MICROGLIAL CELL LINES

An in vitro model of CNS microglia was required to better study a variety of neuroinflammatory and neurodegenerative diseases. Primary human CNS cells are challenging to acquire and require fine-tuned cell culture conditions; therefore an immortalized cell line is advantageous. The history of the development of microglial cell lines is convoluted, and their development has been challenging.

Microglia were first described in the early 20th century by Rio-Hortega, as the "third element" derived from CNS astro- and oligodendroglia [101]. It would not be until the early 21st century that their yolk-sac origin was confirmed, and their complex interactions with the CNS milieu and effects on neuronal development are still being elucidated [102].

Immortalized microglial cultures of human origin began to appear on the scene in 2001 with the development of the HMNO6 embryonic primary microglia cell line. However, in response to LPS exposure HMO6 cells had a far more subdued and less diverse cytokine response than primary microglia [103]. The HOM6 cell line was long the only available human microglial cell line, but its widespread adoption was probably limited due to its patented status. The HMC3 and C13NJ cell lines were both developed using the CHME-5 cell line, which has recently been found to be of rat origin, making these cells less than ideal for the study of human microglia [104]. The most recent development in the attempt to create an immortalized human microglial cell line is the

Immortalized Human Microglia SV40 cell line (IMhu). The IMhu cell line is sold by Applied Biological Material (ABM) and is derived from primary human microglia cells. IMhu have been shown to express the human microglia-macrophage marker CD11b [105], and the cell line has been studied in a variety of microglia associated applications [106–108]. Additionally, IMhu have been characterized to react to proinflammatory stimulation by up regulating inflammatory mediators such as IFNγ, IL-32, and IL-8, as well as showing mechanistic Target of Rapamycin (mTOR) activation in the same patterns as primary human microglia cells [105]. This makes them an ideal microglial model for the study of the innate immune response to CRISPR/Cas.

1.6 Gene Therapy

1.6.1 History of Gene Therapies

In response to the lack of causative therapies for genetic diseases, researchers have long searched for a targeted method to correct the genetic mutations that lead to heritable diseases. A variety of different approaches have been taken at modifying the genome, all of which were facilitated by the discovery of the double helix structure of DNA in 1953 by Watson, Crick, and Franklin. Kornberg's synthesis of DNA in 1958 and the subsequent discoveries of DNA ligases and restriction enzymes in the 1960s were also important stepping-stones on the path to developing gene therapies.

Early experiments in the 1960s attempted to induce mammalian cells to take up, incorporate, and stably express foreign DNA by using specialized cell media. For example, in 1961 Kraus et al altered bone marrow cell hemoglobin by incubating the cells in medium containing foreign DNA [109]. The inefficiency of these processes, though, prevented their widespread uptake.

By the late 1960s, interest in using viral vectors to transfer DNA into target cells was growing. In 1968 Rogers and Pfuderer used the Shope papillomavirus to successfully induce virus-mediated gene transfer [110]. In 1972 Friedman and Robin suggested that viruses could be used to carry DNA into target cells for therapeutic purposes [111]. In 1979, Martin Cline and his team used calcium phosphate transfection to induce human globin gene expression in murine bone marrow cells. In 1980, Cline attempted to correct thalassemia in two patients by transfecting bone marrow stem cells with his human globin

gene vector in vivo [112]. However, Cline had apparently not obtained the required permission for human studies from the institution hosting his work (University of California, Los Angeles) and was ultimately removed from his post and lost most of his funding [113]. The discussions regarding when and how it is appropriate and ethical to test gene therapies on patients remain lively to this day.

The discovery of the polymerase chain reaction (PCR) in 1983 and retroviruses in the early 1980s were monumental breakthroughs in the field of gene therapy. Retroviral vectors were used to restore adenosine deaminase (ADA) in ADA-deficiency severe combined immune deficiency (SCID) in the mid 1980s. The first gene therapy trial in humans, ADA restoration in SCID, was approved in 1990. One of the patients treated, Ashanti DeSilva, showed marked symptom reduction and remains alive to this day [114]. The initial elation over the success of early gene therapy trials was dampened in 1999, though, with the first death of a gene therapy patient. Jesse Gelsinger died four days after the injection of an adenoviral (AdV) vector, as a consequence of a severe immune reaction, presumably to the viral vector [5]. This exposed the need to scrutinize the immunogenicity of gene therapies to improve their safety. The incident also served to slow the initial frenzied development of gene therapies; the next few years saw slower research. The cloning of Dolly the sheep in 1996 and the sequencing of the human genome in 1999 were precursors to the regulatory approval of the first gene-targeted therapy, Glivec, by the FDA in 2001 [115]. The development of viral vector deliveries of genes or gene editing therapies using AdV, AAV, and lentiviral vectors is ongoing, as well as research into the potential immunogenicity of these therapies.

1.6.2 GENOME EDITING

Genome editing is an alternative to gene amplification that allows targeted modification of the genome. Genome editing strategies were pioneered by the discovery of zinc finger nucleases (ZFN), the subsequent discovery of TALENs, and discovery of CRISPR/Cas [116].

1.6.2.1 Inducing Gene Expression

The first step in inducing gene expression is identifying a target gene. Many causative mutations of inherited diseases have been identified and sequenced, facilitating gene editing. Once a gene has been identified it must be isolated from its host cell. One method

of introducing a gene of interest into a target genome is to place it in a plasmid containing promoter and terminator regions. These regions are responsible for the initiation and termination of transcription, and thus, expression. Many plasmids also contain antibiotic resistance genes, which allow for straightforward plasmid replication in bacterial hosts by facilitating the selection of bacteria producing the target plasmid. Once the gene-containing plasmid has been constructed, it must be stably integrated into the target genome to be expressed by the target cell. This can occur through transformation, transfection, or transduction. Transformation is specific to bacteria, which have the ability to directly transfer material through the cell membrane. Inserting DNA into animal cells using chemicals, lipid vehicles, or other methods, is referred to as transfection. Using a viral vector to insert DNA into a cell is referred to as transduction. PCR, western blots, immunofluorescence, or enzyme-linked immunoabsorbent assays (ELISA), can be used to confirm plasmid uptake and expression.

1.6.2.2 Genome Editing Tools

Genome editing requires a nuclease capable of inserting double-stranded breaks (DSB) into a host genome at a pre-determined location. The host cell subsequently repairs these engineered breaks, and these cellular repair mechanisms can be utilized to introduce genes into the host genome through homologous recombination. There are four major classes of engineered nucleases: meganucleases, ZFN, TALENs, and CRISPR/Cas.

1.6.2.2.1 Meganucleases

Meganucleases, also known as homing endonucleases, function as highly specific endonucleases capable of cleaving exon-exon junctions around a specific intron in their host cells [117]. They can recognize a DNA binding sequence of 14-40 base pairs (bp), and their relatively small size makes them attractive targets for viral vector transportation [118]. Meganucleases suffer from off-target binding [119].

1.6.2.2.2 ZFN

ZFN contain a fusion of Zinc–finger domains and a *FokI* nuclease domain [120]. The zinc-finger domain can be engineered to target a specific sequence in the genome, though it still has the potential to bind to off-target sequences which has been shown to lead to cytotoxicity [121]. The challenge of designing ZFNs makes them less attractive targets than other engineered nucleases [122].

1.6.2.2.3 TALENs

TALENs are created by fusing the DNA-binding core of the transcription activator-like effector (TALE) to a *Fokl* nuclease, and bind with great specificity to the genes of a host organism [123]. While TALENs have the capacity to bind specifically they can be difficult to construct due to the presence of repeat sequences; often, complicated procedures like golden gate cloning are required to create the repeat TALE arrays for custom TALENs [124].

1.6.2.2.4 CRISPR/Cas

Research into CRISPR/Cas systems has been ongoing since the 1980s, and in 2012 Doudna and Charpentier described how to harness these systems to cleave DNA in vitro, helping to spark their rapid adoption [125]. In 2020 the pair received the Nobel prize in chemistry for this discovery [116]. CRISPR/Cas systems were first isolated from the adaptive immune systems of archaea and bacteria and allowed the cells to defend themselves against invading phages.

There are multiple biologic variations of CRISPR/Cas systems, the most well-known being the type II CRISPR/Cas system that includes the Cas9 protease. In the type II CRISPR/Cas system invading DNA or RNA is incorporated into the CRISPR sequence of the host genome, enabling the host organism to store this genetic material. This stored sequence is then transcribed into a crRNA. Mature crRNAs guide the Cas9 protease to insert DSB at a specific site in the invading viral DNA (Fig. 2). Other CRISPR/Cas systems include types I, III, and V-A, and are less commonly utilized in gene editing [126].

Cas proteins can easily be paired with custom-designed gRNA to induce DSB at a target sequence in a genome. The subsequent DNA repair is either unspecific, by cellular DNA repair enzymes, or targeted. When a donor DNA template is provided, it may be used in the double-strand break repair by homologous recombination, leading to an actively engineered novel sequence, e.g. to correct a disease causing point mutation [127]. The advantage of CRISPR/Cas systems lies in the simplicity of their design; generally one must only design a custom gRNA. Additionally, CRISPR/Cas generated DSB are highly specific and relatively efficient [128]. CRISPR systems are efficient at gene disruption, but significantly less efficient at gene correction, though new developments in CRISPR technology promise to improve this. The versatility and simplicity of CRISPR/Cas systems makes them attractive gene editing tools, and the investigation into their immunogenicity is therefore highly relevant to the multitude of gene therapies utilizing CRISPR/Cas currently in development.

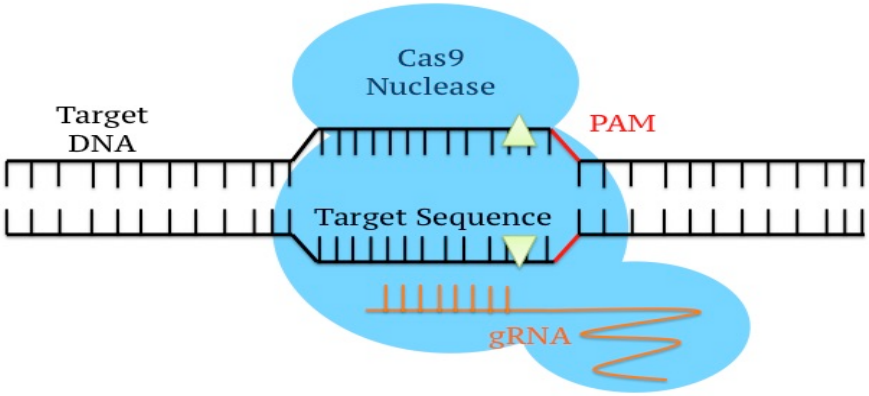

Figure 2**: CRISPR/Cas9 Gene Editing.** The Cas9 nuclease is guided to the correct sequence on the target genome by the gRNA and recognizes the protospacer adjacent motif (PAM) sequence where it induces a single- or double-stranded break. *S. pyogenes* Cas9 (SpCas9) has a 5'-NGG-3' PAM sequence which is found roughly every 8 to 12 base pairs in the human genome [129].

1.6.3 STATE OF THE ART CRISPR/CAS TRIALS

CRISPR/Cas systems have been implemented across many fields of study including medicine, biology, and agriculture, in an attempt to utilize their unique potential. In 2016 CRISPR/Cas9 was used to successfully remove the mutated exon 23 from the dystrophin gene of a Duchenne muscular dystrophy mouse [130]. Also in 2016, the NIH approved the first-in-human Phase 1 CRISPR/Cas9 trial using transgenic T cells to target NY-ESO-1 on tumor cells [1]. CRISPR/Cas technology has been used to target the HIV-1 virus in a variety of modalities [131]. In 2018 the first clinical trial using CRISPR/Cas9 to treat severe sickle cell disease by modifying CD34+ hematopoietic stem cells was launched in the United States [132].

Treatments for IRD using CRISPR/Cas9 are also in development. A treatment for the most common type of LCA, LCA10, caused by an intronic splice mutation in *CEP290,* is "groundbreaking" [133]. Targeted genomic disruption using a self-limiting CRISPR/Cas9 was used to remove the splice mutation and restore wild-type *CPE290* in murine trials in 2017 [134]. In March of 2020 the first-ever CRISPR trial with in vivo gene editing was initiated in a patient with LCA; the CRISPR therapy was injected subretinally to target the splice mutation in *CEP290* responsible for LCA10 [135]. These are only a few of the most recent examples of the expansive spectrum of therapeutic uses of CRISPR/Cas systems.

CRISPR/Cas research is not without its controversies, though. Unprecedented ethical challenges have emerged in response to the potential of CRISPR/Cas systems. In 2018, the Chinese scientist Jiankui He claimed to have used CRISPR/Cas9 to modify the genome of two infants to be resistant to HIV infection [136]. This led to international outrage, a strong rebuke of the use of CRISPR in human embryos from the WHO, and He's eventual incarceration for "illegal medical practices" [137,138]. As with all novel therapies, the ethical implications of further CRISPR/Cas advances remain to be seen.

1.7. IMMUNE RESPONSES TO GENE THERAPY

Immune responses to gene therapy pose a significant hurdle to successfully developing safe and long-lasting treatments for inherited diseases. Varying immune responses, ranging from harmless to fatal, have been recorded in response to gene therapies.

1.7.1 IMMUNE RESPONSES TO VIRAL VECTORS

Viral vectors are attractive in a variety of applications, as they can easily be used to package and transport components of gene therapy such as the wild type genetic sequences of disease genes or expression cassettes used for CRISPR/Cas editing. They can, however, be immunogenic, leading to serious complications. AdV were initially utilized as vectors due to their transduction efficiency and packaging capacity, but their capacity for inducing severe immunotoxicity ultimately led to the death of a patient [139]. Due to the possibility for severe immunotoxicity in AdV, AAV have become the favored viral vectors for gene therapy delivery. While AAV is much less immunogenic then AdV, it too has been noted to induce transient cytokine and chemokine responses in transduced tissues by activating the TLR9 pathway [140]. AAV has been shown to induce humoral adaptive immune responses including the development of AAV-specific cytotoxic T cells and T helper cells as well as AAV-specific antibodies, which may negatively affect the success of future AAV-mediated therapies [141]. Immune responses to viral vectors are broad ranging, but only make up one part of the possible immune responses to gene therapies.

1.7.2 IMMUNE RESPONSES TO CRISPR/CAS

Addressing the potential for immune responses to components of CRISPR/Cas systems is a vital aspect of further developing them for therapeutic uses.

1.7.2.1 gRNA Immune Responses

In vitro transcribed gRNAs containing 5'-triphosphate have been shown to induce a IFN response in macrophages ultimately leading to increased cell death [142]. These immune responses were mitigated in cells transfected with synthetically created gRNAs.

1.7.2.2 Immune Responses in Genetically Modified Cells

The effects of CRISPR/Cas modification on cells may manifest themselves as a reduction of cellular longevity. The p53-mediated damage response has been demonstrated to be activated by gene editing with CRISPR/Cas9 in human RPE cells [7]. This leads to an increase in the rate of cell cycle arrest and eventual cellular mortality. These results indicate a possible need to monitor or inhibit the function of p53 in modified cells to improve the efficacy of CRISPR/Cas modifications.

The production of Type I IFN in response to exposure to viral vectors has been shown to reduce gRNA expression in cells transfected with CRISPR/Cas9 plasmids, reducing the efficiency of CRISPR/Cas9 genome editing [6]. This finding indicates that the future of CRISPR/Cas9 gene editing may be linked to the success of non-viral vectors.

1.7.2.3 Cas9 Immune Responses

1.7.2.3.1 Adaptive Immune Responses

Pre-existing adaptive immunity to Cas9 proteins has also been recorded in humans, likely due to pre-existing adaptive immune responses to *S. pyogenes* and *S. aureus.* Antibodies against SaCas9 were found in 78% of donors and antibodies against SpCas9 in 58% of donors, with associated anti-Sa- or anti-Sp-Cas9 T cells [143]. 96% of donors in another study displayed an activation of effector T cells upon SpCas9 stimulation, with 85% of donors displaying a pre-existing antibody titer against *S. pyogenes* antigens. The T cell activation could not be reproduced in PBMCs from umbilical cord blood, indicating the likely necessity of prior S. pyogenes exposure in triggering an adaptive immune response to SpCas9 [144]. These findings are concerning as CRISPR/Cas systems move toward in vivo clinical trials, particularly due to the increased rates of *Staphylococcus* infections in hospitals which may activate dormant anti-Cas9 T lymphocytes, effectively inactivating CRISPR/Cas9 treatments [145]. However, contrasting these results, it was shown that only 10% of 200 human serum samples from donors originating in the United States contained anti-SaCas9 antibodies, with only 2.5% of samples containing anti-SpCas9 antibodies [146]. These results indicate that while pre-existing antibodies against AAV are present in some human serum samples, their presence may not be as ubiquitous as some studies have indicated.

1.7.2.3.2 Innate Immune Responses

Innate immune responses may also play a key role in inactivating or reducing the efficiency of CRISPR/Cas genome modification. Investigation into the innate immune responses triggered specifically by Cas9 is an avenue of research not yet satisfactorily assessed. The STING-STAT6 pathway has been recorded to drive the immune response to Cas9 protein in human PBMCs, with a pro-inflammatory release of MIP3α, CD40L, and MPO measured; this response was successfully inhibited through inhibition of the STING-STAT6 pathway [147]. Due to the limited research into the innate immune responses

to CRISPR/Cas, further investigation of the innate immune response is necessary to identify potential causes of cellular mortality or reduced CRISPR/Cas modification efficiency.

1.7.3 LONGEVITY OF GENE THERAPY

To be truly therapeutic, gene therapy must produce long-lasting results. Immune responses to modified cells or components of gene therapy may lead to long-term inactivation of modified cells or a reduction of modification efficiency. Due to the relative novelty of gene therapies, there are few reports of their long-term effects.

Gene editing utilizing CRISPR/Cas systems has been shown to be sustained long-term in non-human models. Genome editing for Duchenne muscular dystrophy (DMD) in murine models was sustained for one year after administration of CRISPR via AAV [148]. CRISPR/Cas9 has also been demonstrated to correct hemophilia B via AAV delivery in murine models for up to 210 days post-treatment, but also induced T cell-mediated IFNγ production [2]. The T cell responses were not shown to directly affect the phenotypic correction but require further investigation. The long-term effects of CRISPR/Cas therapies in human trials remain to be reported.

As gene supplementation via AAV vectors has already been utilized in clinical trials, long-term clinical results are available. An AAV-mediated treatment for LCA, which delivered healthy copies of the *RPE65* gene, was shown to be effective in dogs for 5 years post-treatment in areas of the retina which originally had more than 63% or normal PRs [149]. However, both treated and untreated regions of the injected eye showed less degeneration than the control eye, implicating unknown mechanisms of partial treatment effects. The improvements in vision seen post-injection of *RPE65*-AAV in human trials were reported to be sustained at 3 years post-treatment [150].

Nevertheless, the results of gene therapy are not always this promising and are difficult to interpret due to varying measurement modalities of functional improvement. One study reported that adult LCA patients injected subretinally with AAV-*RPE65* showed maintained improvement of vision at three years post-injection, but showed a steady diminution of the area of improved vision at 4.5-6 years post-injection [151]. Another study measured an increase in retinal sensitivity in patients injected with the AAV-*RPE65*

vector, which peaked at 6 to 12 months post-treatment and declined thereafter [152]. Gene therapy in large organs such as the liver utilizing intravenously injected AAV expressing factor VIII have shown a decrease in expression of 30% to 50% at one year post-injection [153]. The implications of the inactivation of gene therapy have yet to be elucidated and may be tied to long-term immune responses to modified cells.

1.8. AIMS

This thesis aims to improve the safety and efficacy of ophthalmological CRISPR/Cas gene therapies by elucidating the innate immune response of macrophage-like cells to Cas9. This was achieved by using macrophage-like cell models to examine the production of cytokines and modeling the reaction of the CNS innate immune system to Cas9-encoding plasmids. Initially, a custom Cas9 plasmid was created. Secondly, the THP-1 cell line was used to examine the innate immune response of systemically derived macrophage-like cells to immune stimuli and plasmid transfection. Finally, IMhu were used to study the microglial cytokine response to a Cas9 plasmid. It is hypothesized that the transfection of macrophage-like cells with Cas9-containing plasmids will induce the production of pro-inflammatory cytokines.

2. MATERIALS AND METHODS

2.1. MATERIALS

2.1.1 TECHNICAL APPLIANCES

Product	Number	Company	Company Location
Heracell 150i CO_2 Incubator, 150 L, Electropolished Stainless Steel	51026282	Thermo Fisher Scientific	Waltham, MA, USA
MSC-Advantage Biological Safety Cabinet Class II	51025411	Thermo Fisher Scientific	Waltham, MA, USA
Sorvall Legend Micro 21 Centrifuge	75002430	Thermo Fisher Scientific	Waltham, MA, USA
Sorvall Legend XT Centrifuge	75004505	Thermo Fisher Scientific	Waltham, MA, USA
KERN Precision Scale	PCB 1000-2	KERN & Sohn	Balingen, Germany
T100 Thermal Cycler	1861096	BioRad	Hercules, CA, USA
Zeiss Axio Observer 5	491916-0001-000	ZEISS	Oberkochen, Germany
Vacusafe Aspiration System	158320	Integra	Plainsboro, NJ, USA
Pipette Controller, PIPETBOY acu 2	612-0926	VWR International	Radnor, PA, USA
Nunc Serological Pipette 2, 5, 10, 25, 50 ml	170372N 170355N 170356N 170357N 170358N	Thermo Fisher Scientific	Waltham, MA, USA
Eppendorf Research plus Pipettes **0.1-2.5 µl** **0.5-10 µl** **2-20 µl** **10-100 µl** **100-1,000 µl**	3123000012 3123000020 3123000098 3123000047 3123000063	Eppendorf	Hamburg, Germany
Eppendorf Safe-Lock Tubes 0.5 ml	0030121023	Eppendorf	Hamburg, Germany
Eppendorf Safe-Lock Tubes 1.5 ml	0030120086	Eppendorf	Hamburg, Germany
Eppendorf Safe-Lock Tubes 2 ml	0030120094	Eppendorf	Hamburg, Germany
PCR Tubes (0.2 ml)	12134102	Fisher Scientific	Waltham, MA, USA
Fisherbrand EasyReader Centrifuge Tube 15 ml	11849650	Fisher Scientific	Waltham, MA, USA
Fisherbrand EasyReader Centrifuge Tube 50 ml	0644318	Fisher Scientific	Waltham, MA, USA

Carl Roth Polystyrene Petri Dishes	N221.2	Fisher Scientific	Waltham, MA, USA
Cole-Parmer Blue Light Transilluminator	GZ-97623-81	Cole-Parmer	Vernon Hills, IL, USA
NanoQuant Plate		Tecan	Männedorf, Switzerland
Tecan Nanoquant Infinite M200	9076655	Tecan	Männedorf, Switzerland
Neon Transfection System	MPK5000	Thermo Fisher Scientific	Waltham, MA, USA
LI-Cor Odyssey FC		LI-COR Biosciences	Lincoln, NE, USA
Spark (Microplate Reader/Luminometer)		Tecan	Männedorf, Switzerland
Nucleofector II	ADD-101	Lonza	Basel, Switzerland
Trypan Blue, 0.4%	15250061	Thermo Fisher Scientific	Waltham, MA, USA
BRAND Counting Chamber BLAUBRAND Neubauer Improved	BR717810	Merk Millipore	Burlington, MA, USA
BRAND Haemocytometer Cover Glass	BR723015-100EA	Merk Millipore	Burlington, MA, USA
Sarstedt Inc T25 TC Flask CN Vent Cap	50-809-257	Fisher Scientific	Waltham, MA, USA
Sarstedt Inc T75 TC Flask CN Vent Cap	50-809-261	Fisher Scientific	Waltham, MA, USA
Sarstedt Inc T175 TC Flask CN Vent Cap	50-809-259	Fisher Scientific	Waltham, MA, USA
Nalgene Cryogenic Vials	V4757-500EA	Sigma Aldrich	St Louis, MO, USA
Mr. Frosty Freezing Container	5100-0001	Thermo Fisher Scientific	Waltham, MA, USA
Nunc Cell-Culture 24-Well Multidish	142475	Thermo Fisher Scientific	Waltham, MA, USA
Nunc Cell-Culture 12-Well Multidish	150628	Thermo Fisher Scientific	Waltham, MA, USA
Nunc Cell-Culture 6-Well Multidish	140675	Thermo Fisher Scientific	Waltham, MA, USA
Corning 96 Well Solit Polystyrene Microplate flat bottom (white)	CLS3362	Merk Millipore	Burlington, MA, USA
Corning 96 Well TC-Treated Microplates, Clear	CLS3997	Merk Millipore	Burlington, MA, USA

2.1.2 Chemicals and reagents

Product	Number	Company	Company Location	Lot #
Invitrogen UltraPure DNase/RNase-Free Distilled Water	Invitrogen 10977023	Fisher Scientific	Waltham, MA, USA	
PBS, pH 7.2	20012027	Thermo Fisher Scientific	Waltham, MA, USA	
Proteome Profiler Human XL Cytokine Array Kit	ARY022B	R&D Systems	Minneapolis, MN, USA	
IRDye 800CW Streptavidin	#926-32230	LI-COR Biosciences	Lincoln, NE, USA	
IL-1β ELISA Kit Deluxe Set	437005	BioLegend	San Diego, CA, USA	8250502
Human IL-8 ELISA	4311501	BioLegend	San Diego, CA, USA	B267771
H_2SO_4 0.1M	68279	Sigma Aldrich	St Louis, MO, USA	
$NaHC0_3$	106329	Merk Millipore	Burlington, MA, USA	
Na_2C0_3	S7795	Sigma Aldrich	St Louis, MO, USA	
Deionized Water	21-520-113	Fisher Scientific	Waltham, MA, USA	

2.1.3 Cell Culture Materials

Product	Number	Company	Company Location
Gibco DMEM, High Glucose	Gibco 11965092	Fisher Scientific	Waltham, MA, USA
Gibco OptiMEM, Reduced Serum Medium	Gibco 31985047	Fisher Scientific	Waltham, MA, USA
Gibco RPMI 1640 Medium	Gibco 21875034	Fisher Scientific	Waltham, MA, USA
Gibco IMDM, GlutaMAX Supplement, HEPES	31980030	Thermo Fisher Scientific	Waltham, MA, USA
2-Mercaptoethanol	M3148-100ML	Sigma Aldrich	St Louis, MO, USA
Collagen I Bovine	A1064401	Fisher Scientific	Waltham, MA, USA
Accutase solution	A-6964-100ML	Sigma Aldrich	St Louis, MO, USA
Dimethyl Sulfoxide	D2650-5X5ML	Sigma Aldrich	St Louis, MO, USA
Glycerol	G5516-100ML	Sigma Aldrich	St Louis, MO, USA
Penicillin-Streptomycin (10,000 U/ml)	15140122	Thermo Fisher Scientific	Waltham, MA, USA
Fetal Bovine Serum qualified, Brazil	10270106	Thermo Fisher Scientific	Waltham, MA, USA
Fetal Bovine Serum, qualified, heat in activated, Brazil	10500064	Thermo Fisher Scientific	Waltham, MA, USA

Trypsin-EDTA solution	T3924-100ML	Sigma Aldrich	St Louis, MO, USA
Tryple Express Enzyme (1X)	12604013	Thermo Fisher Scientific	Waltham, MA, USA
Sodium Pyruvate (100mM)	11360070	Thermo Fisher Scientific	Waltham, MA, USA
MEM Non-Essential Amino Acids Solution (100X)	11140035	Thermo Fisher Scientific	Waltham, MA, USA
HEPES 1M	15630080	Thermo Fisher Scientific	Waltham, MA, USA
L-glutamine 200mM	25030081	Thermo Fisher Scientific	Waltham, MA, USA
Blasticidin	ant-bl-05	InvivoGen	San Diego, CA, USA
Normocin	ant-nr-1	InvivoGen	San Diego, CA, USA
Zeocin	ant-zn-05	InvivoGen	San Diego, CA, USA
Phorbol 12-myristate 13-acetate (PMA)	MKCC9510	Merk Millipore	Burlington, MA, USA
QUANTI-Luc	rep-qlc1	InvivoGen	San Diego, CA, USA
QUANTI-Blue	rep-qb1 rep-qb2	InvivoGen	San Diego, CA, USA
MycoSEQ Mycoplasma Detection Kit with PrepSeq sample preparation	4460626	Thermo Fisher Scientific	Waltham, MA, USA

2.1.4 Immunostimulants

Product	Number	Company	Company Location
Human Recombinant IFN-alpha 2b	#78077	Stemcell Technologies	Cologne, Germany
ODN 2216	tlrl-2216	InvivoGen	San Diego, CA, USA
Adenosine 5'-triphosphate disodium salt (ATP)	tlrl-atpl	InvivoGen	San Diego, CA, USA
Lipopolysaccharides from *Escherichia coli* O55:B5 (LPS)	L2880	Sigma Aldrich	St Louis, MO, USA
dsDNA-EC	tlrl-ecdna	InvivoGen	San Diego, CA, USA
Recombinant Human IL-1α	560002	BioLegend	San Diego, CA, USA
Caspase-1 inhibitor	inh-yvad	InvivoGen	San Diego, CA, USA
Poly (I:C) (LMW)	tlrl-picw	InvivoGen	San Diego, CA, USA
Recombinant human TNF-α	rcyec-htnfa	InvivoGen	San Diego, CA, USA
Recombinant human IL-6	rcyec-hil6	InvivoGen	San Diego, CA, USA
Recombinant human IL-1β	rcyec-hil1b	InvivoGen	San Diego, CA, USA

Recombinant human IL-18	rcyec-hil18	InvivoGen	San Diego, CA, USA
EnGen Cas9 Nuclease NLS, *S pyogenes*	M0646T (400pmol)	New England BioLabs	Ipswich, MA, USA
Imiquimod	Tlrl-imqs	InvivoGen	San Diego, CA, USA

2.1.5 Cell Lines

Product	Number	Company	Company Location
THP-1	ATCC TIB-202	ATCC	Manassas, VA, USA
THP-1 Dual	thpd-nfis	InvivoGen	San Diego, CA, USA
HEK-Blue IFN α/β	hkb-ifnab	InvivoGen	San Diego, CA, USA
HEK-Blue IL-6	hkb-hil6	InvivoGen	San Diego, CA, USA
HEK-Blue TFNα	hkb-tnfdmyd	InvivoGen	San Diego, CA, USA
HEK-Blue IL-1β	hkb-il1b	InvivoGen	San Diego, CA, USA
HEK-Blue IL-18	hkb-hmil18	InvivoGen	San Diego, CA, USA
Immortalized Human Microglia SV40	T0251	abm	Richmond, BC, Canada

2.1.6 Transfection Reagents

Product	Number	Company	Company Location
Lipofectamine 3000	L3000015	Thermo Fisher Scientific	Waltham, MA, USA
GeneJuice Transfection Reagent	70967	Merk Millipore	Burlington, MA, USA
Lipofectamine LTX with Plus Reagent	15338030	Thermo Fisher Scientific	Waltham, MA, USA
Trans-IT 2020 Transfection Reagent	MIR 5404	Mirus Bio	Madison, WI, USA
TransIT-X2 Transfection Reagent	MIR 6003	Mirus Bio	Madison, WI, USA
Neon Transfection System 100 µl kit	MPK10025	Thermo Fisher Scientific	Waltham, MA, USA
Neon Transfection System 10 µl kit	MPK1025	Thermo Fisher Scientific	Waltham, MA, USA
Human Monocyte Nucleofector Kit	#VPA-1007	Lonza	Basel, Switzerland
pLenti-green fluorescent protein (GFP) Control Lentivirus	LV006	abm	Richmond, BC, Canada

2.1.7 Plasmids

Plasmid	Synonym	Tag	Cas9	Origin	Plasmid #	Size (bp)
pRGEN-CMV-Campylobacter jejuni Cas9	CjCas9 Plasmid	None	CjCas9	Addgene	89752	6300
Backbone	Backbone	None	None	pRGEN-cytomegalovirus (CMV)-Campylobacter jejuni Cas9 plasmid with CjCas9 sequence removed		4000
Experimental SpCas9 Plasmid	SpCas9 Plasmid	None	SpCas9	Backbone + SpCas9 sequence from pSPCas9(BB)GFP (PX458) created by Mario Bonillo	See **Appendix A**	8068
Experimental Negative Control Plasmid	NC Plasmid	None	None	Backbone modified by Mario Bonillo	See **Appendix A**	3973
pME-Cas9-T2A-GFP	None	GFP	SpCas9	Addgene	63155	8000
pX601-mCherry Plasmid	mCherryCas9 Plasmid	mCherry	SaCas9	Addgene	84039	7400
pSPCas9(BB)GFP (PX458)	GFP SpCas9 Plasmid	GFP	SpCas9	Addgene	48138	9300
pCMV-mKate	mKate Plasmid	mKate	None	Casebia		6000
pU6-(Bbsl)_CBh-Cas9-T2A-BFP	Blue Fluorescent Protein (BFP) SpCas9 Plasmid	BFP	SpCas9	Addgene	64323	9280
pSpCas9(BB)-2A-miRFP670	miRFP SpCas9 Plasmid	miRFP	SpCas9	Addgene	91854	8800
Lonza GFP Positive Control Plasmid	Lonza GFP	GFP	None	Lonza		4700

2.1.8 Cloning Materials

Product	Number	Company	Company Location
KOD Hot Start DNA polymerase	71086-3	Merk Millipore	Burlington, MA, USA
10mM dNTP Mix	71004-3	Merk Millipore	Burlington, MA, USA
Magnesium Sulfate ($MgSO_4$) 100mM	B1003S	New England BioLabs	Ipswich, MA, USA
QIAquick Gel Extraction Kit	28706	Quiagen	Venlo, Holland
CutSmart Buffer	B7204S	New England BioLabs	Ipswich, MA, USA
BstEll-Hf	R0162S	New England BioLabs	Ipswich, MA, USA
Xbal	R0145S	New England BioLabs	Ipswich, MA, USA
BstZ17I-HF	R3594S	New England BioLabs	Ipswich, MA, USA
6X DNA Loading Dye	R0611	Thermo Fisher Scientific	Waltham, MA, USA
GeneRuler 1kb DNA-Ladder	SM0311	Thermo Fisher Scientific	Waltham, MA, USA
50X TAE-Buffer	B49	Thermo Fisher Scientific	Waltham, MA, USA
UltraPure Agarose	16500100	Thermo Fisher Scientific	Waltham, MA, USA
SYBR Safe DNA-Gel-Stain	S33102	Thermo Fisher Scientific	Waltham, MA, USA
Calf Intestinal Alkaline Phosphatase	M0290	New England BioLabs	Ipswich, MA, USA
T4 DNA Ligase buffer (10X)	B0202S	New England BioLabs	Ipswich, MA, USA
T4 DNA Ligase	M0202S	New England BioLabs	Ipswich, MA, USA
XL-10 Gold Ultracompetent Cells	200314	Agilent	Santa Clara, CA, USA
SOC Medium	15544034	Thermo Fisher Scientific	Waltham, MA, USA
Luria Broth Base	12795027	Thermo Fisher Scientific	Waltham, MA, USA
Ampicillin 100 mg/ml	A5354	Sigma Aldrich	St Louis, MO, USA
Mix2Seq Kit	3094-000 SSK	Eurofins Genomics	Luxemburg, Luxemburg
EndoFree Plasmid Mega Kit	12381	Quiagen	Venlo, Holland
Quiagen Plasmid Maxi Kit	12162	Quiagen	Venlo, Holland
PureLink HiPure Plasmid-Filter Maxiprep-Kit	K210017	Thermo Fisher Scientific	Waltham, MA, USA
GenElute Plasmid Miniprep Kit	PLN10	Sigma Aldrich	St Louis, MO, USA

2.1.9 Primers

Name	Sequence	Company	Company Location
BstEll_FW2 primer	CTGGTCACCCCCCTGATGCTGG	biomers.net	Ulm, Germany

SV40_ing2 primer	CGTGTAGATACTTTTCTCTTTTTCTTTGGAGG	biomers.net	Ulm, Germany
5,947F	ACCAAGGACATGCAGGAACC	biomers.net	Ulm, Germany
3,322R	ATACGGCAAGGTGCACAAGA	biomers.net	Ulm, Germany
4,911F	GCGTATACACTCGAGCATGCATCTAGAGG	biomers.net	Ulm, Germany
4,910F	GCGTATACAACTCGAGCATGCATCTAGAGG	biomers.net	Ulm, Germany
4,907F	GCGTATACAATAACTCGAGCATGCATCTAGAGG	biomers.net	Ulm, Germany
5,236R	AATGCAGCTGGTTCTTTCCG	biomers.net	Ulm, Germany
5,242R	TTCATTAATGCAGCTGGTTCTTTCC	biomers.net	Ulm, Germany
3,322Rev	TCTTGTCACCTTGCCGTAT	biomers.net	Ulm, Germany

2.1.10 Primary Antibodies

Name	#	Company	Source/Target/ Clone.	Isotype	Mol. Weight	Dilution	Technique
Cas9 (7A9-3A3)	14697S	Cell Signaling Technology, Danvers, MA, USA	Mouse mAb/SpCas9/Monoclonal	IgG1	160 kDa	1:600	ICC

2.1.11 Secondary antibodies

Name	#	Company	Source/Target/ Cloe.	Conjugation	Isotype	Stock Concentration (mg/ml)	Dilution	Technique
Donkey Anti-Mouse IgG H&L (Alexa Fluor 488)	ab150105	abcam, Cambridge, UK	Donkey/Mouse IgG/Polyclonal	Alexa Fluor 488 (Ex: 488, Em: 519 nm)	IgG	2	1:300	ICC
Donkey Anti-Mouse IgG (Alexa Fluor 568)	ab175472	abcam, Cambridge, UK	Donkey/Mouse IgG/Polyclonal	Alexa Fluor 568 (Ex: 578, Em: 603 nm)	IgG	2	1:500	ICC

2.1.12 Staining Materials

Product	Number	Company	Company Location
Triton X-100 Surfactant-Ams Detergent	28314	Thermo Fisher Scientific	Waltham, MA, USA
Methanol, anhydrous, 99.8%	322415-1L	Sigma Aldrich	St Louis, MO, USA
Normal Donkey Serum	Ab7475	abcam	Cambridge, UK
Tween-20	P9416-100ml	Sigma Aldrich	St Louis, MO, USA
Bovine Serum Albumin	15561020	Thermo Fisher Scientific	Waltham, MA, USA
Carl Zeiss Coverslips	10474379	Fisher Scientific	Waltham, MA, USA
FlourSave Reagent	345789	Merk Millipore	Burlington, MA, USA
DAPI	10236276001	Sigma Aldrich	St Louis, MO, USA
Dako Antibody Diluent	S0809	Agilent	Santa Clara, CA, USA

2.1.13 Software

Software	Version	Company
Image Studio Lite	5.2.5	LI-COR Biosciences
GraphPad PRISM	8	GraphPad Software, Inc.
JMP	14.2.0	SAS Institute
SnapGene Viewer	4.1.9	GSL Biotech LLC
NanoQuant-Plate-Software	1.4	Tecan
Odyssey Fc Imaging System	1	LI-COR Biosciences
geneious Prime	R10.1	Biomatters
ImageJ/FIJI	1	ImageJ/FIJI
Microsoft Excel	14.5.9	Microsoft
Microsoft PowerPoint	14.5.9	Microsoft
Microsoft Word	14.5.9	Microsoft

2.2. METHODS

2.2.1 CLONING

2.2.1.1 PCR

PCR was performed to amplify DNA sequences. The protocol was adapted from the PCR protocol developed by addgene [154]. First, the PCR primers were diluted to a working concentration of 0.1 µM. Then, the reagents for one reaction were pipetted into a PCR tube: 33.9 µl UltraPure DNase/RNase-Free Distilled Water, 5 µl dNTPs, 3 µl $MgSO_4$, 0.1 µl DNA template (10-100 ng/µl), 1.5 µl forward primer, 1.5 µl reverse primer, 1 µl KOD polymerase, and 5 µl of the included KOD reaction buffer. The reagents were gently mixed, and the tube was placed into the thermal cycler. A 2 minute activation period at 95°C was followed by 35 cycles of the following PCR parameters: a 20 second denaturation phase at 95°C, a 10 second annealing phase at 63°C, and a 40 second extension phase at 70°C.

2.2.1.2 Agarose Gel Electrophoresis

Agarose gel electrophoresis was performed to separate DNA sequences by size. Agarose gel was prepared by dissolving 4 g agarose (1% agarose gel) in 200 ml TAE buffer. The mixture was then heated in the microwave until homogenous. After cooling to room temperature, 2 µl SYBR Safe DNA-Gel-Stain were added and the gel was stirred. The mixture was then poured into a gel mold and well forms were inserted. The gel was left to set at room temperature for 30 minutes. 25 µl sample DNA and 5 µl loading dye were pipetted together in an eppendorf tube and mixed. The agarose gel was placed in the electrophoresis machine and submerged in TAE buffer. 5 µl GeneRuler 1 kb DNA-Ladder were pipetted into the first and last wells. 30 µl sample DNA + loading dye were pipetted per well. The electropohoresis machine was set to 110V, and the gel was allowed to run until the fragments were satisfactorily separated. Results were examined using the Cole-Parmer Blue Light Transilluminator. Photos were captured using the LI-Cor Odyssey FC.

2.2.1.3 Gel Extraction

To facilitate further usage, amplified DNA fragments were extracted from the agarose gel using the QIAquick Gel Extraction Kit. First, the agarose gel containing DNA fragments was excised from the remaining gel. Then the manufacturer's recommended protocol was followed, with two modifications. During the washing step, the drainage

time was increased from one to four minutes. During the elution step, the incubation time was increased to 3 minutes. Both modifications were intended to increase the quantity of purified DNA. The concentration and purity of eluted DNA was assessed using a NanoQuant plate and a Tecan Nanoquant Infinite M200.

2.2.1.4 Restriction Digestion

Restriction digestion of plasmids was performed to induce double-stranded breaks at predetermined sites. The addgene restriction digest protocol was used as a template [155]. The following reagents were pipetted into a 1.5 ml eppendorf tube and mixed gently: 2.5 µl CutSmart Buffer, 1 µl of each restriction enzyme, 1 µg plasmid DNA, and X µl water (enough to bring the total reaction volume to 25 µl). The mixture was then incubated in a water bath for two hours at 37°C. The results were assessed using agarose gel electrophoresis and extracted from the gel prior to further use.

2.2.1.5 Restriction Digestion with Calf Intestinal Alkaline Phosphatase (CIP)

CIP dephosphorylates the 5'-ends of DNA sequences, and therefore prevents vector re-closure during restriction digestion. Restriction digestion with CIP was performed to minimize self-ligation of the digested plasmid. The CIP restriction digest protocol from NEB was used in a modified form [156]. 4 µg plasmid DNA, 2.5 µl CutSmart Buffer, 3 µl of each restriction enzyme, and X µl water (to bring the total reaction volume to 20 µl) were pipetted into a 1.5 ml eppendorf tube and mixed gently. The mixture was incubated at 37°C for 60 minutes. CIP was added after incubation (1 unit CIP per pmol of DNA ends), and the reagents were incubated for an additional 60 minutes at 37°C. The DNA was then assessed using agarose gel electrophoresis and extracted from the gel before ligation.

2.2.1.6 Plasmid Ligation

To ligate two DNA sequences together, a general ligation protocol was utilized, which was adapted from the ligation protocol provided by addgene [157]. Various ratios of insert to vector DNA were utilized, generally: (3 insert: 1 vector), to create a total of 100 ng of DNA. These 100 ng DNA were mixed with 1 µl T4 DNA Ligase buffer (10x), 1 µl T4 DNA Ligase, and X µl water (to bring the total reaction volume to 10 µl). The mixture

was then incubated at room temperature for 24 hours. Various control samples were ligated simultaneously to control for potential causes of failed ligation.

2.2.1.7 XL-10 Gold Transformation

The results of DNA ligation were transformed into XL-10 gold ultracompetent cells per manufacturer's protocol. The transformation and following antibiotic selection allow for confirmation of successful ligation. The manufacturer's protocol was modified at these following points: 75 µl of XL-Gold cells were used instead of 100 µl. 3 µl of 2-Mercaptoethanol were used instead of 4 µl. SOC medium was substituted for NZY+ broth. 2 µl of ligation mixture were added and the tubes were incubated for 1.25 hours instead of 1 hour at 37° after the addition of the SOC medium.

2.2.1.8 Preparation of Agar Plates

The products of the XL-10 gold transformation were plated on agar plates prepared with an appropriate selection antibiotic. All plasmids transformed contained an ampicillin-resistant gene; therefore LB-ampicillin agar plates were used. 3.12 g Luria Broth Base was weighed and mixed with 1.8 g of UltraPure Agarose. 125 ml water was added in an autoclavable container. The mixture was autoclaved under 'liquid' settings, using Select Autoclave Tape to control for appropriate heat exposure. After the mixture had cooled, 125 µl of Ampicillin 100 mg/ml were added. 25 ml LB Agar was poured into each petri dish. The dishes were kept under the hood at room temperature for at least 1 hour before being stored at 8°C until use.

2.2.1.9 DNA Sequencing using the Mix2Seq Kit

Plasmid DNA was analyzed using the Mix2Seq Kit to confirm the sequence of the sample. 15 µl of purified DNA with a concentration between 50-100 ng/µl were added to a 0.2 ml eppendorf tube. 2 µl of an appropriate 10 uM primer were added to the tube. 17 µl of this mixture was transferred to the provided tube and sent to the manufacturer for sequencing.

2.2.1.10 Plasmid Megaprep

The Endofree Plasmid Mega kit was used to amplify the concentration of plasmids. The manufacturer's protocol was followed, with modifications designed to increase the DNA yield. At Step 10, the QIAGEN-tip was washed with 50 ml Buffer QC instead of

200 ml. At step 11, the DNA was eluted with 35 ml Buffer QN at 65°C instead of at room temperature. After the initial DNA elution, Step 11 in the Endofree Plasmid Mega Kit protocol, the DNA purification was continued using a PureLink HiPure Plasmid-Filter Maxiprep-Kit. The PureLink protocol was followed as per manufacturer's protocol beginning at step 1: "*precipitate DNA with a purelink hipure precipitator module*". Step 8 was performed with 500 µl TE buffer instead of 1 ml. The optional elution (Step 9) was performed. The concentration and purity of the plasmid DNA was assessed using a NanoQuant plate and the Tecan Nanoquant Infinite M200.

2.2.1.11 Plasmid Miniprep

The GenElute Plasmid Miniprep Kit was used to amplify the concentration of plasmids from ligation colonies of transformed XL-10 gold cells. 1 colony was picked from a ligation plate using a sterile pipette tip and placed in a 15 ml centrifuge tube filled with 7 ml LB medium containing 7 µl Ampicillin. These tubes were placed in an incubator at 37° for 12-16 hours with shaking at 135 RPM. The cap of the centrifuge tube was left unscrewed and secured loosely with tape to facilitate oxygenation of the medium. After incubation, the tubes were centrifuged at 12,000g for 1 minute. The supernatant was discarded and the cell pellet frozen at -20°C. The manufacturer's miniprep protocol was followed from there on.

2.2.1.12 Plasmid Maxiprep

To amplify the concentration of plasmid samples, the Quiagen Plasmid Maxi Kit was used as per manufacturer's protocol. After step 9 of the Quiagen Plasmid Maxi Kit protocol, DNA purification was continued using a PureLink HiPure Plasmid-Filter Maxiprep-Kit. The PureLink protocol was followed as per manufacturer's protocol beginning at step 1: "*precipitate DNA with a purelink hipure precipitator module*". Step 8 was performed with 500 µl STE buffer instead of 1 ml. The optional elution (Step 9) was performed. The concentration and purity of the plasmid DNA was assessed using a NanoQuant plate and a Tecan Nanoquant Infinite M200.

2.2.2 CELL CULTURE

2.2.2.1 Cell Counting with Trypan Blue

To assess the quantity and vitality of cells in a cell culture sample, cells were trypsinized and assessed using trypan blue. 10 µl cell suspension was combined with 10

µl trypan blue in a 0.2 ml eppendorf tube. 10 µl of this mixture were pipetted onto a Neubauer Haemocytometer, covered with a coverslip, and assessed under a light microscope. The cells on all four quadrants of the Haemocytometer were counted and the average of these counts was used for the calculations.

Average cells per quadrant × 10 × dilution factor (2) = cells/µl

2.2.2.2 Mycoplasma Testing

The cells were declared mycoplasma free through the use of a MycoSEQ PCR based mycoplasma detection kit as per the manufacturer's protocol.

2.2.2.3 IMhu Culture

IMhu were cultured in T25, T75, and T175 flasks. The flasks were treated with Human Collagen type I at 6-10 µg/cm^2 in PBS for 1 hour at room temperature. The collagen solution was aspirated and the flasks were allowed to dry for 1 hour at room temperature. The flasks were then washed twice with PBS before storage at 4°C until use. Cells were cultured in DMEM high glucose medium supplemented with 10% FBS and 1% pen/strep. IMhu were passaged using Tryple Express. Cultures maintained at 37°C with 5% CO_2.

2.2.2.4 THP-1 Thawing

THP-1 cells were thawed carefully to maximize cell viability. The cryovial containing THP-1 cells was partially submerged in a 37°C water bath until only a small ice chip remained. The vial was removed from the water and decontaminated using 70% ethanol. Under the cell culture hood the contents of the cryovial were resuspended in 5 ml pre-warmed RPMI containing 20% FBS, 1% pen/step, and 1% L-glutamine and centrifuged at 300g for 5 minutes. The supernatant was discarded and the cell pellet resuspended in RPMI containing 20% FBS and 1% L-glutamine at a concentration of 500,000 cells/ml in a T25 flask. The flask was incubated upright for 1-3 days at 37°C with 5% CO_2. Once a total of 1×10^6 cells had grown, the cells were transferred to a T75 flask in 10 ml medium. The flask was incubated lying down and the cells were passaged at a concentration of 6×10^5 cells /ml.

2.2.2.5 THP-1 Cryopreservation

To preserve THP-1 cells in a liquid nitrogen stock, the cells were centrifuged at 300g for 5 minutes and the supernatant was discarded. The centrifuged cell pellet was resuspended in 90% PBS and 10% glycerol at a concentration of 2×10^6 cells/ml. 1 ml cell suspension was pipetted into each cryovial and the vials were placed in the Mr. Frosty Freezing Container. The freezing container was stored at -80°C for 24 hours. The vials were then transferred to the liquid nitrogen tank for long-term storage.

2.2.2.6 THP-1 Cell Culture

THP-1 cells were cultured in RPMI growth medium containing: 2mM L-glutamine, 10% heat inactivated FBS, and 100 µg/ml Pen-Strep. Cells were passaged when the density reached 2×10^6 cells/ml. Cells were seeded at 2×10^6 cells in a T75 flask and 4×10^6 cells in a T175 flask.

2.2.2.7 PMA-Induced THP-1 Differentiation

To induce a macrophage-like phenotype, THP-1 cells were incubated in the presence of PMA. The THP-1 cells were seeded at the desired concentration in growth medium containing X ng/ml PMA (Initially, 500 ng/ml PMA were used). The cells were then incubated at 37°C for 48 hours. After 48 hours the PMA-medium was aspirated and replaced with RPMI containing no additives. The cells were then incubated at 37°C for 24 or 48 hours, prior to experimental use.

2.2.2.8 THP-1 Dual Cell Culture

THP-1 Dual cells were cultured in RPMI growth medium containing: 2mM L-glutamine, 25mM HEPES, 10% heat inactivated FBS, 100 µg/ml Normocin, 30 µg/ml blasticidin, and 100 µg/ml Pen-Strep. Cells were passaged every 3 days, or when the density reached 2×10^6 cells/ml. Cells were frozen in freezing medium containing: 90% FBS and 10% DMSO at 1×10^6 cells/ml. The THP-1 Dual cells were thawed as per the THP-1 cell thawing protocol.

2.2.2.9 Human embryonic kidney (HEK)-Blue Cell Culture

The HEK-Blue IFN α/β, HEK-Blue TNFα, HEK-Blue IL-1β, HEK-Blue IL-18, and HEK-Blue IL-6 cell lines were cultured in DMEM high glucose growth medium containing: 10% heat inactivated FBS, 1% Penicillin-Streptomycin 10,000 U/mL, 30

μg/ml Blasticidin, 100 μg/ml Zeocin, and 100 μg/ml Normocin at 37°C with 5% CO_2. Cells were cultured in T25, T75, and T175 flasks and passaged at 70-80% confluency.

2.2.2.10 HEK-Blue Passaging

Culture medium was removed from the vial, and cells were rinsed once with PBS. Pre-warmed Trypsin was added, and the flask was incubated at 37°C for 5 minutes. 2 ml of Trypsin were added to a T25 flask, 5 ml to a T75 flask, and 10 ml to a T175 flask. The flask was then assessed under a light microscope to confirm that the cells had dislodged. Growth medium was added to halt trypsination: 5 ml in a T25 flask, 10 ml in a T75 flask, and 20 ml to a T175 flask. This mixture was pipetted into a 15 ml or 50 ml centrifuge tube and centrifuged at 400g for 5 minutes. The supernatant was discarded and the cell pellet resuspended in a small amount of growth medium. The cells were then counted before seeding at the desired concentration.

2.2.2.11 HEK-Blue Thawing

To thaw cryovials stored in liquid nitrogen tanks, vials were submerged in a 37°C water bath. The cap was kept above water to reduce contamination. As soon as the frozen cells were almost completely thawed the vial was removed from the water and decontaminated using 70% ethanol. Under the cell culture hood the cells were transferred to a 15 ml centrifuge tube containing 14 ml pre-warmed growth medium without Zeocin and Blasticidin and centrifuged at 250g for 5 minutes. The supernatant containing the cryoprotective agent was discarded, cells resuspended in 1 ml of growth medium and transferred into a T25 flask containing 5 ml growth medium. The cells were incubated at 37°C with 5% CO_2 until they reached 80% confluency whereupon they were transferred to a T75 flask and cultured as per the cell culture protocol.

2.2.2.12 HEK-Blue Cryopreservation

To preserve HEK cells in a liquid nitrogen stock, the cells were centrifuged at 400g for 5 minutes and the supernatant was discarded. The centrifuged cell pellet was resuspended in 90% PBS and 10% DMSO at a concentration of 1×10^6 cells/ml. 1 ml cell suspension was pipetted into each cryopreservation vial and the vials were placed in the Mr. Frosty Freezing Container. The freezing container was stored at -80°C for 24 hours. The vials were then moved to the liquid nitrogen tank for long-term storage.

2.2.2.13 Scaling Cell Culture Volumes

"Useful Numbers for Cell Culture" from Thermo Fischer was referenced to calculate the volume of medium or concentration of cells for culture in flasks or well plates [158].

2.2.3 CYTOKINE ASSESSMENT

2.2.3.1 IL-β ELISA

The concentration of IL-1β in supernatant samples was quantified using the IL-1β ELISA Kit Deluxe Set from Biolegend as per the manufacturer's protocol. PBS containing 0.05% Tween-20 was used as the wash solution. 1M H_2SO_4 was used as the stop solution. Plastic cling film and aluminum foil were used to seal the plates.

2.2.3.2 IL-8 ELISA

The concentration of IL-8 in supernatant samples was quantified using the Human IL-8 ELISA Set from Biolegend as per the manufacturer's protocol. PBS containing 0.05% Tween-20 was used as wash solution; 1M H_2SO_4 was used as the stop solution. The coating buffer contained: 8.4g $NaHC0_3$, 3.56 g Na_2C0_3, and 1L deionized water. Plastic cling film and aluminum foil were used to seal the plates.

2.2.3.3 Detection of NF-κB Activation in THP-1 Dual Cells

THP-1 Dual cells facilitate the study of the activation of the NF-κB pathway, as NF-κB activation triggers the excretion of secreted embryonic alkaline phosphatase (SEAP). Through monitoring of excreted SEAP, the activation of the NF-κB pathway can be assessed. QUANTI-Blue was used to assess the SEAP concentration in supernatant from THP-1 Dual cells. First, the QUANTI-Blue was prepared as per manufacturer's protocol. Then 200 µl QUANTI-Blue were aliquoted per well in a 96-well plate. 20 µl supernatant from THP-1 dual cells was then added per well. 20 µl culture medium was used as a negative control. The 96-well plate was then incubated at 37°C for 15 minutes to 24 hours. SEAP activity was then assessed using a microplate reader, which measured the optical density at 625-650 nm.

2.2.3.4 Detection of IFN Activation in THP-1 Dual Cells

THP-1 Dual cells facilitate the study of the activation of the IRF pathway, as IRF activation triggers the excretion of luciferase. Through monitoring of excreted luciferase,

the activation of the IRF pathway can be assessed. QUANTI-Luc was used to assess the luciferase concentration in supernatant from THP-1 Dual cells. QUANTI-Luc was prepared as per the manufacturer's protocol. The manufacturer's protocol for end-point readings using a luminometer without an injector was followed. The luminometer was set for end-point measurements with a 4 second start time and a 0.1 second reading time. 20 µl of sample supernatant were pipetted per well of an opaque 96-well plate. 50 µl QUANTI-Luc was then added to each well. The plate was gently tapped several times and the measurements were taken using a Tecan Spark microplate reader.

2.2.3.5 HEK-Blue Cytokine Detection

HEK-Blue cells were incubated with supernatant from various experiments as per the manufacturer's protocol to assess cytokine production. The subsequent activation of NF-κB and activator protein-1 in the HEK-Blue cells in response to cytokines in their supernatant induced the production of SEAP. This HEK-Blue supernatant containing SEAP was analyzed using the SEAP reporter assay. The results of this assay were determined using a Tecan plate reader at a wavelength of 640 nanometers.

2.2.3.6 Human Dot-Blot Proteome Profiler

Semiquantitative immunodetection of human cytokines, chemokines, growth factors, angiogenesis markers, and other proteins in supernatant was performed using the Proteome Profiler Human XL Cytokine Array Kit. The manufacturer's recommended protocol was followed. The protocol utilizing IRDye 800CW to create a chemiluminescent signal corresponding to the amount of cytokine bound was followed. Starting at step 14 of the proteome profiler's protocol, the protocol for "*Use of Proteome Profiler Arrays with LI-COR Detection*" was followed. Chemiluminescence was detected using a LI-Cor Odyssey FC scanner. The Odyssey scan was run with a resolution of 84 µm, an intensity of 5, 800 nm, an absorbance of 774 nm, and an emission of 789 nm. The signal intensity, measured in pixel density, was analyzed using ImageStudioLite Software. For each measured analyte, the average signal of the duplicate spots was determined and normalized to the average signal of the reference spots after being corrected with the background signal.

2.2.4 TRANSFECTION

2.2.4.1 THP-1 Nucleofection

To efficiently transfect THP-1 macrophages, the established protocol published by Maeß, Buers, Robenek, and Lorkowski was followed [159]. The Human Monocyte Nucleofector Kit from Lonza was utilized in conjunction with the Nucleofector II from Lonza.

2.2.4.2 Electroporation using the Neon Electroporation System

The Neon Electroporation System was utilized to electroporate cells with plasmid DNA. 100 µl and 10 µl tips were utilized. Cells were resuspended in the Resuspension buffer R at the manufacturer's recommended concentration. The manufacturer's protocol was followed, and various electroporation settings were tested to optimize transfection efficiency.

2.2.4.3 GeneJuice

The manufacturer's protocol was followed to transfect cells with plasmid DNA. An example for transfection in a 12-well plate follows: Pipet 50 µl OptiMEM per well + x µl GeneJuice per well together in a sterile tubule. Vortex and incubate at room temperature for 5 minutes. Add 2 µg DNA per well and gently mix. Incubate at room temperature for 15 minutes. Add drop-wise to cells and gently rock plate to distribute. Add 1 ml medium per well. Incubate for 24-72 hours at 37°C before assessment using fluorescence microscopy.

2.2.4.4 Lipofectamine 3000

The manufacturer's protocol was followed to transfect cells with plasmid DNA. An example for transfection in a 12-well plate follows: Pipet 1000 ng DNA per well + 100 µl OptiMEM + 1.5 µl Lipofectamine 3000 + 2 µl P3000 reagent into a sterile tubule. Mix gently and incubate at room temperature for 15 minutes. Add drop-wise to cells and gently rock plate to distribute. Add 1 ml medium. Incubate for 24-72 hours at 37°C before assessment using fluorescence microscopy.

2.2.4.5 Lipofectamine LTX

The manufacturer's protocol was followed to transfect cells with plasmid DNA. An example for transfection in a 12-well plate follows: Add 0.5 µg DNA to 100 µl OptiMEM per well to a sterile tubule. Add 0.5 µl Plus reagent to the diluted DNA and incubate for 15 minutes at room temperature. Dilute 1-2.25 µl Lipofectamine LTX into the DNA solution. Incubate for 25 minutes at room temperature. Add 100 µl of the LTX-DNA solution drop-wise onto the cells. Add 400 µl RPMI medium and incubate for 18-24 hours before assessment using fluorescence microscopy.

2.2.4.6 TransIT-2020

The manufacturer's protocol was followed to transfect cells with plasmid DNA. An example for transfection in a 12-well plate follows: Place 50 µl OptiMEM per well in a sterile tubule. Add x µg (0.5, or 1) Plasmid DNA and pipet gently to mix. Add x µl (0.5, 1, 1.5, 2) TransIT-2020 and pipet gently to mix. Incubate at room temperature for 30 minutes. Add drop-wise to cells and top off with 0.45 ml RMPI medium. Incubate for 24-72 hours at 37°C before assessment using fluorescence microscopy.

2.2.4.7 TransIT-X2

The manufacturer's protocol was followed to transfect cells with plasmid DNA. An example for transfection in a 12-well plate follows: Place 50 µl OptiMEM per well in a sterile tubule. Add x µg (0.5, or 1) Plasmid DNA and pipet gently to mix. Add x µl (0.5, 1, 1.5, 2) TransIT-X2 and pipet gently to mix. Incubate at room temperature for 30 minutes. Add drop-wise to cells and top off with 0.45 ml RMPI medium. Incubate for 24-72 hours at 37°C before assessment using fluorescence microscopy.

2.2.5 Immunostaining

2.2.5.1 Immunocytochemistry (ICC)

18 mm diameter round coverslips were placed in a 24-well plate. The 24-well plate was then disinfected using UV light for 1 hour. Cells were seeded and experiments performed. At the desired time point, the cells were washed twice using wash buffer (WB) containing: 1% NDS and 0.05% Tween20 in PBS. All steps aside from incubation with the primary antibody took place at room temperature. After washing, the cells were fixed with 4% paraformaldehyde (PFA) in PBS for 10 min at room temperature. The cells were washed three times with WB following fixing. Permeabilization with PBS containing

0.05% Triton X-100 for 10 minutes was performed. After three washes with WB the cells were blocked with 10% NDS and 0.05% Tween20 in PBS for one hour. The cells were then washed with the WB twice before being incubated overnight at 8°C in the presence of the primary antibody, Cas9 (7A9-3A3) Mouse mAb, at a concentration of 1:600. After three washes in WB, the cells were incubated for two hours with the secondary antibody in Dako antibody diluent. The secondary antibody, Donkey Anti-Mouse IgG Alexa Fluor 488, was added at a concentration of 1:500. Cells were washed with WB three times before being incubated with DAPI for 2 minutes in the dark. The coverslips were mounted to slides using a drop of Fluor Save Reagent. Immunostaining was assessed and images were captured using fluorescence microscopy.

2.2.6 Statistical Analyses

2.2.6.1 JMP

JMP version 14.2 was used for all statistical analyses. Data was initially assessed for normality using the Shapiro-Wilk test. Normally distributed data was further assessed using One-way ANOVA or Student's T tests. Post hoc analysis of One-way ANOVAs was performed using Tukey's tests. Non-normally distributed data was assessed using non-parametric Mann-Whitney tests or Kruskal-Wallis tests. Post hoc assessment of Data analyzed with Kruskal-Wallis tests was performed using Dunn's test with control for joint ranks and Bonferroni adjustment.

2.2.6.2 GraphPad PRISM

GraphPad PRISM version 8 was used to create graphs.

2.2.6.3 ImageJ/FIJI

ImageJ/FIJI version 1 was used to assess the pixel density of images.

3. Results

3.1. Optimization of Cloning Protocols

Initially, the project aimed to assess the immune reaction to the *C. jejuni* Cas9 (CjCas9) sequence. The pRGEN-CMV-Campylobacter jejuni Cas9 plasmid from Addgene was chosen due to its small size and simple construction. To reduce immunogenicity triggered by sequences other than the Cas9 sequence, the SV40 NLS/HA tag was removed (Fig. 3).

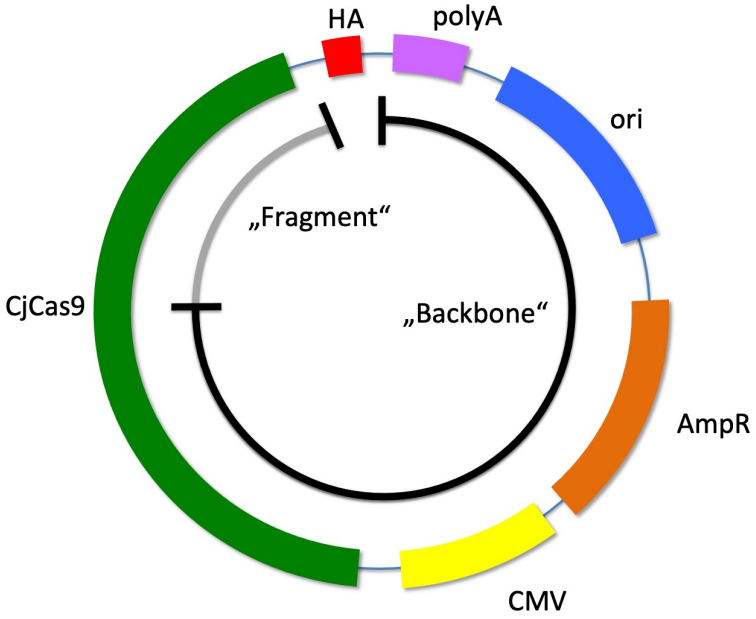

Figure 3: **CjCas9 Plasmid with „Fragment“ and „Backbone“ labeled**. HA: SV40 NLS/HA tag, polyA: polyA signal, ori: Origin of replication, AmpR: Ampicillin resistance gene and promoter, CMV: Cytomegalovirus (CMV) enhancer and promoter, CjCas9: CjCas9 sequence.

Established protocols for PCR, restriction digestion, and ligation were initially utilized and modified as needed.

3.1.1 PCR

3.1.1.1 Initial Results

PCR amplification was performed using primers designed to create a fragment lacking the SV40 NLS/HA tag. The established PCR protocol was followed as described (Chapter 2.2.1.1) and a fragment of the projected size (1.7 kb) was produced.

3.1.1.2 Primer Design

Due to issues with possible plasmid self-ligation, new primers (4,911F, 4,910F, 4,907F, and 5,236R, 5,242R, 5,245R) were designed using geneious Prime to create non-self-ligating restriction sites. The initial PCR protocol (Chapter 2.2.1.1) was followed and the resulting fragments separated using gel electrophoresis. Fragments created were of the projected size (1.6 kb), and were extracted using the established gel extraction protocol (Chapter 2.2.1.2), which was modified to increase the final DNA concentration: elution was performed with 30 µl elution buffer at 70°C for 4 minutes.

3.1.1.3 DNA Sequencing

To control for appropriate primer functioning, fragments produced by both the initial and subsequent primers were sent for sequencing (Chapter 2.2.1.9), as fragments lacking restriction sites for the restriction enzymes would be unable to be digested and ligated. The fragments were sequenced using the Mix2Seq Kit and geneious Prime was used to confirm that the restriction sites on both ends of the fragment were intact and correlated with the projected PCR results.

3.1.2 RESTRICTION DIGESTION

3.1.2.1 Initial Results

Restriction digestion was initially performed on the PCR fragments and unmodified plasmid using the established protocol and the restriction enzymes BstEII and XbaI (Chapter 2.2.1.4). The results of this restriction digestion were separated using gel electrophoresis and extracted from the gel using the established gel extraction protocol (Chapter 2.2.1.3). This initially led to the extraction of plasmid backbones with a relatively low average DNA concentration of 1 ng/µl. To increase the DNA yield, the initial plasmid solution volume was increased from 5 µl to 9 µl. The restriction digestion was repeated, leading to an average increase in DNA concentration of 20 ng/µl.

3.1.2.2 Modified Agarose Gel Settings

To reduce the concentration of unrestricted backbone in digestion samples, the settings of the agarose gel electrophoresis (Chapter 2.2.1.2) were modified to increase the degree of separation between the digested backbone and undigested plasmid in the gel. The initial settings were: 1% agarose, 110V, and a 1-hour run time. These were adjusted to: 2% agarose, 140V, and a 4-hour run time.

3.1.2.3 New Restriction Enzymes

After the development of custom primers, new restriction enzymes were selected to better fit the new fragment produced. Restriction digestion was performed using PvUII and BstZ17I and the modified protocol (Chapter 3.1.2.1).

3.1.2.4 Backbone Dephosphorylation with CIP

To reduce backbone self-ligation, restriction digestion was performed with the addition of CIP. CIP dephosphorylates the 3' and 5' ends of DNA and thereby prevents re-ligation of linearized DNA. The backbone was dephosphorylated with CIP and digested as per protocol (Chapter 2.2.1.5). The volume of restriction enzymes was increased from 1 µl to 4 µl to increase the amount of restricted plasmid. The result of this restriction digestion was purified using agarose gel electrophoresis.

3.1.3 LIGATION

3.1.3.1 Initial Results

The backbone and fragment were ligated as per protocol (Chapter 2.2.1.6) and transformed into XL-10 gold ultracompetent cells (Chapter 2.2.1.7). A ligation sample and a negative control containing the DNA backbone and the DNA ligase were plated. After incubation, neither plate showed colony growth.

3.1.3.2 Optimized Controls

To control for the function of the XL-10 gold cells, all following ligation attempts included a control containing XL-10 gold cells and the positive control plasmid (pUC18) included in the XL-10 gold kit. Additionally, controls containing the backbone and ligase but without the fragment were run to control for self-ligation as well as controls containing only XL-10 gold cells and H_2O (Fig. 4).

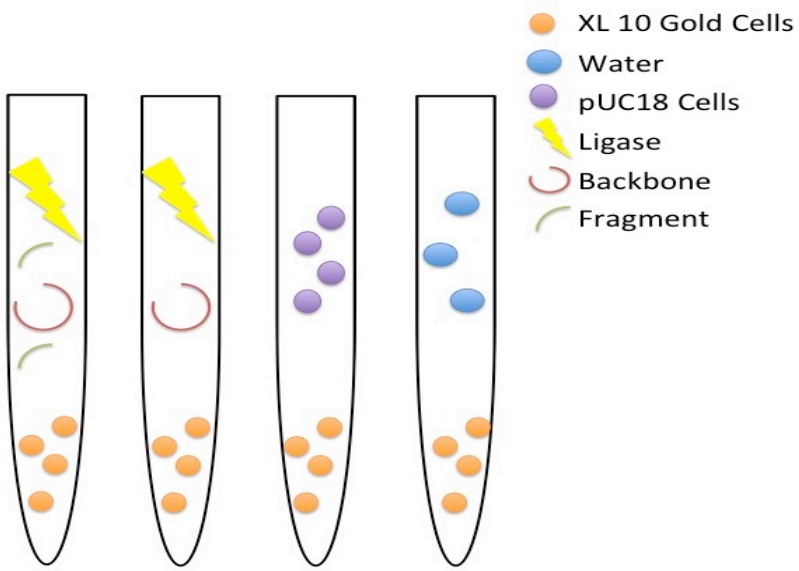

Figure 4: **Ligation Positive and Negative Controls.**

The first self-ligation negative control containing backbone and ligase was plated and showed colony growth. This was an indication of self-ligation and led to the adoption of modified protocols.

3.1.3.3 Modifying Ligation Ratios

3.1.3.3.1 Initial Restriction Enzymes and Primers

A modified ligation protocol (Chapter 2.2.1.6) was utilized containing varying rations of vector (backbone) and insert (fragment): vector 1:3 insert, vector 1:10 insert, vector 1:1 insert, and vector 1:0 insert. The ligation results were transformed into XL-10 gold cells and plated on agarose gel. The plates containing ligation with vector 1:10 insert grew tightly seeded colonies, and 20 colonies were picked and amplified via miniprep (Chapter 2.2.1.11). Picked colonies were initially placed in a 15 ml centrifuge tube with 7 ml LB and 1% ampicillin. They were incubated for 12 hours at 37°C with shaking at 160 RPM prior to miniprep. The negative controls containing a H_20 control and vector 1:0 insert did not show growth. The pUC18 transformed cells grew as expected.

The 20 amplified ligated plasmids were digested with BstEII-HF and Xbal. The results of this restriction should have proven that the ligated plasmids contained the restriction sites by being digested into a fragment (1.8 kb) and backbone (4.5 kb), indicating successful ligation (Fig. 5).

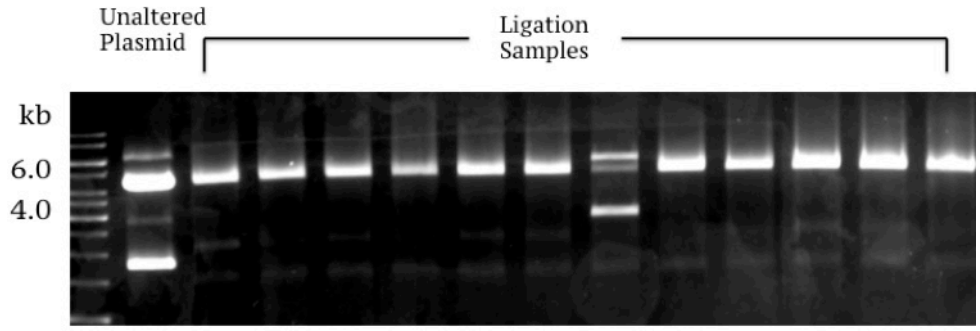

Figure 5: **Restriction Digestion of Ligated Plasmids with BstEII-HF and XbaI.** Well 1, on the left, contained the unmodified plasmid and was digested into a backbone and fragment. All other wells contained plasmids from the ligation sample and were not digested into a backbone and fragment, as expected.
kb: kilo base pairs

This lack of digestion indicated that the ligation results seen might have been caused by self-ligation of the plasmid backbone. As a result of this, measures against self-ligation including CIP phosphorylation and the development of new primers were initialized.

3.1.3.3.2 New Restriction Enzymes and Primers

The fragment was ligated with the newly prepared backbone. Samples contained: vector 1:3 insert (100 ng insert), vector 1:3 insert (50 ng insert), and vector 1:0 insert. The ligation mixtures were then incubated at room temperature overnight, prior to transformation in XL-10 gold cells. Transformation and ligation controls containing the pUC18 positive control plasmid, and vector 1:0 insert, respectively, were included. The ligation samples, as well as the vector 1:0 insert negative control grew a lawn of bacterial colonies. The pUC18 sample grew individual, distinct colonies. This indicated an issue with undigested plasmid or self-ligation of the samples.

3.1.3.3.3 Ligating the CIP Restricted Plasmid

Restriction digestion was performed with CIP (Chapter 3.1.2.4) to reduce self-ligation of the plasmid backbone. Ligation was performed with the CIP modified vector 1:3 insert (100 ng insert), and two control samples: vector 1:0 insert, and vector 1:0 insert with no ligase. Transformation in XL-10 gold cells was performed as per protocol. The ligation plate grew closely packed colonies; the two control plates showed minimal growth. 10 colonies were miniprepped as per protocol and 6 of the samples were sent for sequencing

using the Mix2Seq sequencing kit. The sequencing results, assessed using geneious Prime, showed that the HA tag had been successfully removed in 2 samples. A maxiprep (Chapter 2.2.1.12) was performed as per protocol, resulting in a modified HA tag-free plasmid with a final concentration of approximately 1μg/ml.

3.2. CHARACTERIZATION OF CYTOKINE RELEASE IN THP-1 CELLS

To establish the baseline response of THP-1 cells to established PAMPs and DAMPs, THP-1 cells were exposed to a variety of immunostimulants targeting specific PRPs, including CpG ODN, a TLR9 agonist.

3.2.1 PMA- DIFFERENTIATED THP-1 STIMULATION WITH LPS AND CPG ODN

THP-1 cells were differentiated using 500 ng/ml PMA (Chapter 2.2.2.7), adherence and viability were confirmed using light microscopy and trypan blue staining (Chapter 2.2.2.1) prior to stimulation. The cells were stimulated in triplicate wells with OptiMEM containing either LPS (100 ng/ml or 1000 ng/ml) or CpG ODN (3 μM or 30 μM). Supernatant was sampled from each well at 3, 6, 12, 24, and 52 hours post-stimulation and immediately placed on dry ice prior to storage at -80°C. The IFN I/II response in the sampled supernatant was assessed using HEK-Blue IFN I/II cells as per protocol (Chapter 2.2.3.5). It was noted that the THP-1 cells showed morphological signs of stress at all time points after 24 hours including cytoplasmic volume variation, and detachment of previously adherent cells.

Kruskal-Wallis Testing was conducted to examine the effect of THP-1 stimulation on IFN I/II production. No significant change in cytokine production was seen at 6 hours ($H(5)=10.4$, $p=0.065$) and 12 hours ($H(5)=8.23$, $p=0.083$) post-stimulation. At 3 hours ($H(5)=10.63$, $p=0.031$), 24 hours ($H(5)=10.17$, $p=0.038$), and 52 hours ($H(5)=12.9$, $p=0.012$) post-stimulation Kruskal-Wallis tests showed significant differences in IFN I/II between groups. Post-hoc pairwise comparisons using Dunn's test with control for joint ranks and Bonferroni adjustment for all values at 24, 48, and 52 hours post-stimulation showed no significance for all groups assessed (all ps>0.05).

3.2.1.1 Comparing Cytokine Concentrations in Frozen and Refrigerated Supernatant

To assess the effect of immediate refrigeration or flash freezing (immediate placement on dry ice prior to storage at -80°C) on cytokines in supernatant, PMA-differentiated (500 ng/ml) THP-1 cells (Chapter 2.2.2.7) were stimulated with CpG ODN in triplicate wells . Cells were stimulated with CpG ODN (either 1 μM, 3 μM, 5 μM, 7 μM, or 10 μM) in OptiMEM. Supernatant samples were collected at 3, 6, 9, 24, 48, and 54 hours post-stimulation. One sample per time point was immediately placed on dry ice and directly transferred to -80°C storage. Another sample was placed into a 4°C fridge for 8 hours before transfer to the -80°C freezer. The IFN I/II production was assessed using HEK-Blue IFN I/II cells as per protocol (Chapter 2.2.3.5). One-way ANOVA assessment showed a statistically significant differences in IFN I/II production between groups at 3 hours ($F(11,14) = 2.61$, $p = 0.047$) , 6 hours ($F(10,12) = 9.49$, $p < 0.01$), 9 hours ($F(11,14) = 9.22$, $p < 0.01$), 24 hours ($F(11,14) = 4.70$, $p = 0.01$), and 54 hours ($F(11,14) = 3.05$, $p = 0.027$) post-stimulation. There was no statistical significance seen between groups at 48 hours ($F(11,14) = 1.73$, $p > 0.1$) post-stimulation.

Post hoc Tukey's tests showed that the optical density (OD) readout from HEK-Blue IFN I/II cells in response to refrigerated THP-1 supernatant was significantly higher (all $p < 0.05$) than flash frozen supernatant at 6 hours (for 1, 3, and 5 μM CpG ODN) and 9 hours (for 3, 5, 7, and 10 μM CpG ODN) post-stimulation. At 3, 24, and 54 hours there was no significant difference between the IFN OD values of refrigerated and flash frozen

supernatant seen when comparing all groups (all *p*s >0.05). OD values at 9 hours post-stimulation are shown below (Fig. 6).

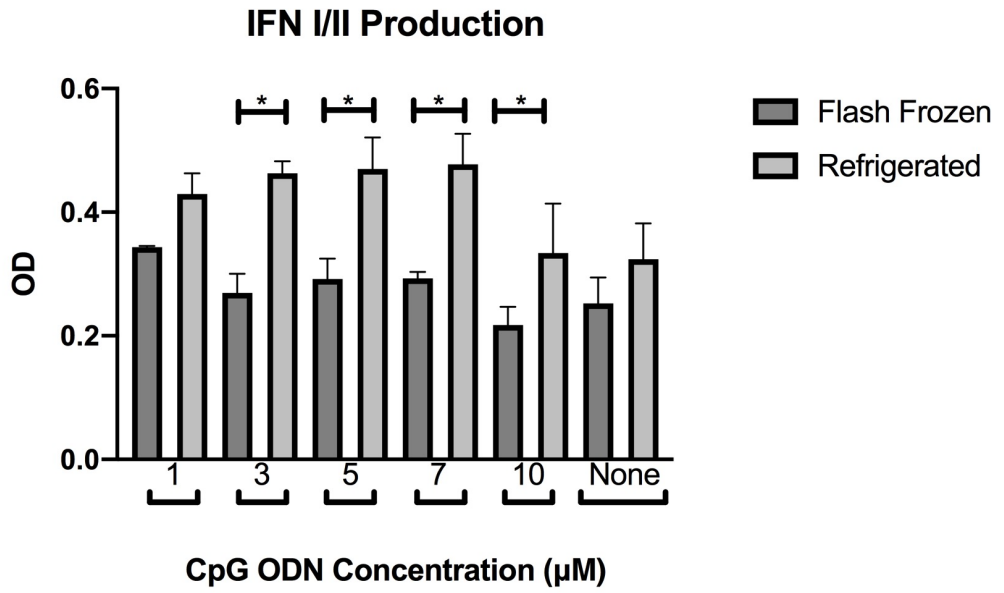

Figure 6: **Comparison of IFN in Flash Frozen and Refrigerated Supernatant Samples from CpG ODN-Stimulated THP-1 cells at 9h Post-stimulation.**
Supernatant from THP-1 cells stimulated with 3 μM, 5 μM, 7 μM, or 10 μM CpG ODN and refrigerated contained significantly higher (Tukey's Test, $p < 0.05$) n=3, levels of IFN I/II than supernatant from cells stimulated with 3 μM, 5 μM, 7 μM, or 10 μM CpG ODN and flash frozen at -80°C. Error bars indicate standard deviation.
OD: Optical Density

3.2.1.2 PMA-Differentiated THP-1 Stimulation with CpG ODN

PMA-differentiated (500ng/ml) THP-1 cells (Chapter 2.2.2.7) were stimulated in triplicate in OptiMEM containing either 3 μM or 5 μM CpG ODN, or exposed only to OptiMEM. Supernatant was collected at 3, 6, 24, and 48 hours post-transduction and refrigerated at 4°C for 8 hours prior to storage at -80°C. HEK-Blue cells were used to assess IFN I/II concentration in the THP-1 supernatant (Chapter 2.2.3.5).

One-way ANOVA assessment showed no significant output of IFN I/II in response to CpG ODN stimulation at 3 hours ($F(2,6) = 0.76$, $p = 0.51$), 6 hours ($F(2,6) = 0.56$, $p = 0.60$), 24 hours ($F(2,6) = 1.60$, $p = 0.28$), or 48 ($F(2,6) = 0.18$, $p = 0.84$) hours post-stimulation.

3.2.2 Inflammasome Activation and IL-1B Production in PMA-Differentiated THP-1 cells

THP-1 cells were differentiated with 500 ng/ml PMA (Chapter 2.2.2.7) and assessed for adherence and viability using trypan blue staining prior to stimulation. The cells were then incubated in OptiMEM in triplicate wells containing LPS (either 100 ng/ml, 10 ng/ml, or no LPS) for 3 hours. Then, the cells were incubated in OptiMEM containing ATP (either 1 mM, 5 mM, or no ATP) and supernatant was sampled at 30 min, 1 hour, and 3 hours post-stimulation. These samples were stored at 4°C for 8 hours prior to storage at -80°C. THP-1 cells were stimulated with various combinations of ATP and LPS: 100ng/ml LPS+no ATP, 100 ng/ml LPS+5 mM ATP, 100 ng/ml LPS+1 mM ATP, 10 ng/ml LPS+5 mM ATP, 10 ng/ml LPS+1 mM ATP. Negative controls containing neither LPS nor ATP were included. The Human IL-1β ELISA MAX Deluxe set was used to identify the presence and concentration of IL-1β in the supernatant samples as per manufacturer's protocol (2.2.3.1).

One-way ANOVA analysis showed no significant production of IL-1β at 30 minutes ($F(4,2)=8.6$, $p=0.11$), 1 hour ($F(5,2)=0.69$, $p=0.68$), or 3 hours ($F(5,2)=0.28$, $p=0.90$) post-stimulation.

3.3. Characterization of the Activation of Inflammatory Pathways and Cytokine Production in THP-1 Dual cells

To establish the baseline response of THP-1 cells to PAMPs and DAMPs, THP-1 Dual cells were exposed or transfected with well-known immunostimulants. The activation of the NF-κB and IRF pathways was assessed as a measurement of pro-inflammatory activation.

3.3.1 THP-1 Dual cell Stimulation with ds-DNA-EC and CpG ODN

THP-1 Dual cells were stimulated in triplicate wells with dsDNA (1 μg/ml) and Lipofectamine 3000, CpG ODN (3 μM), or a negative control containing endotoxin free water, to induce NF-κB and IRF activation in cells without PMA differentiation. Cells were incubated for 48 hours at 37°C and supernatant samples were removed at 16, 24, and 48 hours post-transduction. The samples were assessed for NF-κB and IRF (cGAS-

Sting) pathway activation using QUANTI-Blue (Chapter 2.2.3.3) and QUANTI-Luc (Chapter 2.2.3.4).

One-way ANOVA analysis of NF-κB activation showed a significant difference between groups at 16 hours ($F(2,6)=10.89$, $p=0.01$), 24 hours ($F(2,6)=22.67$, $p=0.001$), and 48 hours ($F(2,6)=96.11$, $p<0.0001$) post-stimulation. Post hoc Tukey's tests showed that the OD of the control group was significantly higher than that of the CpG ODN or dsDNA groups ($p<0.01$) at 16 hours post-stimulation. At 24 hours post-stimulation, Tukey's test showed that the OD values of the control group were significantly higher than those of the dsDNA group ($p=0.004$). At 48 hours post-stimulation post hoc Tukey's tests showed that the OD values of the CpG ODN group were significantly higher than those of the control group ($p<0.001$) and dsDNA groups ($p<0.001$). All other inter-group analyses were not statistically significant (all ps>0.05). NF-κB production in stimulated THP-1 Dual cells is shown below (Fig. 7).

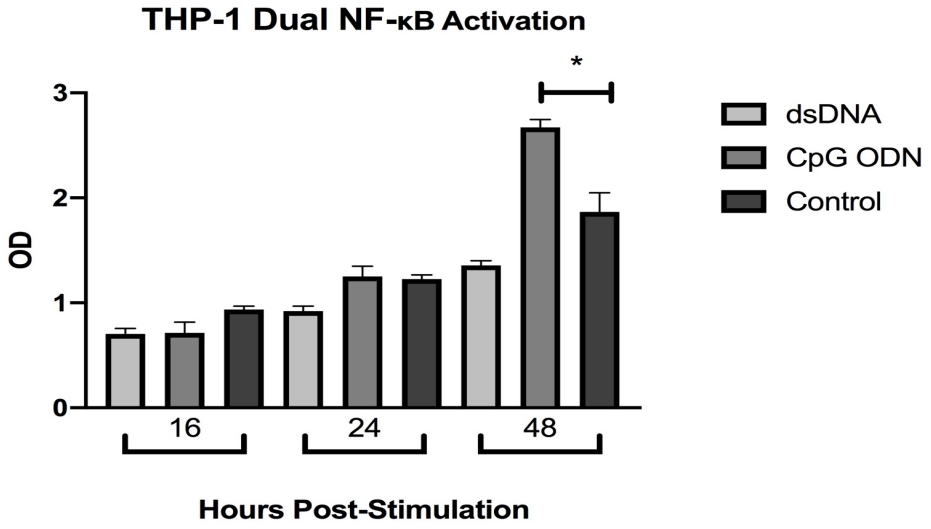

Figure 7**: NF-κB Pathway Activation in Response to ds-DNA-EC and CpG ODN stimulation in THP-1 Dual Cells.** At 48 hours post-transduction a significant upregulation (Tukey's Test, $p<0.01$) n=3, of the NF-κB pathway was seen in response to CpG ODN stimulation when compared to non-stimulated controls or cells exposed to dsDNA. Error bars indicate standard deviation.
OD: Optical Density

One-way ANOVA analysis of IRF pathway activation showed a significant difference between groups at 16 hours ($F(2,6)=36.79$, $p=0.0004$) and 24 hours ($F(2,6)=2691.22$, $p<0.0001$) post-stimulation. Group values at 48 hours post-stimulation were not statistically significantly different ($p>0.05$). Post hoc Tukey's tests showed that the OD of the dsDNA group was significantly higher than that of the CpG ODN ($p= 0.0007$) and control ($p=0.0008$) groups at 16 hours post-stimulation. At 24 hours post-stimulation, post hoc Tukey's tests showed that the OD of the dsDNA group was significantly higher than that of the CpG ODN ($p<0.0001$) and control ($p<0.0001$) groups. Results of the analysis are shown below (Fig. 8)

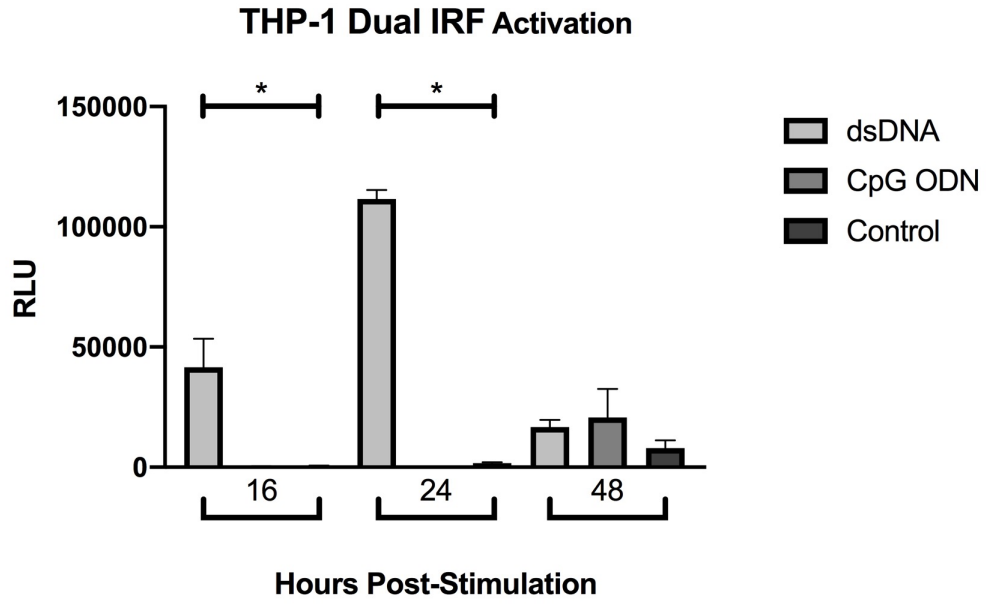

Figure 8: **IRF Pathway Activation in Response to ds-DNA-EC stimulation in THP-1 Dual Cells.** At 16 and 24 hours post-transduction there was a significant upregulation (Tukey's Test $p < 0.001$) n=3, of the IRF pathway in response to ds-DNA-EC when compared to cells stimulated with CpG ODN or non-stimulated controls. Error bars indicate standard deviation.
RLU: Relative light units

3.3.2 Inflammasome Activation and IL-1β Production in PMA-Differentiated THP-1 Dual cells

THP-1 Dual cells were differentiated using 500 ng/ml PMA (Chapter 2.2.2.7) and stimulated with LPS and ATP in triplicate wells to induce inflammasome activation and the production of IL-1β. Non-differentiated THP-1 Dual cells were also stimulated with

LPS and ATP to assess the effects of PMA differentiation on IL-1β production. After PMA differentiation, cells were initially stimulated with OptiMEM containing LPS (either 100 ng/ml, 10 ng/ml, or no LPS) and incubated at 37°C for three hours. After incubation, the medium was removed and replaced with OptiMEM containing ATP (either 1 mM, 5 mM, or no ATP). Supernatant samples were removed at 30 min, 1 hour, and 3 hours post-stimulation and immediately stored at -80°C prior to cytokine assessment. IL-1β concentration in the supernatant samples was assessed (Fig. 9) using the Human IL-1β ELISA MAX Deluxe set as per manufacturer's protocol (Chapter 2.2.3.1).

One-way ANOVA analysis of IL-1β production showed a significant difference between groups at 30 minutes ($F(5,9)=35.98$, $p<0.0001$) and 3 hours ($F(5,8)=9.22$, $p=0.0036$) post-stimulation. Kruskal-Wallis testing showed significant differences in IL-1β production between groups at 1 hour post-stimulation ($H(5)=13.3$, $p=0.021$)

Post hoc Tukey's tests for values at 30 minutes and 3 hours post-stimulation showed that samples stimulation with 5 mM ATP and either 100 or 10 ng/ml LPS contained significantly more IL-1β than samples stimulated only with or without PMA ($p<0.05$). Additionally, at 30 minutes post-stimulation samples containing 100 ng/ml LPS and 5 mM ATP contained significantly more IL-1β than samples stimulated with 100 ng/ml LPS and 1 mM ATP ($p<0.05$). At 3 hours post-stimulation, samples containing 100 ng/ml LPS and 5 mM ATP contained significantly more IL-1β than samples stimulated with 100 ng/ml LPS and 1 mM ATP ($p=0.035$). All other comparisons were not statistically significant ($p>0.05$).

Post hoc pairwise comparisons using Dunn's test with control for joint ranks and Bonferroni adjustment for all values at 1 hour post-stimulation showed significant production of IL-1β in samples stimulated with 100 ng/ml LPS and 5 mM ATP when compared to samples without PMA and with no stimulation ($p=0.032$). All other comparisons showed no statistical significance (all ps>0.05).

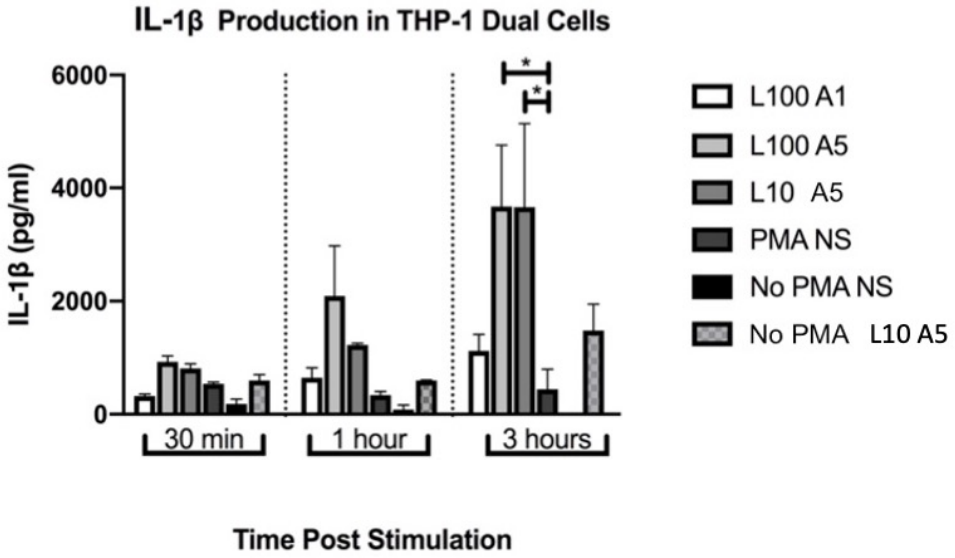

Figure 9: **IL-1β Production in THP-1 Dual cells Stimulated with LPS and ATP.** Cells were stimulated with LPS (L) and ATP (A) or not stimulated (NS) with either 500 ng/ml PMA-differentiation (L 100 A1, L 100 A5, L 10 A5, PMA NS), or no differentiation (No PMA). Supernatant was sampled at 30 minutes, 1 hour, and 3 hours post-stimulation. Significant production (Tukey's Test $p < 0.05$) n=3, of IL-1β in PMA differentiated cells in response to 100 ng/ml or 10 ng/ml LPS and 5 mM ATP, when compared to cells exposed only to only PMA, was seen at 3 hours post-stimulation. Error bars indicate standard deviation.

3.4. TRANSFECTING THP-1 CELLS

To assess the innate immune responses to Cas9 in THP-1 cells, THP-1 cells were to be transfected with plasmids containing Cas9. To facilitate this, a transfection protocol was to be established. Summaries of various transfection reagents and protocol modifications trialed can be seen in Fig. 38, Fig 39, and Fig. 40.

3.4.1 LIPOSOMAL TRANSFECTION REAGENTS

3.4.1.1 Lipofectamine 3000

3.4.1.1.1 THP-1 Dual Transfection

THP-1 Dual cells were seeded in a 12-well plate and differentiated with 100 ng/ml PMA as per protocol (Chapter 2.2.2.7). On day three, the cells were transfected with the mKate plasmid using Lipofectamine 3000. 1.5 or 3 µl Lipofectamine 3000 were combined with 1 µl mKate plasmid DNA per well. Control wells were included which

were neither transfected nor exposed to DNA. Transfection was performed following the manufacturer's recommended protocol (2.2.4.4). The transfected cells were evaluated using fluorescence microscopy at 24, 48, and 72 hours post-transfection. No mKate signal was visualized.

3.4.1.1.2 Adjusting Lipofectamine and DNA ratios

THP-1 Dual cells were differentiated with 100 ng/ml PMA in 24-well plate (Chapter 2.2.2.7). On day three, multiple combinations of plasmid DNA concentration and transfection reagent volume were tested to identify the optimal conditions for transfection (see **Appendix B**). The transfection efficacy was assessed using fluorescence microscopy at 24 and 48 hours post-transfection. No mKate signal was identified in any sample at any time point.

3.4.1.1.3 HEK-Blue Transfection Control

Due to the challenging transfection in THP-1 cells, HEK-Blue IFN I/II cells were transfected with the mKate plasmid using Lipofectamine 3000. Successful transfection could indicate that the transfection challenges in THP-1 cells were mainly due to the transfected cell line. The transfection protocol was modified for HEK cells: cells were seeded in DMEM in a 24-well plate one day prior to transfection with 0.5 µg mKate plasmid DNA and 1.5 µl Lipofectamine 3000. The results were analyzed using fluorescence microscopy at 24 hours post-transfection (Fig. 10).

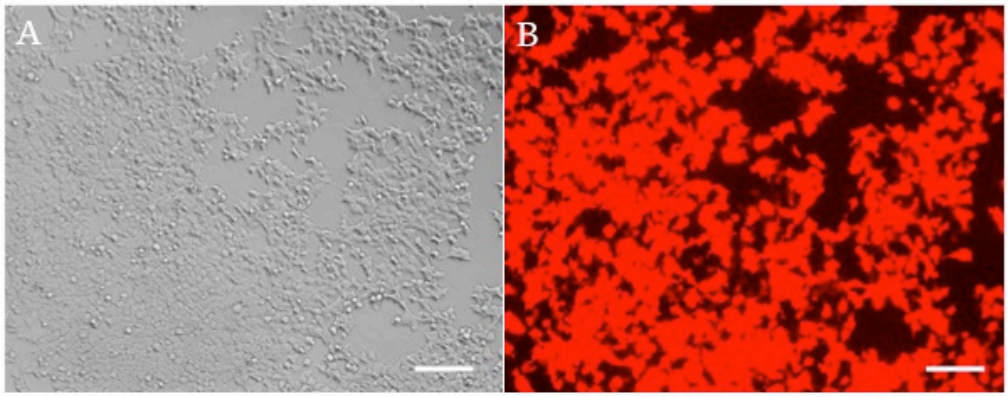

Figure 10: **HEK-Blue IFN I/II Cells Transfected with 0.5 µg mKate Plasmid DNA and 1.5 µl Lipofectamine 3000 at 24 Hours Post-Transfection**. HEK cells are viewed under brightfield (A) and fluorescence microscopy (B). >80% of cells expressed an mKate signal. Scale bars: 100 µm.

3.4.1.2 Lipofectamine LTX

3.4.1.2.1 THP-1 Dual Transfection

THP-1 Dual cells were seeded in a 24-well plate and differentiated using 100 ng/ml PMA as per protocol (Chapter 2.2.2.7). On day 3, the cells were transfected with the mKate plasmid using Lipofectamine LTX per manufacturer's protocol (Chapter 2.2.4.5). The transfected wells contained 0.5 µg mKate plasmid and varying amounts of Lipofectamine LTX (1 µl, 1.5 µl, 2 µl, 2.25 µl, or 2.5 µl). Control wells were included which were not transfected or exposed to DNA. The transfection efficacy was assessed at 24 hours post-transfection using fluorescence microscopy (Fig. 11). Single cells expressed an mKate signal.

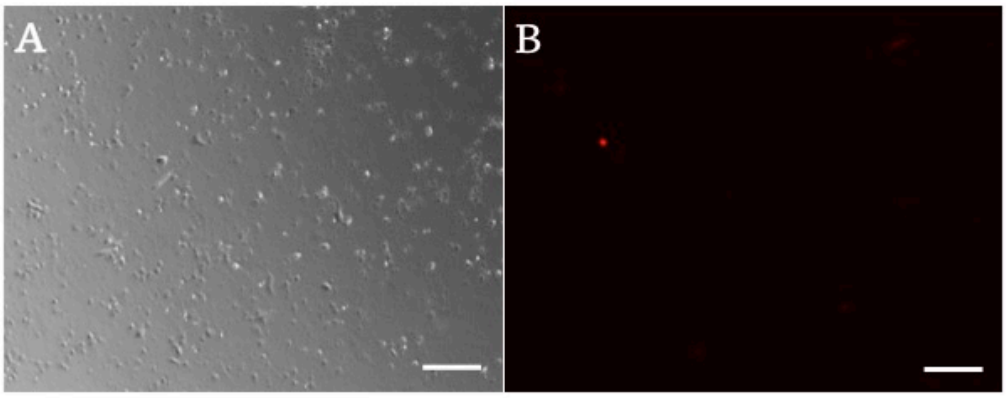

Figure 11: **THP-1 Dual Cells Transfected with mKate Plasmid using Lipofectamine LTX.** 1.5 µl Lipofectamine LTX and 0.5 µg mKate were used per well. Images were captured at 24 hours post-transfection. THP-1 Dual cells are viewed under brightfield (A) and fluorescence microscopy (B). Single cells (< 1%) expressed an mKate signal. Scale bars: 100 µm

3.4.1.2.2 HEK-Blue Transfection Control

To evaluate the effectiveness of the transfection protocol, HEK-Blue IFN I/II cells were seeded in a 24-well plate in DMEM and transfected with 0.5 µg mKate plasmid and 1.5 µl Lipofectamine LTX. The protocol from Chapter 3.4.1.2.1 was followed. The results of this transfection were analyzed at 24 hours post-transfection using fluorescence microscopy. >80% of transfected HEK cells expressed an mKate signal.

3.4.1.2.3 Increased THP-1 Dual Cell Seeding Density

THP-1 Dual cells were seeded at a higher density (5×10^5 cells/well) in OptiMEM and differentiated with 100 ng/ml PMA (Chapter 2.2.2.7) in a 24-well plate, to improve cell viability and induce a higher rate of transfection. On day 3, the cells were transfected with 0.5 µg mKate plasmid and 1 µl, 1.5 µl, or 2 µl Lipofectamine LTX. The results of this optimization were assessed after 24 hours of incubation at 37° using fluorescence microscopy to assess mKate expression. The rate of transfection was <1%.

3.4.1.2.4 Addition of a Rest Day

Modifications designed to further improve cell viability and transfection efficacy were endeavored: the rest day in RPMI medium after PMA exposure and before transfection was increased to two days. THP-1 Dual cells were seeded at 5×10^5 cells/well in OptiMEM with 100 ng/ml PMA (Chapter 2.2.2.7) in a 24-well plate, and on day 4 the cells were transfected with 0.5 µg mKate plasmid and 1 µl, 1.5 µl, or 2 µl Lipofectamine LTX. Cells were assessed via fluorescence microscopy at 24 hours post-transfection for mKate expression. <1% of THP-1 Dual cells expressed an mKate signal.

3.4.1.2.5 Addition of Washing Steps

The protocol from Chapter 3.4.1.2.4 was modified further: in addition to the higher seeding density and the added rest day, washing was introduced to further optimize the transfection protocol. The cells were incubated in the Lipofectamine LTX-mKate plasmid DNA transfection medium for 4 hours before being gently washed with PBS. The cells

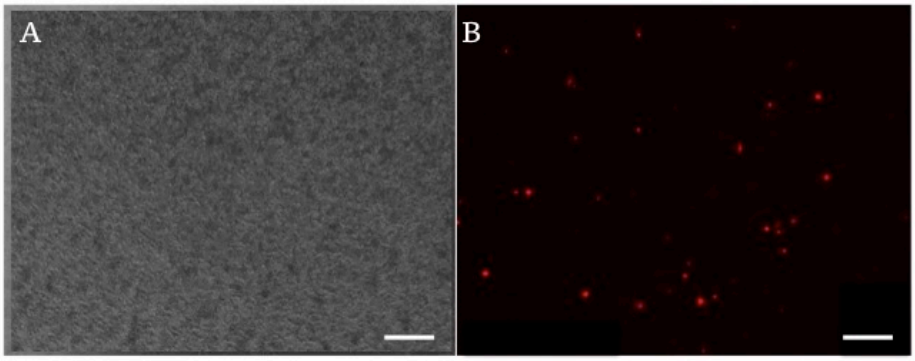

Figure 12**: THP-1 Dual Cells Transfected with the mKate Plasmid using Lipofectamine LTX with Washing Post-Transfection.** 1.5 µl Lipofectamine LTX and 0.5 µg mKate were used. Images were captured at 24 hours post-transfection. THP-1 Dual cells are viewed under brightfield (A) and fluorescence microscopy (B). Approximately 1% of cells expressed an mKate signal. Scale bars: 100 µm.

were then incubated in plain RMPI medium for 24 hours at 37°C before assessment for mKate expression using fluorescence microscopy (Fig. 12).

3.4.1.2.5.1 Optimizing Washing Steps

The transfection protocol from Chapter 3.4.1.2.5 was repeated with modified transfection reagent concentrations and washing times. THP-1 Dual cells were transfected with 2 µg mKate plasmid DNA and 3 µl Lipofectamine LTX. The transfection medium was removed and cells were washed with PBS at 3, 4, or 5 hours post-transfection before incubation in plain RPMI. The cells were assessed for mKate expression using fluorescence microscopy at 24 hours post-transfection (Fig. 13).

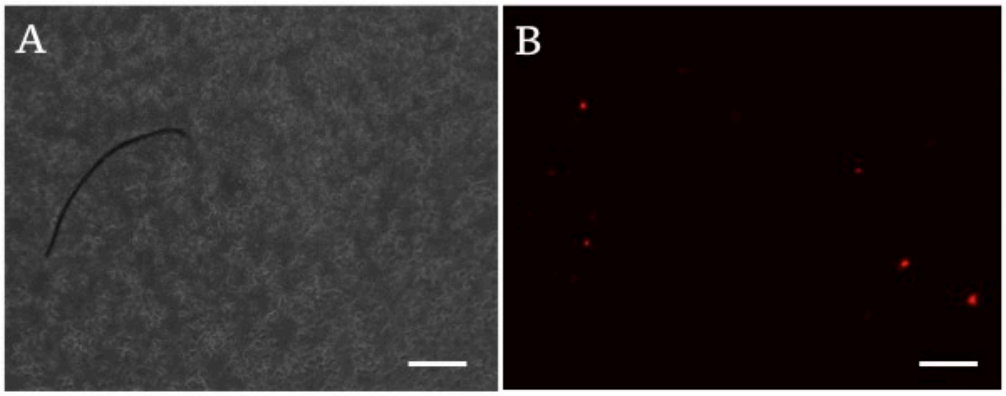

Figure 13: **THP-1 Dual Cells Transfected with the mKate Plasmid using Lipofectamine LTX with Optimized Washing Steps.** 3 µl Lipofectamine LTX and 2 µg mKate were used. Cells were washed at 4 hours post-transfection and images were captured at 24 hours post-transfection. THP-1 Dual cells are viewed under brightfield (A) and fluorescence microscopy (B). The rate of transfection was <1%. Scale bars: 100 µm.

3.4.1.2.6 Optimizing Transfection Component Concentrations

THP-1 Dual cells were seeded at 5×10^5 cells/well in OptiMEM with 100 ng/ml PMA (Chapter 2.2.2.7) in a 24-well plate. Transfection was repeated with modified mKate plasmid DNA and LTX concentrations; 1 µg DNA was paired with 1.5 µl Lipofectamine LTX and the cells were washed at either 3 or 4 hours post-transfection. Plasmid expression was assessed at 24 hours post-transfection using fluorescence microscopy. The rate of mKate plasmid transfection was < 1%.

3.4.1.2.7 Optimizing PMA Concentration

THP-1 Dual cells were seeded at 5×10^5 cells/well in a 24-well plate in OptiMEM with PMA differentiation (Chapter 2.2.2.7) in 10 ng/ml PMA, in an attempt to more gently differentiate the cells and thereby improve the transfection conditions. Cells were transfected with 1 µg DNA and 1.5 µl Lipofectamine LTX. Plasmid expression was assessed at 24 hours post-transfection using fluorescence microscopy. The rate of transfection with the mKate plasmid was < 1%.

3.4.1.2.8 Comparison of THP-1 and THP-1 Dual Transfection Efficacy

To compare the relative transfection efficacy seen in THP-1 and THP-1 Dual cells, both were transfected using an identical protocol. The cells were differentiated with 10 ng/ml PMA using the established differentiation protocol (Chapter 2.2.2.7). Cells were transfected with 1 µg mKate plasmid DNA and 1.5 or 2 µl of Lipofectamine LTX per the established transfection protocol (Chapter 3.4.1.2.5) on day 3, prior to incubation at 37°C for 24 hours. Plasmid expression was assessed using fluorescence microscopy at 24 hours post-transfection. The transfection rate seen in THP-1 and THP-1 Dual cells was equal, both cell lines were <1% transfected in all transfection samples.

3.4.1.2.9 Transfection of Monocyte-like THP-1 and THP-1 Dual Cells

To assess the efficacy of transfecting THP-1 cells in suspension, THP-1 and THP-1 Dual cells were transfected with the mKate plasmid using Lipofectamine LTX. THP-1 cells were seeded in a 24-well plate in OptiMEM containing 1.5 µl Lipofectamine LTX and 0.5 µg mKate plasmid on the day of transfection. Plasmid expression was assessed 24 hours post-transfection using fluorescence microscopy. The rate of transfection was <1% in both the THP-1 and THP-1 Dual cells when transfected in a non-differentiated state

3.4.1.3 Transfection of THP-1 Dual cells using TransIT-2020

THP-1 Dual cells were differentiated in 100 ng/ml PMA (Chapter 2.2.2.7) with two rest days in RPMI in a 24-well plate. On day four, the medium was removed, and the cells were transfected with 0.5, 1, 1.5, or 2 µl TransIT-2020 and 0.5 or 1 µg mKate plasmid as per protocol (Chapter 2.2.4.6). Plasmid expression was evaluated at 24 hours post-transfection using fluorescence microscopy. Single cells (< 1%) expressed the mKate signal.

3.4.2 ELECTROPORATION USING THE NEON ELECTROPORATION KIT

To establish a method for transfecting THP-1 cells, electroporation was utilized, as it has been described as being effective in transfecting this challenging-to-transfect cell line [160].

3.4.2.1 Establishment of an Electroporation Protocol

Initially, THP-1 Dual cells were differentiated with 10 ng/ml PMA as per differentiation protocol (Chapter 2.2.2.7). Then, cells were prepared for electroporation: cells were detached from the flask using accutase and centrifuged at 300G for 5 minutes. The cell pellet was washed once with PBS. The cells were then, again, centrifuged before being resuspended in Resuspension buffer R at 1×10^7 cells/ml. 24-well plates were prepared and filled with 0.5 ml pre-warmed RPMI per well. The NEON electroporation kit was prepared and utilized per manufacturer's protocol (2.2.4.2). Various electroporation settings were tested to identify the most efficient settings and minimize cell death (see **Appendix C**). 2.77 µg mKate plasmid DNA and 3.5×10^5 cells were electroporated per well. Two control wells were included which were exposed to 2.77 µg DNA but not electroporated. After 24 hours of incubation at 37°C, the cells were evaluated for mKate signal expression using fluorescence microscopy and trypan blue staining: non-electroporated control cells had re-adhered to the wells and showed >80% cell viability. All electroporated samples showed 0% mKate expression and had cell viabilities of <10%.

3.4.2.2 Optimized Electroporation Settings

To increase cell viability post-electroporation and improve transfection efficiency, THP-1 Dual cells were electroporated using the protocol described in Chapter 3.4.2.1 with alternate electroporation settings (see **Appendix C**). The cells were assessed for mKate plasmid expression at 24 hours post-electroporation using fluorescence microscopy. Single cells (<1%) were transfected per well.

3.4.2.2.1 Repeated Electroporation Setting Optimization

Electroporation was repeated using the same protocol (Chapter 3.4.2.1), and modified electroporation settings (see **Appendix C**). Settings with voltages under 900V led to increased cell viabilities (>60%) post-electroporation, when compared to wells electroporated using settings with voltages higher than 900V (<50% viable). The transfection efficacy measured at 24 hours post-electroporation with fluorescence microscopy was negligible, with only single cells transfected in any well (Fig. 14).

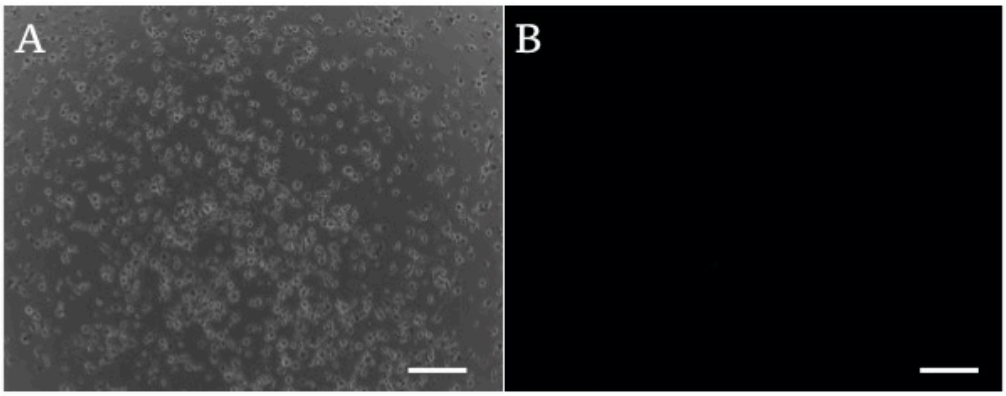

Figure 14: **THP-1 Dual Cells Electroporated with mKate Plasmid.** 3.5×10^5 cells were electroporated with 2.77 µg mKate plasmid at 500V for 10 ms with 1 pulse. Cells were assessed for mKate signal at 24 hours post-electroporation. THP-1 Dual cells are viewed under brightfield (A) and fluorescence microscopy (B). 0% of cells expressed an mKate signal. Scale bars: 100 µm.

3.4.2.3 Optimization of the Transfection Medi

To further improve cell viability and transfection efficacy, the electroporation protocol (Chapter 3.4.2.1) was modified. THP-1 Dual cells were seeded in 20 ml optimized medium in a T175 flask containing: 1% PSG, 1% sodium pyruvate, 1% nonessential amino acids, 100 ng/ml PMA, and 50 µM 2-mercaptoethanol in RPMI. The cells were incubated at 37°C for 48 hours in this optimized medium. The cells were then lysed by applying 6 ml of accutase and incubating at 37°C for 30 minutes. PBS solution was used to rinse the cells off the flask, before the cells were pelleted through centrifugation at 500G for 5 minutes. The cells were counted and resuspended in Resuspension buffer R at 5×10^4 or 1×10^5 cells/ml. The cells were then electroporated as per manufacturer's protocol (Chapter 2.2.4.2) using several varying electroporation settings (see **Appendix C**). Each electroporation setting was applied to samples containing 5×10^4 or 1×10^5 cells and either 0.5 or 3 µg mKate plasmid. The electroporated

cells were placed in a 24-well plate containing 1.5 ml pre-warmed recovery medium: RPMI containing 20% FBS, 1% sodium pyruvate, 1% nonessential amino acids, 1% L-glutamine, 1% pen/strep, and 50 µM 2-mercaptoethanol. Four hours post-electroporation, this medium was aspirated and replaced with fresh recovery medium containing 100 ng/ml PMA.

Cells were assessed using fluorescence microscopy at 24 hours post-electroporation. Cell viability was assessed using trypan blue: all wells showed cell viability of >70%. The highest transfection rate (1%) was recorded at 1250V, 30ms, 1 pulse at all cell and DNA concentrations. All other electroporation samples had only single transfected cells per well (< 1%).

3.4.3 CHEMICAL TRANSFECTION REAGENTS

3.4.3.1 THP-1 Dual Transfection with GeneJuice

THP-1 Dual cells were seeded in a 12-well plate and differentiated with PMA as per protocol (Chapter 2.2.2.7). On day three, the cells were transfected with the mKate plasmid using GeneJuice. 3 or 6 µl GeneJuice were combined with 2 µg DNA per well. Transfections were performed following the manufacturer's recommended protocol (Chapter 2.2.4.3). The transfected cells were evaluated using fluorescence microscopy at 24, 48, and 72 hours post-transfection. There was 0% mKate expression visible at any time point.

3.4.3.1.1 Optimization of the GeneJuice Protocol

The protocol above (Chapter 3.4.3.1) was repeated in a 24-well plate, with transfection reagent and plasmid concentrations scaled down accordingly (Chapter 2.2.2.13). Multiple combinations of plasmid concentration and transfection reagent volume were tested to identify the optimal transfection conditions (see **Appendix D**). The transfection efficacy was assessed using fluorescence microscopy at 24 and 48 hours post-transfection. 0% mKate signal was identified in any sample at any time point.

3.4.3.2 Transfection of THP-1 Dual cells with TransIT-X2

THP-1 Dual cells were differentiated using 100 ng/ml PMA (Chapter 2.2.2.7) and transfected with TransIT-X2 as per protocol (Chapter 2.2.4.7). Cells were transfected with 0.5 µg mKate plasmid and 1, 1.5, 2, 2.5, or 3 µl TransIT-X2 in a 24-well plate.

Plasmid expression was analyzed at 24 hours post-transfection using fluorescence microscopy. The rate of mKate expression was < 1%.

3.4.3.2.1 Optimization of PMA Concentration in THP-1 and THP-1 Dual cell Transfection

The experiment above (Chapter 3.4.3.2) was repeated using both THP-1 and THP-1 Dual cells, with differentiation in 10 ng/ml PMA (Chapter 2.2.2.7). Fluorescence microscopy at 24 hours post-transfection identified a rate of transfection of < 1% in all samples.

3.4.3.2.2 Transfection of Monocyte-like THP-1 cells

To compare the transfection efficacy of differentiated and non-differentiated cells, THP-1 cells were transfected in suspension. Undifferentiated cells were transfected with 0.5 µg mKate plasmid and 1.5 µl TransIT-X2 in OptiMEM. The transfection rate measured using fluorescence microscopy was < 1%.

3.4.3.2.2.1 Differentiation of Transfected Monocyte-like THP-1 cells

In an attempt to create transfected macrophage-like cells, monocyte-like cells were transfected and then differentiated using 100 ng/ml PMA (Chapter 2.2.2.7). Undifferentiated cells were transfected with 0.5 µg mKate plasmid and 1.5 µl TransIT-X2 in OptiMEM. They were then incubated in 100 ng/ml PMA at 24 hours post-transfection. Over 80% cell mortality was observed using trypan blue staining, with 0% transfected cells after 24 hours of PMA incubation visible when assessed using fluorescence microscopy.

3.4.3.2.3 Transfection of Monocyte-like THP-1 and THP-1 Dual cells with the BFP SpCas9 Plasmid

THP-1 Dual and THP-1 cells were seeded at 3.5×10^5 cells/well in a 24-well plate in 1 ml optimized RPMI medium containing: 20% FBS, 1% nonessential amino acids, 1% sodium pyruvate, 50 µM 2-mercaptoethanol, and 1% L-glutamine. This initial medium also contained TransIT-X2 and plasmid DNA. The cells were transfected with 0.5 µg plasmid DNA, either mKate or BFP SpCas9, and either 1 or 2 µl TransIT-X2. They were incubated at 37°C for 24 hours. Plasmid expression was assessed using fluorescence microscopy at 24 hours post-transfection. Cells transfected with the BFP SpCas9 plasmid

showed a 0% transfection rate and cells transfected with the mKate plasmid a < 1% transfection rate.

3.4.3.2.4 Transfection of Monocyte-like THP-1 Dual cells with mCherryCas9 Plasmid

To transfect THP-1 cells with an alternate large plasmid, THP-1 Dual cells were transfected with the mCherryCas9 plasmid. The mKate plasmid contained 6000 bp, while the mCherryCas9 plasmid had 7400 bp. THP-1 Dual cells were seeded in suspension and transfected as per established protocol (Chapter 3.4.3.2.3), in optimized RPMI medium containing: 20% FBS, 1% nonessential amino acids, 1% sodium pyruvate, 50 µM 2-mercaptoethanol, and 1% L-glutamine. Combinations of different DNA and TransIT-X2 concentrations were tested to determine the best transfection conditions. 0.5, 1, 1.5, 2, 2.5, or 3 µg DNA were combined with either 1, 1.5, 2, or 2.5 µl TransIT-X2. Cells were assessed using fluorescence microscopy to detect plasmid expression at 24 hours post-transfection. Cells transfected with 2.5 µg mCherryCas9 DNA and 2.5 µl TransIT-X2 showed a <1% rate of transfection, all other samples were transfected at a rate of 0%.

3.4.4 NUCLEOFECTION

3.4.4.1 Nucleofection of THP-1 Dual cells using the Lonza Nucleofector

Due to published accounts of effective nucleofection of THP-1 cells, an attempt was made to emulate these successes. The only modification of the published protocol (Chapter 2.2.4.1) was the substitution of IMDM medium for Human Monocyte Nucleofector Medium. 2×10^6 THP-1 Dual cells were nucleofected with 5 or 10 µg mKate plasmid or 10 µg BFP SpCas9 plasmid. These high concentrations of DNA were added inadvertently, the intended concentrations were 0.5 or 1 µg DNA. After 24 hours of incubation at 37°C, cell viability and plasmid expression was assessed using fluorescence microscopy. The cell viability was >50% in all samples upon trypan blue staining assessment. Of the cells transfected with the mKate plasmid, single cells (< 1%) expressed an mKate signal. 0% of cells transfected with the BFP SpCas9 plasmid expressed a BFP signal.

3.4.4.1.1 Nucleofection Optimization

The protocol described above (Chapter 3.4.4.1) was repeated, and 2×10^6 THP-1 Dual cells were nucleofected with mKate, mCherryCas9, or Lonza GFP control plasmid DNA.

Cells were nucleofected with 0.5 µg or 1 µg per plasmid. THP-1 cells transfected with the Lonza GFP control plasmid expressed a GFP signal at a rate of 65% (Fig. 15). The rate of transfection, with plasmid expression measured at 24 hours post-nucleofection using fluorescence microscopy, was <1% in cells nucleofected with the mKate or mCherryCas9 plasmids

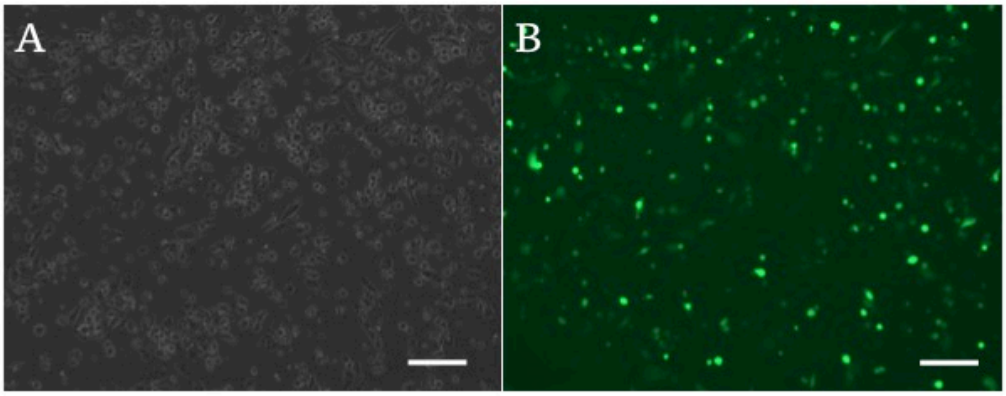

Figure 15: **2×10^6 THP-1 Dual Cells Nucleofected with 0.5 µg Lonza GFP Control Plasmid DNA.** Cells were assessed for GFP expression at 24 hours post-nucleofection via fluorescence microscopy. 65% of cells expressed a GFP signal. THP-1 Dual cells are viewed under brightfield (A) and fluorescence microscopy (B). Scale bars: 100 µm.

3.4.4.2 Electroporation of THP-1 Dual cells using GFP Positive Control Plasmid

To identify whether plasmid size was the limiting factor in improving transfection efficiency in THP-1 cells, THP-1 Dual cells were electroporated with the Lonza GFP positive control plasmid, which had shown a high transfection rate in the previous nucleofection experiment. The electroporation protocol was performed as previously established (Chapter 3.4.2.3), and the optimized electroporation medium was utilized. 5×10^4 or 1×10^5 cells were electroporated with 0.5 or 1 µg DNA at two differing settings. Non-electroporated cells were included as controls (see **Appendix E**). Cells electroporated with 0.5 µg DNA at a concentration of 1×10^5 cells at 1400V for 20ms and 2 pulses were transfected at a rate of 1-2% when assessed for plasmid expression using fluorescence microscopy at 24 hours post-electroporation.

3.4.4.3 Comparison of Lonza GFP and GFP SpCas9 Plasmid Electroporation

To confirm that plasmid size and not the fluorescent tag was responsible for the successful electroporation with the Lonza GFP plasmid, THP-1 Dual cells were electroporated with

the Lonza GFP and GFP SpCas9 plasmids. The established electroporation protocol was followed (Chapter 3.4.2.3). THP-1 Dual cells were electroporated at a concentration of 1×10^6 or 2×10^6 cells/electroporation tip and 0.5 µg DNA at 1400V for 20ms with two pulses. Cells were assessed for GFP expression at 24 hours post-electroporation using fluorescence microscopy (Fig. 16)

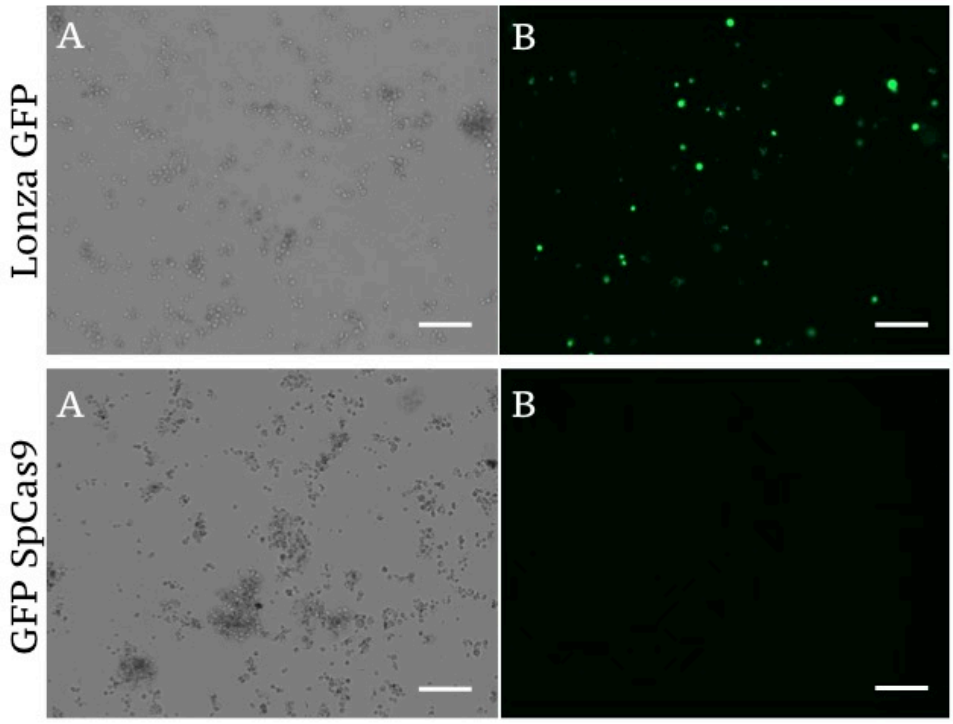

Figure 16: **THP-1 Dual Cells Electroporated with Lonza GFP or GFP SpCas9 Plasmids.** Cells were electroporated at 1400V for 20ms with 2 pulses at a concentration of 2×10^6 cells/tip with 0.5 µg Lonza GFP or GFP SpCas9 plasmid DNA. Fluorescence microscopy for plasmid expression was performed at 24 hours post-electroporation. The Lonza GFP plasmid was expressed at a rate of 3%, the GFP SpCas9 plasmid at a rate of 0%. THP-1 Dual cells are viewed under brightfield (A) and fluorescence microscopy (B). Scale bars: 100 µm.

3.4.5 Lentiviral Transduction of THP-1 Dual Cells

THP-1 Dual cells were transduced with a GFP-tagged lentivirus to test the efficacy of lentiviral transduction in THP-1 cells. THP-1 Dual cells were seeded at a concentration of 5×10^4 cells/well in a 96-well plate in RPMI with 100 ng/ml PMA three days prior to transduction. The medium was replaced with plain RPMI one day before transduction. Helen Pan kindly transduced two wells each using 50 or 100 µl pLenti-GFP lentivirus. Three control wells were not transduced. The cells were examined for GFP signal using

fluorescence microscopy at 24, 48, and 72 hours post-transduction. 0% of cells expressed a GFP signal at any time point.

3.5. TRANSFECTION OF THP-1 CELLS WITH CAS9 PROTEINS

Due to the large size of Cas9-containing plasmids and the limitation plasmid size placed on transfection in THP-1 cells, it was attempted to establish a protocol for transfection with Cas9 in protein form.

3.5.1 CAS9 PROTEIN TRANSFECTION WITH LIPOFECTAMINE 3000

Lipofectamine 3000 was used to transfect THP-1 cells with Cas9 proteins due to previous relative transfection successes involving its use in THP-1 cells. Liposome complexes were formed with the Cas9 protein by combining Lipofectamine 3000 and OptiMEM with the Cas9 protein. 2 µl Lipofectamine and 1 µl plus reagent were added to 6 µl Cas9 protein (120nM) per well of a 24-well plate. The mixture was incubated at room temperature for 20 minutes. THP-1 cells were seeded in 100 ng/ml PMA on untreated glass coverslips in 24-well plates to be 70-80% confluent on the day of transfection. Prior to transfection, the medium was aspirated from the THP-1 cells and the liposome-Cas9 protein complexes were added to the cells drop-wise. OptiMEM was added to bring the total medium concentration per well to 1 ml. The cells were incubated at 37°C with 5% CO_2 for 24, 48, and 72 hours until fixation for ICC staining with the SpCas9 primary antibody and Alexa Fluor 488 secondary antibody as per protocol (Chapter 2.2.5.1). When assessed using fluorescence microscopy, stained cells expressed an intracellular DAPI signal, <1% of cells expressed an Alexa Fluor 488 signal.

3.5.1.1 HEK Positive Controls

Due to the low transfection rate seen in THP-1 cells transfected with Cas9 protein using Lipofectamine 3000, Cas9 protein transfection using Lipofectamine 3000 was repeated with HEK-Blue IFN I/II and THP-1 cells, using the same protocol as above (Chapter 3.5.1). HEK-Blue cells were utilized as a positive control for transfection due to the relative ease with which they had previously been transfected. The concentrations of Cas9 protein and Lipofectamine 3000 were modified: 2.5 or 5 µl of Cas9 protein were combined with 2 or 4 µl Lipofectamine 3000. HEK cells were additionally transfected with the miRFP SpCas9 plasmid and Lipofectamine 3000 as per the Lipofectamine 3000 protocol (Chapter 2.2.4.4) to control for staining. Cells were fixed for staining at 10, 24,

and 48 hours post-transfection. Cells stained at 24 hours post-transfection as per ICC protocol (Chapter 2.2.5.1) are shown below (Fig. 17). At all time points there was no Alexa Fluor signal visible in HEK or THP-1 cells transfected with Cas9 protein when assessed using fluorescence microscopy. HEK-Blue cells transfected with the miRFP SpCas9 plasmid showed a 30% rate of miRFP expression at 24 hours post-transfection when assessed with fluorescence microscopy. After staining, HEK-Blue cells transfected with the miRFP SpCas9 plasmid showed a 1-2% rate of Alexa Fluor 488 staining

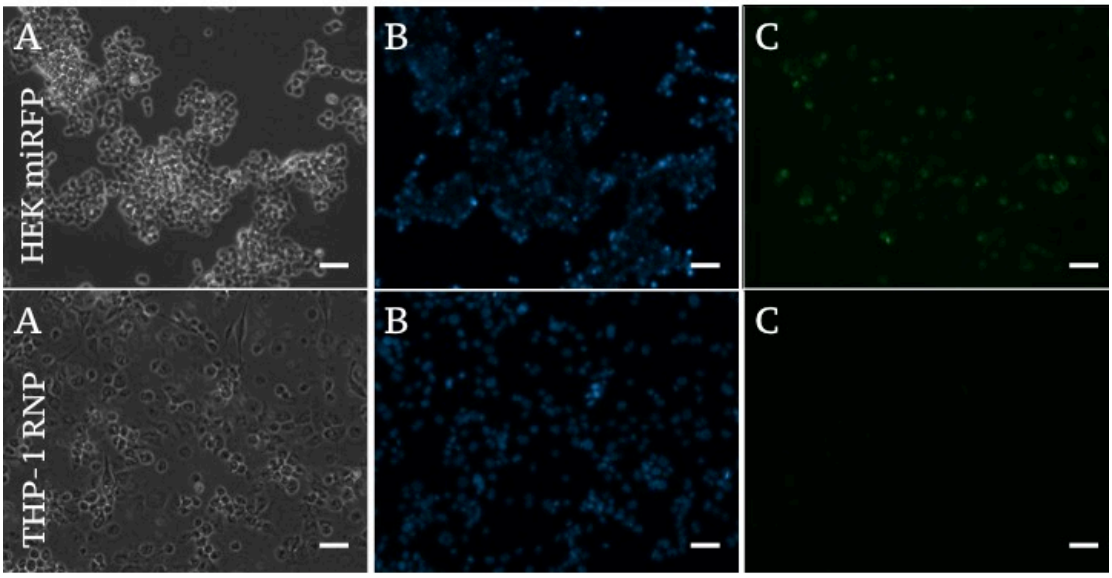

Figure 17: **HEK and THP-1 Cells Transfected with miRFP SpCas9 Plasmids and Cas9 Protein, respectively.** HEK cells were transfected with miRFP SpCas9 plasmid and fixed for staining at 24 hours post-transfection. THP-1 cells were transfected with 5 µl Cas9 protein and 2 µl Lipofectamine 3000 fixed for staining at 24 hours post-transfection. The cells were stained with the SpCas9 primary antibody and Alexa Fluor 488 secondary antibody. The THP-1 cells expressed 0% Alexa Fluor 488 signal, 1-2% of the HEK cells showed an Alexa Fluor 488 signal. THP-1 and HEK cells are viewed under brightfield (A) and fluorescence microscopy DAPI (B) and 488 nm (C) channels. Scale bars: 100 µm.

3.5.2 Electroporation of THP-1 Cells with Cas9 Proteins

Electroporation was utilized to transfect THP-1 cells with Cas9 protein more effectively. The electroporation protocol (Chapter 3.4.2.3) from the last THP-1 electroporation attempt was followed, including the optimized THP-1 transfection medium. THP-1 Dual cells were electroporated with 1 µg Cas9 protein at 1400V, 20ms, and with 1 or 2 pulses. Controls with HEK cells were run in parallel using the same settings. Cells were electroporated at a cell concentration of 2×10^6 cells/well. Controls

with electroporation and without Cas9 protein, and without electroporation and Cas9 protein were included. ICC staining was performed at 24 hours post-electroporation as per protocol (Chapter 2.2.5.1). 0% Alexa Fluor 488 signal was seen at any setting, in HEK or THP-1 Dual cells, when assessed for Cas9 staining using fluorescence microscopy. A DAPI signal was visible intracellularly on all stains. Due to the lack of a positive control for the staining protocol, i.e. HEK cells transfected with miRFP SpCas9, an unsatisfactory stain could not be ruled out.

3.5.2.1 ICC Fixation Optimization

Initially, ICC fixation was performed using ice-cold methanol fixation (Chapter 2.2.5.1). A method using 4% PFA for 10 minutes at room temperature was trialed and the results were compared, to optimize the stain. HEK cells were transfected with 0.5 µg miRFP SpCas9 plasmid and 1 µl Lipofectamine 3000 and fixed at 24 hours post-transfection. Cells were fixed for staining using either 4% PFA or ice-cold methanol. The ICC stain was performed per protocol (Chapter 2.2.5.1) (Fig. 18).

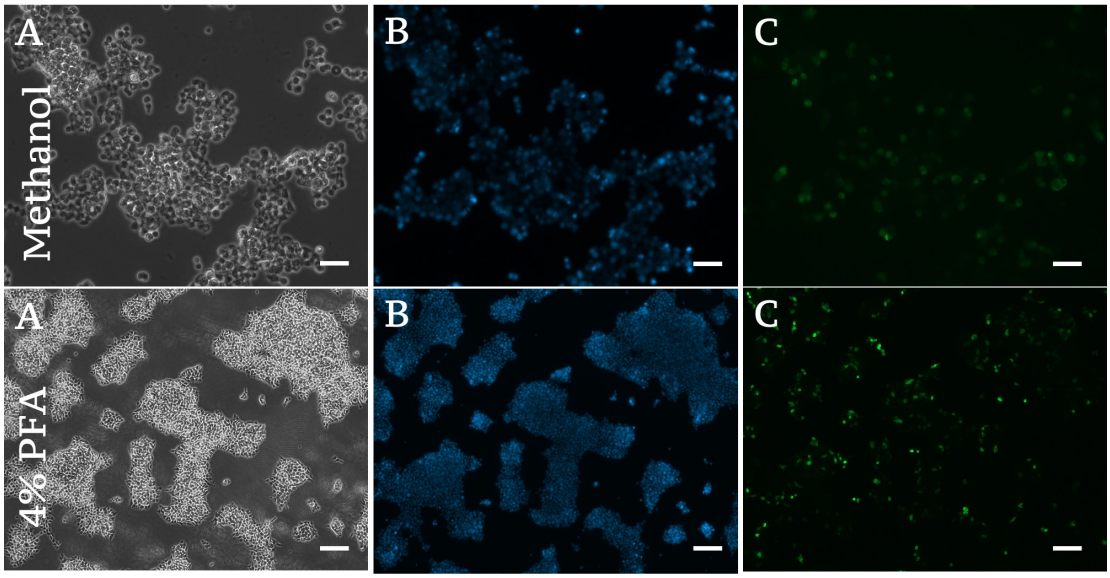

Figure 18: **HEK-Blue cells Transfected with the miRFP SpCas9 Plasmid using Lipofectamine 3000 and Fixed for Staining with Methanol or 4% PFA.** HEK cells were stained using the SpCas9 primary antibody and Alexa Fluor 488 secondary antibody after fixing with methanol or 4% PFA at 24 hours post-transfection. 1% of the cells fixed with methanol showed an Alexa Fluor 488 signal. 1-2% of the cells fixed with 4% PFA showed an Alexa Fluor 488 signal. HEK cells are viewed under brightfield (A) and fluorescence microscopy DAPI (B) and 488 nm (C) channels. Scale bars: 100 µm.
4% PFA.: 4% Paraformaldehyde

3.5.2.2 Electroporation Optimization

Electroporation of THP-1 Dual cells with Cas9 protein was repeated using the same settings (Chapter 3.4.2.3), with HEK-Blue cells were used as a control to optimize the electroporation protocol. The amount of electroporated cells was increased to 1×10^7 cells per electroporation tip. THP-1 Dual cells were electroporated with or without prior PMA differentiation (100 ng/ml) (Chapter 2.2.2.7). Cells were electroporated with 5 µg Cas9 protein at 1400V, 20ms, and with 2 pulses. Additional THP-1 Dual cells with and without PMA differentiation were electroporated with the Lonza GFP plasmid, as a positive control for the electroporation settings. 1×10^6 cells were transfected with 0.5 µg Lonza GFP DNA at 1400V, 20ms, and with 2 pulses. 1×10^6 HEK cells were electroporated with 5 µg Cas9 protein at 1200V, 20ms, and with 2 pulses. Additional HEK cells were transfected using Lipofectamine 3000 with the miRFP SpCas9 plasmid as a positive control for staining. Cells were fixed for staining at 1, 3, and 6 hours post-electroporation and stained using the established ICC protocol modified with 4% PFA fixation (2.2.5.1). The results of the stain were assessed using fluorescence microscopy. 1% of the HEK cells transfected with the Cas9 protein stained at 1-hour post-electroporation were positively stained for SpCas9; the HEK cells fixed for staining at 3 hours post-electroporation no longer expressed a Cas9/Alexa Fluor 488 signal. Otherwise, there was 0% Cas9 signal seen in all stained samples.

3.5.2.3 Staining Time Point Optimization

A repeat of the THP-1 Cas9 protein electroporation (3.5.2.2) was performed to optimize the staining time points. The electroporation protocol was unchanged: 1×10^7 cells and 5 µg Cas9 protein per electroporation tip. Cells were fixed for staining at 30 minutes, 45 minutes, 1 hour, and 1.5 hours post-transfection. The cells were stained using an optimized ICC protocol (Chapter 2.2.5.1) containing higher antibody concentrations: primary AB 1:300, secondary AB 1:250. <1% of THP-1 cells expressed an Alexa Fluor 488 signal at 30 minutes post-electroporation when assessed using fluorescence microscopy. All other time points showed 0% Alexa Fluor 488 staining.

3.5.2.4 Electroporation of PMA-Differentiated and Non-Differentiated THP-1 cells

To assess the effects of PMA on transfection with Cas9 proteins, PMA differentiated (Chapter 2.2.2.7) and non-differentiated THP-1 Dual cells were transfected. The established electroporation protocol was used (Chapter 3.5.2.2), with either 5 µg or 10 µg Cas9 protein and staining at 30 minutes, 60 minutes, or 1.5 hours post-electroporation. A faint Alexa Fluor 488 signal was visible in cells fixed at 30 minutes post-electroporation when assessed using fluorescence microscopy (Fig. 19). All other time points and samples showed 0% Alexa Fluor 488 signal.

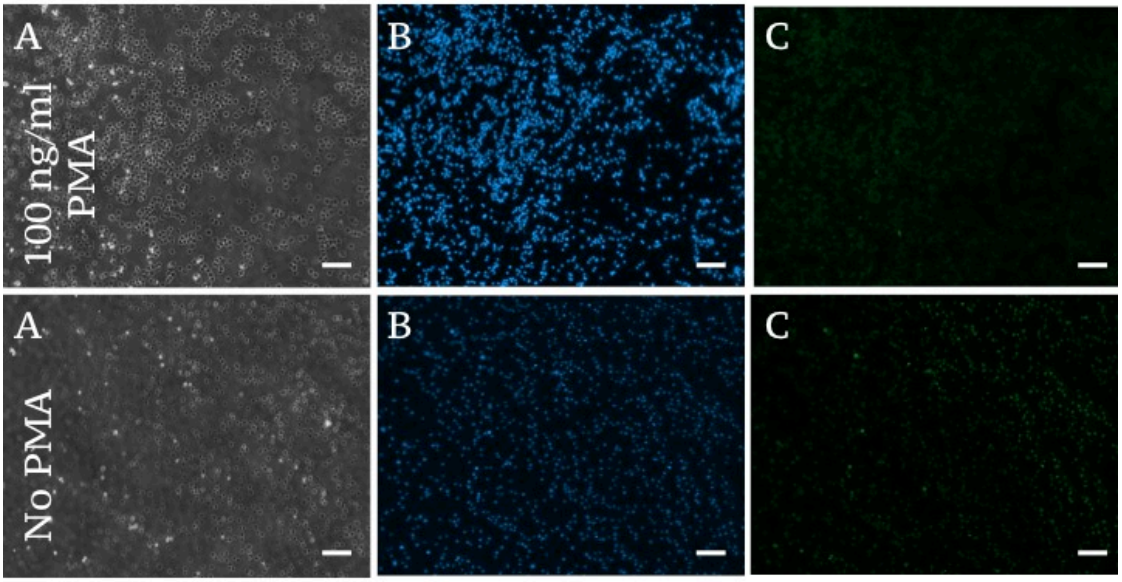

Figure 19: **THP-1 Dual cells Electroporated with Cas9 Protein and Fixed for Staining at 30 Minutes Post-Electroporation.** THP-1 Dual cells were electroporated with 5 µg Cas9 protein and ICC stained with an SpCas9 primary antibody and an Alexa Fluor 488 secondary antibody. THP-1 Dual cells with and without 100 ng/ml PMA differentiation showed a faint ubiquitous Cas9 signal when ICC stained after fixation at 30 minutes post-electroporation. THP-1 Dual cells are viewed under brightfield (A) and fluorescence microscopy DAPI (B) and 488 nm (C) channels. Scale bars: 100 µm.

3.5.2.5 Repeated Electroporation of Differentiated and Non-Differentiated THP-1 cells

Due to the ambiguity of the previous staining result, the experiment was repeated with additional controls to confirm the authenticity of the Cas9 stain. The established electroporation protocol (Chapter 3.5.2.2) was repeated using THP-1 Dual cells with and without PMA (100 ng/ml) differentiation (Chapter 2.2.2.7) and 5 or 10 µg Cas9 protein;

negative controls without Cas9 protein were also electroporated. Additionally, THP-1 cells without PMA were electroporated with 5 µg miRFP SpCas9 DNA to establish a positive control for a Cas9 signal. The established ICC protocol (Chapter 2.2.5.1) with increased antibody concentrations (primary AB 1:300, secondary AB 1:250) and 4% PFA fixation was utilized. A faint, ubiquitous Cas9 signal was seen in the PMA differentiated THP-1 cells transfected with 5 µg Cas9 protein and fixed at 30 minutes post-electroporation when assessed using fluorescence microscopy. The entire experiment was repeated, identically, whereupon 0% Cas9 signal was visible in any stained sample.

3.5.2.6 Electroporation with Additional Controls and Viability Assessment

The transfection of THP-1 Dual cells with Cas9 protein (Chapter 3.5.2.2) was repeated with additional controls to assess the staining and transfection protocols, those controls are shown below (Fig. 20).

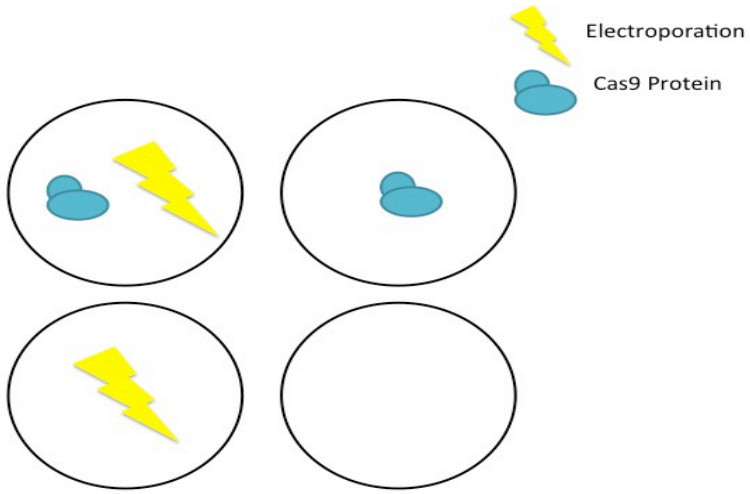

Figure 20: **Electroporation Negative Controls for Electroporation of THP-1 Dual Cells with Cas9 Protein.** THP-1 Dual cells were electroporated with and without Cas9 protein, exposed to only Cas9 protein, or neither electroporated nor exposed to Cas9 proteins.

The cells were fixed at 30 minutes post-transfection and stained as per modified ICC protocol (2.2.5.1). Additionally, parallel wells were assessed with trypan blue staining at 9 hours post-electroporation to evaluate cell viability. 0% Cas9 signal was seen in any stained sample, the DAPI stain was intracellularly expressed in all samples when assessed using fluorescence microscopy. At 9 hours post-electroporation, cell viability was 61% in cells which were electroporated with Cas9 protein, 53% in cells which were

electroporated without Cas9 protein, 58% in cells exposed to Cas9 but not electroporated, and 64% in cells which were neither exposed to Cas9 protein nor electroporated.

3.5.2.7 HEK-Blue Staining Control with mCherryCas9

To ascertain the efficacy of the staining protocol, HEK-Blue cells were transfected with the mCherryCas9 plasmid using Lipofectamine 3000 and plus reagent. Cells were assessed for plasmid expression at 24 hours post-transfection using fluorescence microscopy and then fixed for ICC staining (Chapter 2.2.5.1). When assessed using fluorescence microscopy at 24 hours post-transfection, 40% of HEK-Blue cells expressed an mCherry signal. 20% of those cells, when stained for SpCas9 and assessed using fluorescence microscopy, were positively stained for SpCas9 (Fig. 21).

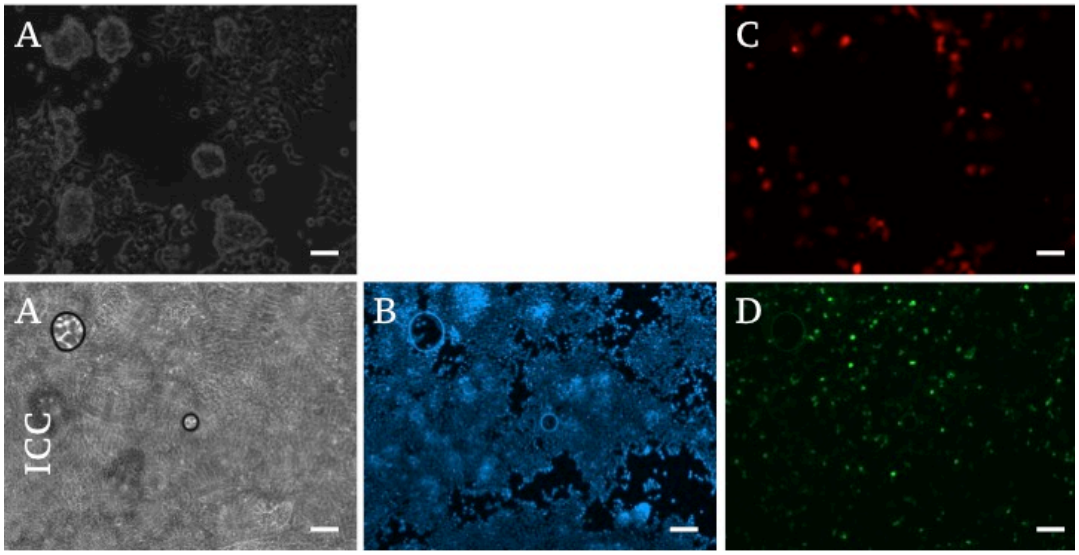

Figure 21: **HEK-Blue cells Transfected with mCherryCas9 Plasmid and Fixed for SpCas9 Staining at 24 Hours Post-Transfection.** Cells were transfected with 500ng mCherryCas9 and 3 µl Lipofectamine 3000. mCherry Cas9 fluorescence images (A, C) were captured at 24 hours post-transfection, prior to fixation. HEK cells are viewed under brightfield (A) and fluorescence microscopy DAPI (B), mCherry (C), and 488 nm (D) channels. Scale bars: 100 µm.

3.5.2.8 Repeated THP-1 Dual Electroporation with Cas9 protein

THP-1 Dual cells were electroporated as per the established protocol (Chapter 3.5.2.2) and ICC stained in tandem to the HEK-Blue cells from above (Chapter 2.2.5.1). Fixation for staining took place at 30 minutes, 1 hour, and 3 hours post-electroporation. 0% Alexa Fluor 488 fluorescence signal was visible at any time point in any sample when assessed using fluorescence microscopy.

3.5.2.9 THP-1 Dual Electroporation with Cas9 Protein

It was planned that THP-1 cells be transfected with Cas9 protein and supernatant be sampled at various time points for cytokine analysis. The THP-1 Dual cells were electroporated (Chapter 3.5.2.2) and fixed (Chapter 2.2.5.1) as per the established protocols. HEK-Blue controls were also transfected and stained using the same protocols. Supernatant was sampled from parallel wells of THP-1 cells at 1, 3, 6, 9, 24, and 48 hours post-electroporation. The THP-1 cells, which were not electroporated and not exposed to Cas9 protein, were 80% confluent at 48 hours post-electroporation when assessed using trypan blue. All other cell groups were approximately 50% confluent at the same time point. This experiment was performed three times, with 0% Alexa Fluor fluorescence signal expressed in any sample when assessed using fluorescence microscopy. Therefore no cytokine assessment was performed. The DAPI stain showed an intracellular DAPI signal in all stained samples.

3.6. TRANSFECTION WITH SUPERNATANT ASSESSMENT

3.6.1 THP-1 DUAL PLASMID TRANSFECTION WITH TRANSIT-X2 AND SUPERNATANT CYTOKINE ASSESSMENT

To assess the activation of the NF-κB and IRF pathways in THP-1 Dual cells transfected with plasmids, THP-1 Dual cells were transfected in triplicate wells using TransIT-X2 (Chapter 2.2.4.7). The cells were seeded in the optimized THP-1 transfection medium without PMA and transfected on the day of seeding. Cells were transfected with either the CjCas9 plasmid containing the HA tag, the mCherryCas9 plasmid, or the mKate plasmid, at 0.5 µg plasmid DNA with 1 µl TransIT-X2 per well of a 24-well plate. Additional controls containing only TransIT-X2 or optimized transfection medium were included. THP-1 Dual cells were also stimulated with 1 µg/l dsDNA or 3 µM CpG ODN as per the established protocol (Chapter 3.3.1), to serve as positive controls for pathway activation. The cells were incubated in the transfection or stimulation mediums at 37°C for 24 hours. 50 µl supernatant samples were removed at 16, 24, 48, and 72 hours post-transfection and stored at -80°C (Fig. 22). The removed samples of medium were replaced with the same volume of plain RPMI. The cells were assessed for plasmid expression using fluorescence microscopy at 24 and 48 hours post-transfection. The activation of the

NF-κB and IRF pathways were assessed using QUANTI-Luc and QUANTI-Blue as per protocol (Chapters 2.2.3.3 and 2.2.3.4).

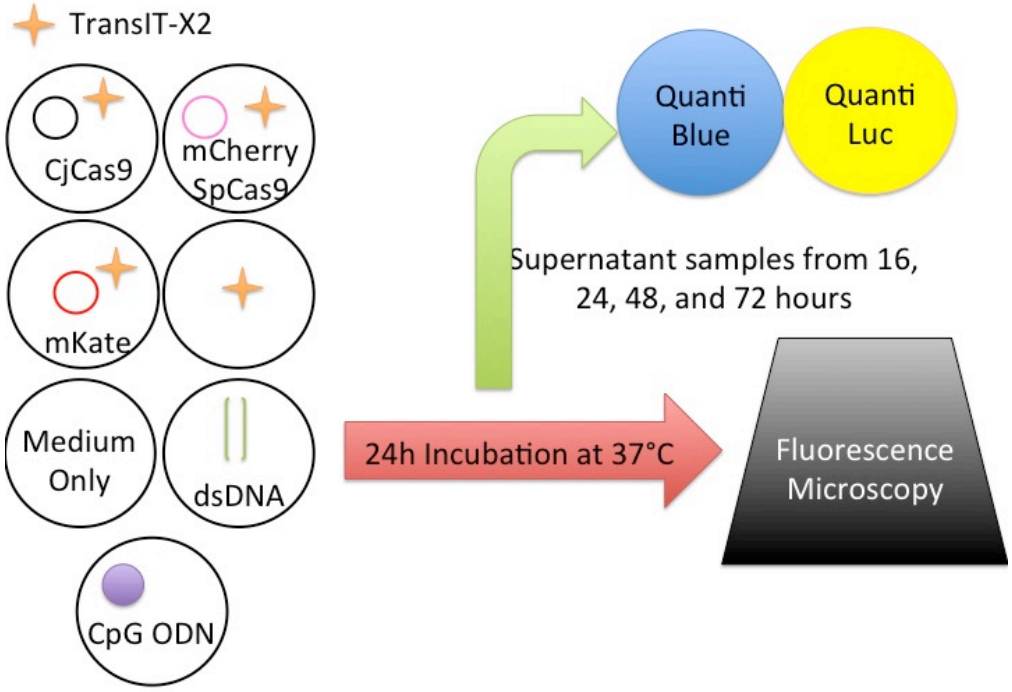

Figure 22: **Experimental Design for Transfection of THP-1 Dual Cells with Plasmids using TransIT-X2.** THP-1 Dual cells were transfected with 0.5 µg of multiple plasmids using 1 µl TransIT-X2 or exposed to 1 µg/l dsDNA or 3 µM CpG ODN prior to incubation, supernatant sampling, and fluorescence microscopy analysis.

While cells transfected with the mKate plasmid showed a <1% rate of transfection, cells transfected with the mCherryCas9 plasmid showed a 0% rate of transfection. Cells transfected with the CjCas9 plasmid could not be stained, due to a lack of primary antibodies capable of recognizing the plasmid.

Kruskal-Wallis Testing was conducted to examine the effect of THP-1 Dual stimulation and transfection on IRF pathway activation. Statistically significant changes in IRF activation were seen at 16 hours ($H(6)=18.18$, $p=0.006$), 24 hours ($H(6)=19.36$, $p=0.0036$), 48 hours ($H(6)=19.64$, $p=0.0032$), and 72 hours ($H(6)=19.36$, $p=0.0036$) post-stimulation. Post-hoc pairwise comparisons using Dunn's test with control for joint ranks and Bonferroni adjustment showed statistically significant upregulation of the IRF pathway in response to transfection with the mCherry Cas9 plasmid when compared to cells only exposed to TransIT-X2 at 16 and 24 hours post-transfection ($p<0.05$). All other

comparisons were not statistically significant (all *p*s>0.05). Data from the 16-hour post-transfection analysis is displayed below (Fig. 23).

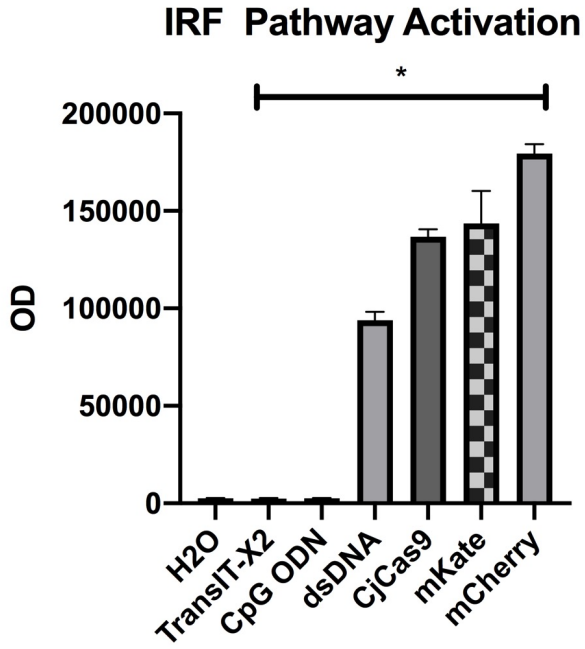

Figure 23: **THP-1 Dual Cells Transfected with mCherryCas9 Showed Significant Up-regulation of the IRF Pathway.** There was significant upregulation or the IRF pathway (Tukey's Test $p < 0.05$) seen in cells transfected with the mCherryCas9 plasmid when compared to cells exposed to TransIT-X2 at 16 hours post-transfection. Error bars indicate standard deviation.
OD: Optical Density

Kruskal-Wallis Testing was conducted to examine the effect of THP-1 Dual transfection on NF-κB pathway activation. Statistically significant differences in NF-κB activation were seen at 16 hours ($H(6)=18.12$, $p=0.006$), 24 hours ($H(6)=18.34$, $p=0.0054$), 48 hours ($H(6)=17.85$, $p=0.0066$), and 72 hours ($H(6)=15.9$, $p=0.014$) post-stimulation. Post-hoc pairwise comparisons using Dunn's test with control for joint ranks and Bonferroni adjustment showed statistically significant upregulation of the NF-κB pathway in response to transfection with the mCherryCas9 plasmid when compared to cells only exposed to H_2O at 16, 24, 48, and 72 hours post-transfection (all $p<0.05$). Additionally, Dunn's test with control for joint ranks and Bonferroni adjustment showed statistically significant upregulation of the NF-κB pathway in response to transfection with the mKate plasmid when compared to cells only exposed to H_2O at 16, 24, and 48 hours post-transfection (all $p<0.05$). All other comparisons were not statistically

significant (all *p*s>0.05). Data from the 24-hour post-transfection analysis is displayed below (Fig. 24).

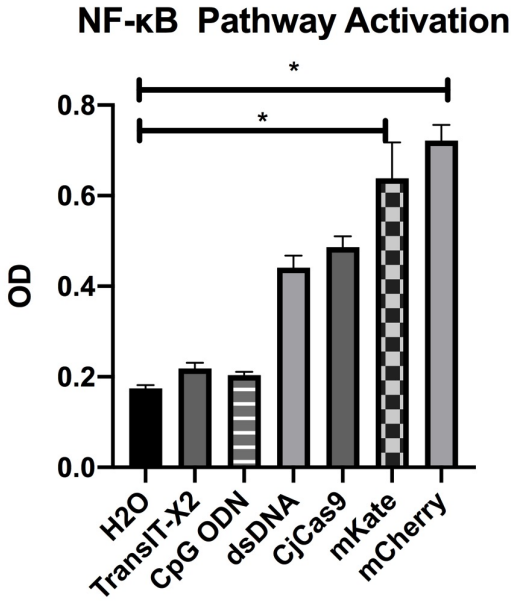

Figure 24: **THP-1 Dual Cells Transfected with Plasmids Showed Upregulation of the NF-κB Pathway.** There was significant upregulation of the NF-κB pathway (Tukey's test $p < 0.05$) seen in cells transfected with the mKate or the mCherryCas9 plasmids when compared to cells exposed to H_2O at 24 hours post-transfection. Error bars indicate standard deviation.
OD: Optical Density

3.6.2 THP-1 DUAL NUCLEOFECTION AND PATHWAY ACTIVATION ASSESSMENT

The established nucleofection protocol was used to nucleofect 2×10^6 THP-1 Dual cells with the mKate, mCherryCas9, or Lonza GFP control plasmid (Chapter 3.4.4.1.1). Cells were nucleofected with 0.5 µg or 1 µg DNA of each plasmid. THP-1 cells transfected with the Lonza GFP control plasmid expressed a GFP signal at a rate of 65% when assessed using fluorescence microscopy (Fig. 15). The rate of transfection with the mKate or mCherryCas9 plasmids was <1%. THP-1 Dual cells nucleofected without plasmid DNA served as negative controls.

Supernatant samples were taken at 24, 48, and 72 hours post-nucleofection and stored at -80°C. QUANTI-Luc and QUANTI-Blue assessments of IRF and NF-κB pathway activation were performed as per protocol (Chapters 2.2.3.3 and 2.2.3.4).

One-way ANOVA analysis showed no significant up-regulation (all *p*s> 0.05) of the NF-κB pathway in any sample.

Kruskal-Wallis testing of supernatant from IRF pathway analysis at 24 hours post-nucleofection showed no significant IRF pathway up-regulation (H(7)=7.93, *p*=0.34). One-way ANOVA analysis showed significant up-regulation of the IRF pathway at 48 hours (F(7,1) =4812.6, *p*=0.011),and 72 hours (F(7,1) =46728.48, *p*=0.0036) post-nucleofection. Post-hoc Tukey's tests showed significant up-regulation of the IRF pathway in response to nucleofection with the mCherryCas9 plasmid, the mKate plasmid, and the Lonza GFP plasmid at both 0.5 µg or 1 µg plasmid DNA when compared to non-nucleofected samples at 48 and 72 hours post-transfection (all *p*<0.05). This activation of the IRF pathway at 48 hours post-electroporation is displayed below (Fig. 25).

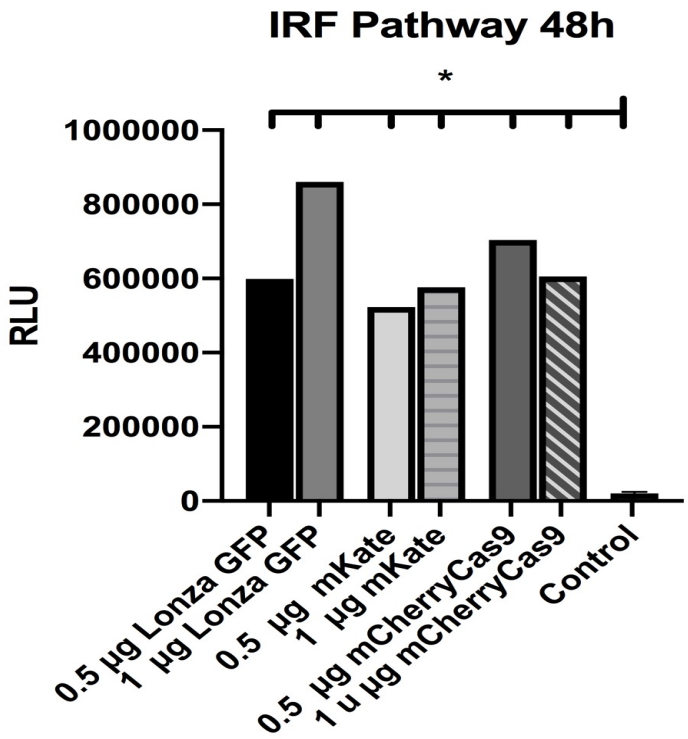

Figure 25: **The IRF Pathway is Upregulated in THP-1 Dual cells in Response to Nucleofection with Plasmids.** Significant upregulation (Tukey's Test *p*=<0.05) of the IRF pathway was recorded in response to nucleofection with the 0.5 µg or 1 µg Lonza GFP, mKate, and mCherryCas9 plasmids when compared to non-nucleofected control cells. Error bars indicate standard deviation
RLU: Relative light units

3.7. ASSESSING IMMUNE RESPONSES IN IMHU CELLS

To establish baseline IMhu immune responses prior to Cas9 stimulation trials, IMhu were stimulated with a variety of commercially available immunostimulants. A summary of cytokine production in response to immunostimulants can be seen in Table 4.7.

3.7.1 INFLAMMASOME ACTIVATION AND IL-1B PRODUCTION IN IMHU

IMhu were stimulated with LPS and ATP to activate the NLRP3 inflammasome and induce production of IL-1β. IL-1α co-stimulation was included, as IL-1α has been described to aid in inflammasome activation. IMhu were seeded on collagen-coated plates in triplicate wells and incubated at 37°C for 24 hours. On day two, the cells were transduced with LPS, IL-1α, and ATP. First, the medium was aspirated from the wells and replaced with OptiMEM containing: LPS 500 ng/ml + IL-1α 25 ng/ml, LPS 10 μg/ml + IL-1α 25 ng/ml, LPS 5 μg/ml + IL-1α 25 ng/ml, LPS 5 μg/ml, IL-15 25 ng/ml, or only OptiMEM, and incubated for 6 hours. Then, the medium was replaced with OptiMEM containing 5 mM ATP or no ATP and cells were incubated at 37°C. Supernatant samples were removed at 1, 3, 5, and 24 hours post-transduction. The samples were immediately placed on dry ice prior to storage at -80°C. IMhu cytokine production was assessed using HEK-Blue IL-1β cells as per manufacturer's protocol (Chapter 2.2.3.5).

One-way ANOVA of samples from 3 hours post-stimulation revealed no significant IL-1β production (p=0.67). Kruskal-Wallis testing of supernatant from 1 hour post-stimulation showed no significant IL-1β production (H(7)=10.16, p=0.18).

Kruskal-Wallis testing of supernatant from 5 hours (H(7)=16.76, p=0.019) and 24 hours (H(7)=14.0, p=0.03) post-stimulation showed significant differences in IL-1β production between groups. Post hoc pairwise comparisons using Dunn's test with control for joint ranks and Bonferroni adjustment revealed statistically significant production of IL-1β in response to stimulation with 5 μg/ml LPS + 5mM ATP at 24 hours post-stimulation when compared to cells only exposed to ATP (p=0.046). Results of

supernatant collection at 24 hours post-transfection are shown below (Fig. 26) All other comparisons were not statistically significant (all *p*s>0.05)

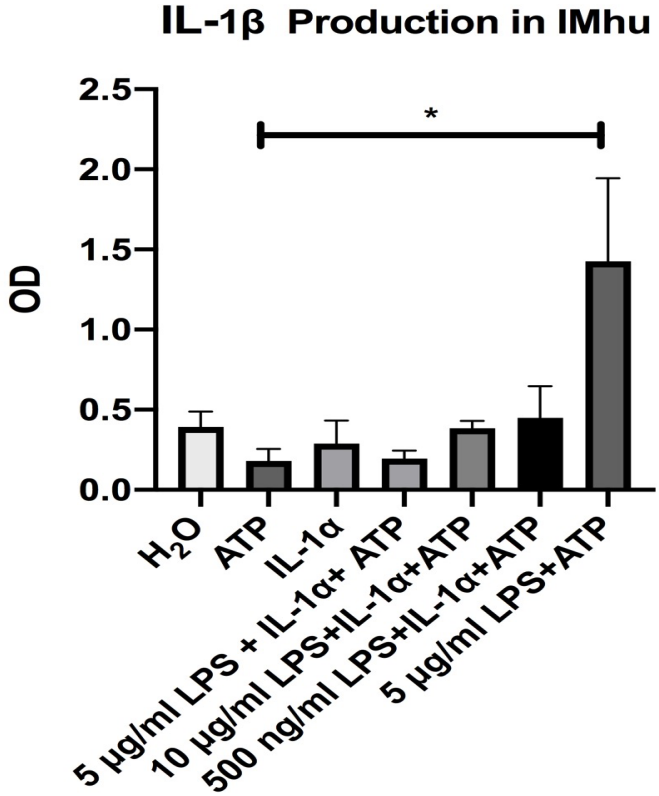

Figure 26: **Production of IL-1β in IMhu Stimulated with LPS +/- ATP +/- IL-1α with 6 Hours of LPS Incubation and 24 Hours of ATP Incubation.** A significant production (Tukey's Test *p*= 0.046) of IL-1β was recorded in response to stimulation with 5 µg/ml LPS + 5mM ATP when compared to cells only exposed to 5mM ATP at 24 hours post-ATP- stimulation. Error bars indicate standard deviation
ATP: 5mM ATP
OD: Optical Density

3.7.2 Cytokine Production in IMhu upon ds-DNA-EC and Poly I:C Stimulation

IMhu were seeded in growth medium on collagen-coated plates in triplicate wells 1 day prior to stimulation with stimulants of the TLR9 pathway/cytosolic DNA sensors (ds-DNA-EC) and TLR3 (Poly I:C) pathways to assess the baseline responses of IMhu to known immunostimulants. On day two, the cells were stimulated with dsDNA (1 or 5 µg/ml with Lipofectamine 3000, 1 or 5 µg/ml without Lipofectamine 3000), Poly I:C (5 µg/ml or 10 µg/ml), or H_2O in OptiMEM. The cells were incubated at 37°C and supernatant samples were taken at 3, 6, 24, and 48 hours post-stimulation and stored at -

80°C until assessment. The resulting cytokine production was analyzed using HEK-Blue IFN I/II, HEK-Blue TNFα, and HEK-Blue IL-6 cells as per manufacturer's protocol (Chapter 2.2.3.5).

Supernatant assessment for IFN production revealed no significant IFN I/II production in response to any stimulant at any time point. One-Way ANOVA at 3 hours post-stimulation ($F(7,8)=1.92$, $p=0.19$) and Kruskal-Wallis tests for values at 6 hours ($H(7)=6.12$, $p=0.52$), 24 hours ($H(7)=13.06$, $p=0.071$), and 48 hours ($H(7)=10.15$, $p=0.18$) were used.

Supernatant assessment for IL-6 production revealed no significant IL-6 production in response to any stimulant at any time point. One-way ANOVA tests for values at 3 hours ($F(7,8)=1.53$, $p=0.28$), 6 hours ($F(7,8)=1.3$, $p=0.36$), 24 hours ($F(7,8)=2.71$, $p=0.093$), and 48 hours ($F(7,8)=1.77$, $p=0.22$) post-stimulation were used.

Supernatant assessment for TNFα production revealed significant production of TNFα at 48 hours post-stimulation when assessed using a One-way ANOVA test ($F(7,8)=6.48$, $p=0.009$). All other time points showed no statistical significance when assessed using Kruskal-Wallis tests: 3 hours ($H(7)=11.9$, $p=0.11$), 6 hours ($H(7)=13.24$, $p=0.067$), and 24 hours ($H(7)=11.38$, $p=0.12$) post-stimulation. Post hoc Tukey's tests for values at 48 hours post-stimulation revealed a significant production of TNFα in response to 10 μg/ml Poly I:C when compared to cells exposed to H_20 ($p=0.0152$).

3.7.2.1 Repeated IMhu Stimulation with dsDNA and Poly I:C

The experiment from Chapter 3.7.2 was repeated to establish a protocol that would induce a robust cytokine response to stimulation. IMhu were stimulated with dsDNA (1 or 5 μg/ml with Lipofectamine LTX, or 5 μg/ml dsDNA without Lipofectamine LTX) or Poly I:C (5 or 10 μg/ml) Additional cells were exposed only to OptiMEM or Lipofectamine LTX. Supernatant was sampled at 6, 24, and 48 hours post-stimulation. Cytokine expression was assessed using HEK-Blue IFN I/II, HEK-Blue TNFα, and HEK-Blue IL-6 cells as per manufacturer's protocol (Chapter 2.2.3.5).

IL 6 production in response to stimulation was assessed using Kruskal-Wallis tests, which showed a significant difference between groups at 6 hours ($H(6)=15.48$, $p=0.017$) and 48 hours ($H(6)=617.42$, $p=0.0079$) post-stimulation; there was no significance seen

at 24 hours post-stimulation (H(6)=616.69, p=0.195). Post hoc pairwise comparisons using Dunn's test with control for joint ranks and Bonferroni adjustment showed a statistically significant production of IL-6 at 6 and 48 hours post-stimulation in cells stimulated with 10 μg/ml Poly I:C when compared to cells only exposed to OptiMEM ($p<0.05$).

TNFα production in response to stimulation was assessed using Kruskal-Wallis tests with a significant difference seen between groups at 6 hours (H(8)=20.85, p=0.0076), 24 hours (H(8)=21.37, p=0.0062), and 48 hours (H(8)=18.45, p=0.0126) post-stimulation. Post hoc pairwise comparisons using Dunn's test with control for joint ranks and Bonferroni adjustment showed a statistically significant production of TNFα at 6, 24, and 48 hours post-stimulation (all $p<0.05$) in cells exposed to Poly I:C 10 μg/ml, when compared to cells only exposed to Lipofectamine LTX. In addition, at 24 hours post-stimulation, cells exposed to 5 μg/ml Poly I:C produced significantly more TNFα than cells exposed only to Lipofectamine LTX (p=0.014).

IFN I/II production in response to stimulation was assessed using Kruskal-Wallis tests with a significant difference seen between groups at 6 hours (H(8)=21.65, p=0.0056), 24 hours (H(8)=19.26, p=0.0135), and 48 hours (H(8)=17.17, p=0.028) post-stimulation. Post hoc pairwise comparisons using Dunn's test with control for joint ranks and Bonferroni adjustment showed a statistically significant production of IFN I/II at 6, 24, and 48 hours post-stimulation (all $p<0.05$) in cells stimulated with 10 μg/ml Poly I:C when compared to cells exposed only to Lipofectamine LTX. In addition, at 6 and 24 hours post-stimulation, cells exposed to 5 μg/ml Poly I:C produced significantly more TNFα than cells exposed only to Lipofectamine LTX ($p<0.05$).

IMhu cytokine production in response to stimulation is shown below (Fig. 27).

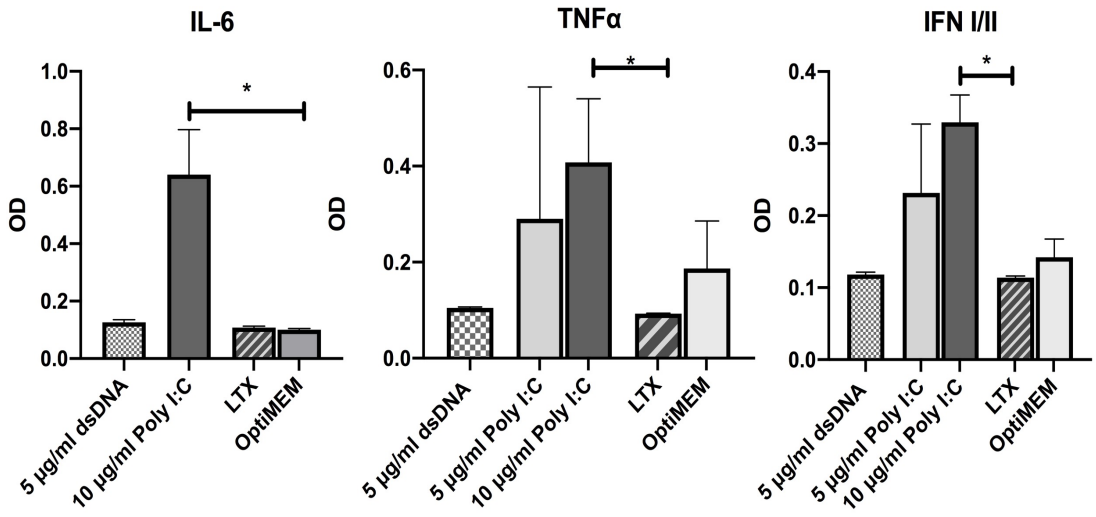

Figure 27: **Cytokine Production in IMhu Stimulated with 10 µg/ml Poly I:C.** A significant production (Tukey's Test $p<0.05$) of IL-6, TNFα, and IFN I/II was recorded in response to stimulation with 10 µg/ml Poly I:C when compared to cells only exposed to OptiMEM or Lipofectamine LTX at 48 hours post-stimulation. Error bars indicate standard deviation.
LTX: Lipofectamine LTX

3.7.3 IMHU STIMULATION WITH IMIQUIMOD AND CPG ODN

IMhu were seeded for stimulation as per protocol to assess the immune responses to stimulants of the TLR7 and TLR9 pathways: on day 2, IMhu were stimulated with CpG ODN (1 µM, 5µM, or 1µM with Lipofectamine LTX), or Imiquimod (1 µg/ml, 5 µg/ml, or 1 µg/ml with Lipofectamine LTX) or not stimulated and only exposed to medium or Lipofectamine LTX. The cells were incubated at 37°C and supernatant samples were taken at 6, 24, and 48 hours post-stimulation and stored at -80°C. Cytokine responses were assessed using HEK-Blue IFN I/II, IL-6, and TNFα cells as per protocol (Chapter 2.2.3.5).

IL-6 concentration in supernatant samples was significantly different between groups assessed using One-way ANOVA tests for values from 6 hours ($F(5,12)=5.42$, $p=0.008$) and 24 hours ($F(5,12)=4.11$, $p=0.021$) post-stimulation. There was no significant difference seen between groups of samples at 48 hours post-stimulation when assessed using Kruskal-Wallis tests ($H(5)=7.29$, $p=0.2$). Post hoc analyses with Tukey's tests of values from 6 and 24 hours post-stimulation showed that at 6 hours post-stimulation 5 µg/ml Imiquimod stimulated a significantly larger output of IL-6 than OptiMEM ($p=0.0034$). This is shown below (Fig. 28). At 24 hours post-stimulation there was no significant production of IL-6 (all ps>0.05).

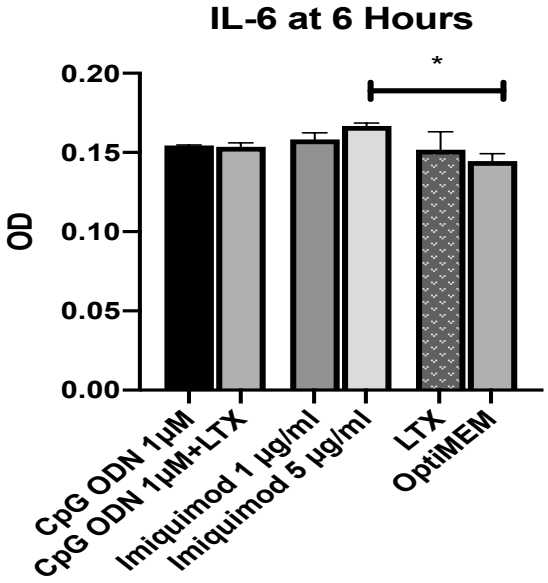

Figure 28: **IL-6 Production in IMhu Stimulated with Imiquimod.** A significant production (Tukey's Test $p=0.0034$) of IL-6 was recorded in response to stimulation with 1 µg/ml Imiquimod when compared to cells only exposed to OptiMEM at 6 hours post-stimulation. Error bars indicate standard deviation.
LTX: Lipofectamine LTX

TNFα concentration in samples was compared using Kruskal-Wallis tests. At 6 hours ($H(7)=16.13$, $p=0.24$) and 48 hours ($H(7)=15.24$, $p=0.33$) post-stimulation significant differences in TNFα concentration were seen between groups. No significant difference was seen in TNFα concentrations in samples gathered at 24 hours ($H(7)=12.77$, $p=0.078$). Post hoc pairwise comparisons using Dunn's test with control for joint ranks and Bonferroni adjustment for values at 6 and 48 hours showed no significance between any groups ($p>0.05$).

IFN I/II concentration in supernatant samples was assessed using Kruskal-Wallis tests for values at 6 hours (H(7)=9.87, *p*=0.2) and 24 hours (H(7)=15.75, *p*=0.028) post-stimulation. The significant difference between groups seen at 24 hours was assessed further using post hoc pairwise comparisons using Dunn's test with control for joint ranks and Bonferroni adjustment and showed no significance between any groups (all *p*s>0.05). One-way ANOVA tests showed a significant difference in IFN I/II concentration between experimental groups at 48 hours post-stimulation (F(7,16)=5.5, *p*=0.0023). Post Hoc Tukey's tests showed a significantly higher concentration of IFN I/II in supernatant samples from cells stimulated with Imiquimod 5 µg/ml at 48 hours when compared to samples from cells stimulated with Lipofectamine LTX (*p*=0.0144). IFN concentration at 48 hours is shown below (Fig. 29).

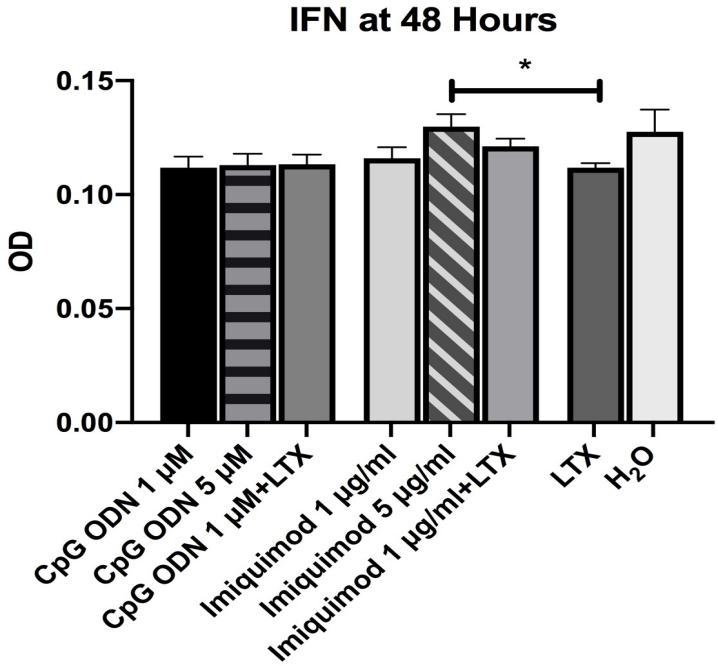

Figure 29: **IFN Production in IMhu Stimulated with Imiquimod.** A significant production (Tukey's Test *p*=0.014) of IFN was recorded in response to stimulation with 5 µg/ml Imiquimod when compared to cells only exposed to Lipofectamine LTX at 48 hours post-stimulation. Error bars indicate standard deviation.
LTX: Lipofectamine LTX

3.7.4 COMPARING COLLAGEN-COATED AND UNCOATED WELLS

IMhu stimulation experiments were repeated comparing collagen-coated and uncoated wells. The same protocols (Chapters, 3.7.2, and 3.7.3) were utilized in two cell cohorts; one cohort was seeded in collagen-coated wells and the other in uncoated wells. Cells were stimulated with 1 μg/ml dsDNA, 1 μg/ml dsDNA with Lipofectamine LTX, 5 μg/ml LPS, or only exposed to OptiMEM or Lipofectamine LTX. Supernatant samples taken at 6, 24, and 48 hours post-stimulation were assessed using HEK-Blue IFN I/II, HEK-Blue IL-6, and HEK-Blue TNFα cells as per manufacturer's protocol (Chapter 2.2.3.5).

Kruskal-Wallis tests showed a significant difference in TNFα production between experimental groups from samples taken at 6 hours ($H(9)=21.39$, $p=0.011$), 24 hours ($H(9)=23.74$, $p=0.0047$), and 48 hours ($H(9)=22.0$, $p=0.0089$) post-stimulation. Post hoc pairwise comparisons using Dunn's test with control for joint ranks and Bonferroni adjustment showed no significant differences in TNFα concentration between matched collagen-coated and uncoated wells (all ps>0.05).

Kruskal-Wallis testing of supernatant samples taken at 6 hours post-stimulation and assessed for IFN I/II concentration showed no significant difference in IFN I/II production between any samples ($H(9)=13.61$, $p=0.14$). At 24 hours post-stimulation, Kruskal-Wallis tests showed a significant difference in IFN I/II concentration between supernatant samples ($H(9)=23.94$, $p=0.0044$). Post hoc pairwise comparisons using Dunn's test with control for joint ranks and Bonferroni adjustment and showed no significantly higher IFN I/II concentrations in samples from collagen-coated wells compared paired uncoated wells (all ps>0.05). One-way ANOVA testing of samples taken at 48 hours post-stimulation showed a significant difference in IFN I/II production between samples ($F(9,20)=2.79$, $p=0.027$). Post hoc Tukey's tests showed no significant difference between any of the tested groups (all ps>0.05).

Supernatant assessments of IL-6 concentration were analyzed using One-way ANOVA. IL-6 values of samples from 6 hours post-stimulation were significantly different between experimental groups ($F(9,20)=9.02$, $p<0.0001$). Post hoc Tukey's tests showed that cells in collagen-coated wells exposed to 1 μg/ml dsDNA produced significantly more IL-6 than cells in collagen-coated wells only exposed to OptiMEM

(p=0.0071). Cells in uncoated wells exposed to 1 µg/ml dsDNA also produced significantly more IL-6 than cells in uncoated wells only exposed to OptiMEM (p=0.025). This is shown in the graph below (Fig. 30).

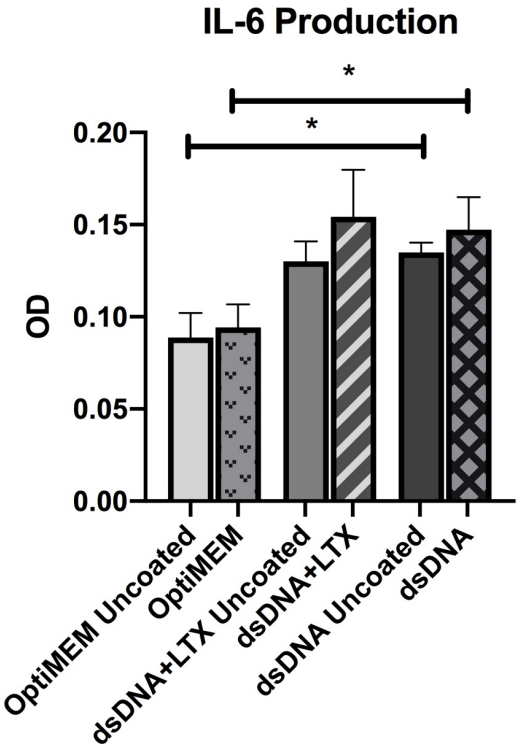

Figure 30: **Comparison of IL-6 Production in IMhu Seeded in Collagen-Coated and Uncoated Wells.** A significant production (Tukey's Test p<0.05) of IL-6 was recorded in response to stimulation with 1 µg/ml dsDNA when compared to cells only exposed to OptiMEM in collagen-coated and uncoated wells at 6 hours post-stimulation. Error bars indicate standard deviation.
LTX: Lipofectamine LTX

One-way ANOVA analysis showed significantly different IL-6 concentrations between experimental groups in supernatant samples from 24 hours post-stimulation ($F(9,20)=5.9$, p=0.0005). Post hoc Tukey's tests revealed no significant differences between paired collagen-coated and uncoated samples (p>0.05). Kruskal-Wallis tests showed significant differences in IL-6 concentrations between experimental groups in supernatant samples from 48 hours post-stimulation ($H(9)=23.0$, p=0.0062). Post hoc pairwise comparisons using Dunn's test with control for joint ranks and Bonferroni adjustment showed no significant differences in IL-6 concentrations between samples from collagen-coated wells and paired uncoated wells (p>0.05).

3.8. TRANSFECTION OF IMHU WITH PLASMIDS

To assess the innate immune response to Cas9 in IMhu, IMhu were to be transfected with plasmids containing Cas9 and the supernatant assessed for cytokine production.

3.8.1 TRANSFECTION OF IMHU WITH LIPOFECTAMINE 3000

It was initially attempted to establish a transfection protocol using serum-free medium, as serum may contain cytokines, which can hinder cytokine output assessment as well as reducing transfection efficacy. Therefore, IMhu were seeded on 96-well collagen-coated plates in OptiMEM one day prior to transfection. They were then transfected with 0.15 µl Lipofectamine 3000 and 200 ng of mKate, GFP SpCas9, or mCherryCas9 plasmid DNA per well. Control wells containing only cells, Lipofectamine 3000, and OptiMEM were also plated. Cells were assessed for fluorescence at 24 hours post-transfection. 5% of cells transfected with the mKate plasmid expressed an mKate signal. 1% of cells transfected with the mCherryCas9 plasmid expressed an mCherry signal at 24 hours post-transfection, and 0% of GFP SpCas9-transfected cells expressed a GFP signal at that time point.

3.8.1.1 Optimization of Lipofectamine 3000 Transfection

To increase transfection rates, IMhu were transfected in a collagen-coated 96-well plate. The cells were seeded in DMEM on the first experimental day. IMhu were then transfected with the GFP SpCas9 plasmid in either DMEM or OptiMEM following the previously established protocol (Chapter 3.8.1). Various ratios of plasmid DNA and Lipofectamine 3000 were combined to ascertain the optimal amounts of transfection reagents when transfecting IMhu (see **Appendix F**). The results of the transfection were assessed at 24 hours post-transfection using fluorescence microscopy. IMhu transfected with 0.4 µl Lipofectamine and 300 ng showed the highest rate of transfection, at 35% IMhu transfected with 0.15, 0.2 or 0.4 µl Lipofectamine 3000 and 300 or 400 ng plasmid DNA were all transfected at rates between 28 and 33%.

IMhu transfected with 0.4 µl Lipofectamine and 300 ng GFP SpCas9 plasmid DNA in OptiMEM serum-free medium were transfected at a rate of 31%, IMhu

transfected in DMEM with 0.4 µl Lipofectamine and 300 ng GFP SpCas9 plasmid DNA were transfected at a rate of 33% when assessed at 24 hours post-transfection (Fig. 31).

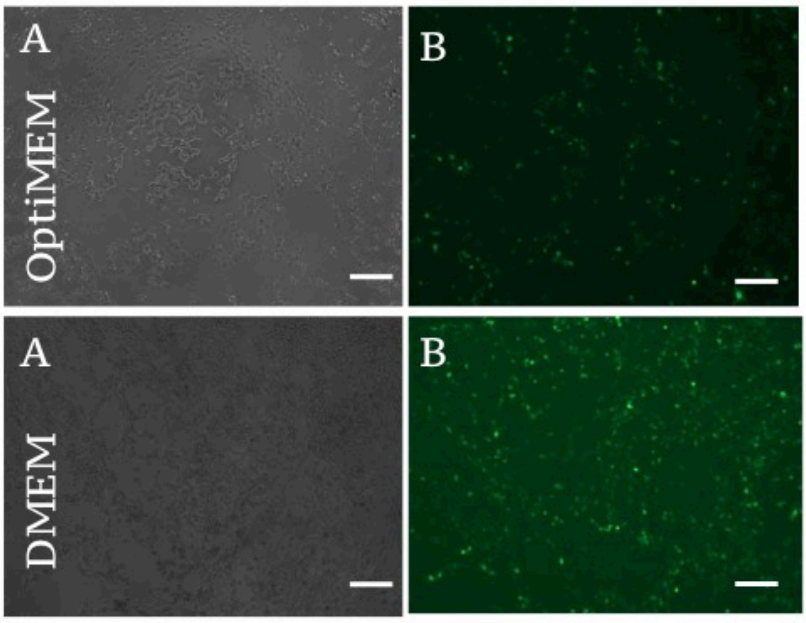

Figure 31: **IMhu Transfected with GFP SpCas9 Plasmid and Lipofectamine 3000 in OptiMEM or DMEM at 24 Hours Post-Transfection.** IMhu were transfected with 200 ng of the GFP SpCas9 plasmid and 0.15 µl Lipofectamine 3000 in a collagen-coated 96-well plate in either OptiMEM or DMEM medium. HEK cells are viewed under brightfield (A) and fluorescence (B) channels. Scale bars: 100 µm.

3.8.2 Transfection of IMhu with Multiple Plasmids using Lipofectamine 3000 with Supernatant Cytokine Assessment

IMhu were transfected with multiple Cas9 plasmids using Lipofectamine 3000 to assess the IMhu immune response to the Cas9 sequence. On day one, coverslips were placed in a 24-well plate and sterilized with UV light for an hour. Then the coverslip-containing wells along with a 96-well plate were coated with human collagen I as per collagen-coating protocol (Chapter 2.2.2.3). Subsequently, IMhu were seeded into the collagen-coated 24-well and 96-well plates and incubated at 37°C for 24 hours. On day two, the cells were stimulated or transfected. Cells in the 24-well plate were transfected using 1.5 µl Lipofectamine 3000 and 1.5 µg SpCas9, NC, or GFP SpCas9 plasmid DNA, shown below (Fig. 32). Concentrations of Lipofectamine 3000 and plasmid DNA were scaled down accordingly for use in the 96-well plate (Chapter 2.2.2.13). Additionally, cells were incubated in the presence of 1.5 µg SpCas9 plasmid DNA without a transfection reagent. Stimulation controls included Poly I:C at 5 µg/ml and Imiquimod at

1µg/ml. Supernatant was sampled at 6, 12, 24, and 48 hours post-transfection from the 96-well plate. The supernatant was then stored at -80°C prior to cytokine assessment with HEK-Blue IL-6, TNFα, IL-1β, and IL-18 cell lines as per protocol (Chapter 2.2.3.5). The IMhu seeded in the 24-well plate were stained using the established ICC protocol (Chapter 2.2.5.1) using the secondary antibody Alexa fluor 568 donkey anti-mouse IgG at 24 hours post-transfection.

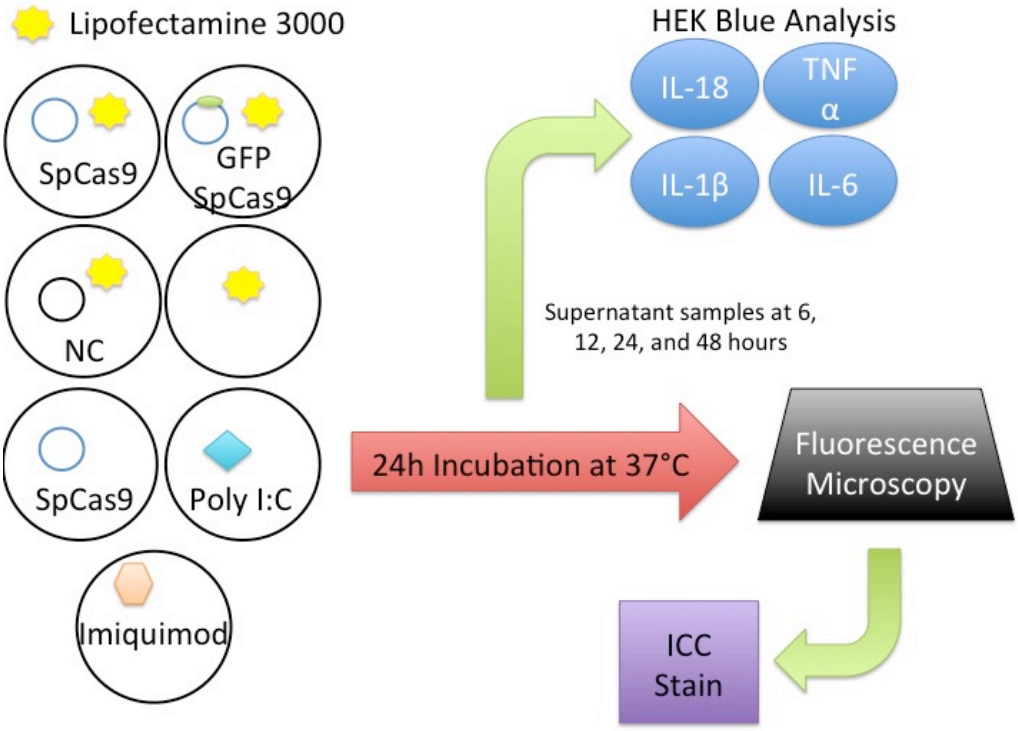

Figure 32: **Experimental Design for Transfection of IMhu with SpCas9 Plasmids using Lipofectamine 3000 with Supernatant Assessment.** IMhu were transfected with 1.5 µl Lipofectamine 3000 and 1.5 µg of an SpCas9 plasmid, a GFP SpCas9 plasmid, or a negative control plasmid containing the same sequence as the SpCas9 plasmid but lacking the SpCas9 sequence. Other IMhu were exposed to positive controls for cytokine production, and the cells were incubated for 24 hours prior to supernatant sampling, fluorescence microscopy, and ICC staining.
NC: Negative Control

At 24 hours post transfection, the cells transfected with the GFP SpCas9 plasmid were assessed for GFP expression using fluorescence microscopy and 25% of cells expressed a GFP signal. The cells were then fixed for ICC staining. Stained samples were assessed using fluorescence microscopy (Fig. 33). A Cas9 signal was positive in the GFP SpCas9 and SpCas9 samples fixed at 24 hours post-transfection. Cells transfected with the GFP

SpCas9 plasmid were 1-2% positively stained for SpCas9. 20% of IMhu transfected with the SpCas9 plasmid stained positively for SpCas9.

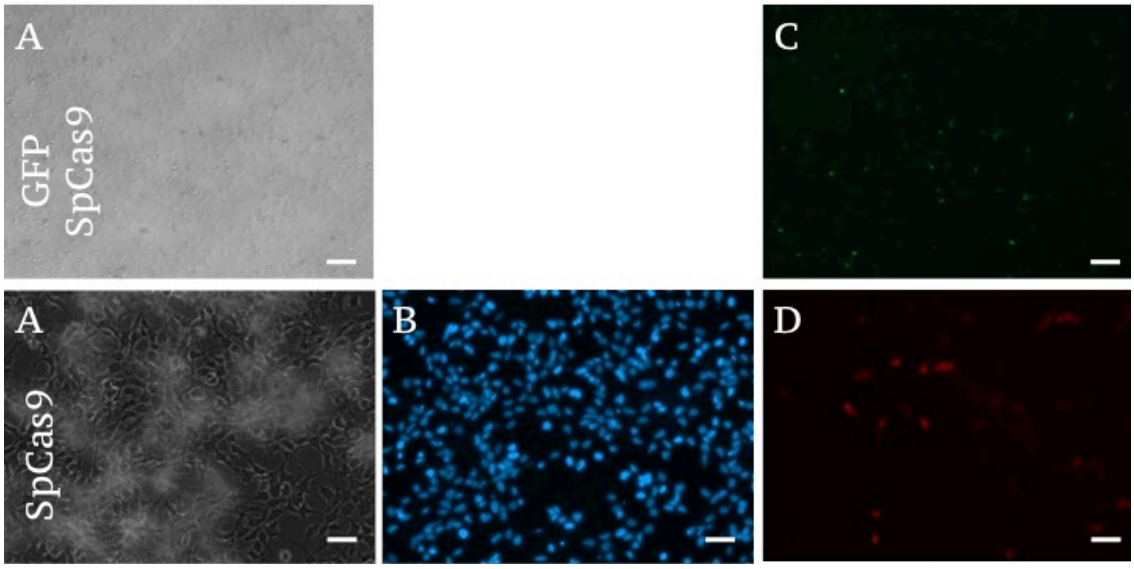

Figure 33: **IMhu Transfected with GFP SpCas9 Plasmid and SpCas9 plasmid and Fixed for SpCas9 Staining at 24 Hours Post-Transfection.** Cells were transfected with 1.5 µg GFP SpCas9 or SpCas9 plasmid DNA and 1.5 µl Lipofectamine 3000 per well in a 24-well plate. GFP SpCas9 fluorescence images (A, C) were captured at 24 hours post-transfection. Cells were fixed for ICC staining at 24 hours post-transfection. IMhu are viewed under brightfield (A) and fluorescence microscopy DAPI (B), GFP (C), and 568nm (D) channels. Scale bars: 100 µm.

Sampled supernatant was assessed for significant differences between experimental groups using Kruskal-Wallis tests.

In supernatant assessed for TNFα concentration Kruskal Wallis tests showed no significant differences between experimental groups in samples taken at 6 hours ($H(6)=12.16$, $p=0.058$), 12 hours ($H(6)=8.85$, $p=0.18$), and 48 hours ($H(6)=6.84$, $p=0.34$) post-stimulation. At 24 hours the differences in TNFα concentration between experimental groups were statistically significant ($H(6)=13.07$, $p=0.042$). Post hoc pairwise comparisons using Dunn's test with control for joint ranks and Bonferroni adjustment showed no significant differences in TNFα concentrations between groups (all ps>0.05).

In supernatant assessed for IL-18 concentration Kruskal Wallis tests showed no significant difference between experimental groups in samples taken at 6 hours

(H(6)=8.76, p=0.187), 12 hours (H(6)=10.15, p=0.119), and 48 hours (H(6)=11.71, p=0.069) post-stimulation. At 24 hours the differences in IL-18 concentration between experimental groups were statistically significant (H(6)=13.03, p=0.043). Post hoc pairwise comparisons using Dunn's test with control for joint ranks and Bonferroni adjustment showed that the IL-18 concentration of supernatant samples taken from cells stimulated with 5 μg/ml Poly I:C was significantly higher than that of cells exposed to the SpCas9 plasmid (p=0.033).

In supernatant assessed for IL-1β concentration Kruskal Wallis tests showed no significant differences between experimental groups in samples taken at 6 hours (H(6)=8.67, p=0.193), 12 hours (H(6)=11.83, p=0.066), 24 hours (H(6)=3.4, p=0.76), and 48 hours (H(6)=10.89, p=0.092) post-stimulation.

In supernatant assessed for IL-6 concentration Kruskal Wallis tests showed no significant differences between experimental groups in samples taken at 12 hours (H(6)=8.087, p=0.232), 24 hours (H(6)=6.68, p=0.35), and 48 hours (H(6)=6.23, p=0.4) post-stimulation. At 6 hours the differences in IL-6 concentration between experimental groups were statistically significant (H(6)=15.4, p=0.017). Post hoc pairwise comparisons using Dunn's test with control for joint ranks and Bonferroni adjustment showed that the IL-6 concentration of supernatant samples taken from cells stimulated with 5 μg/ml Poly I:C was significantly higher than that of cells exposed to the SpCas9 plasmid (p=0.027). The IL-6 values at 6 hours post-transfection are shown below (Fig. 34).

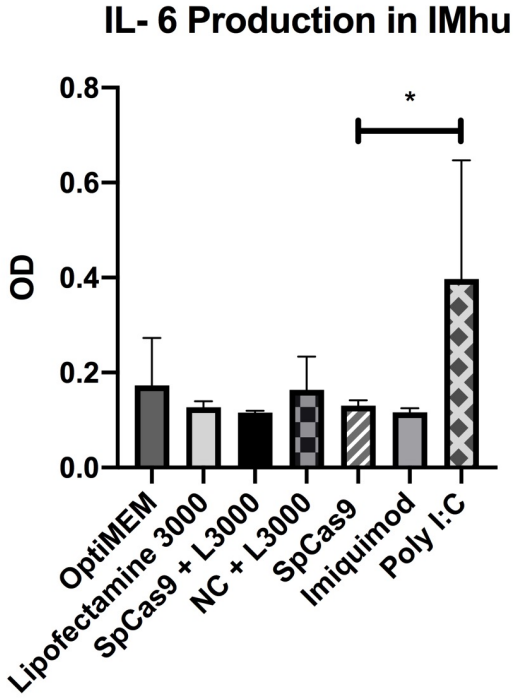

Figure 34: **Production of IL-6 in IMhu Transfected with SpCas9 Plasmid at 6h post-Transfection.** A significant production of IL-6 was recorded in response to stimulation with 5 μ g /ml Poly I:C (Dunn's Test p =0.027) when compared to cells exposed to the SpCas9 plasmid. Error bars indicate standard deviation.
L3000: Lipofectamine 3000
NC: Negative Control

3.9. PROTEOME PROFILER

To assess a broader array of cytokines potentially induced by Cas9 plasmid transfection, the Human XL Cytokine Array was used to analyze supernatant from transfected IMhu. On day one, coverslips were placed in the wells of a 24-well plate and sterilized with UV light for one hour at room temperature before collagen coating as per protocol (Chapter 2.2.2.3). IMhu were seeded in DMEM growth medium and incubated at 37°C for 24 hours. On day two, the cells were transfected using 1.5 at Lipofectamine 3000 and 1 µl Plus reagent per well. 1.5 µg DNA was added per well. IMhu were transfected with: GFP SpCas9 + Lipofectamine 3000, SpCas9 plasmid + Lipofectamine 3000, NC plasmid + Lipofectamine 3000, or only Lipofectamine 3000 (Fig. 35). See **Appendix A** for plasmid maps of the SpCas9 and NC plasmids. The cells were then incubated at 37°C for 24 hours. After 24 hours, 1 ml supernatant was removed and stored

at -80°C until assessment. The IMhu were assessed for GFP expression using fluorescence microscopy before staining using the established ICC protocol (Chapter 2.2.5.1) with 1:500 primary antibody and 1:500 Alexa Fluor 568 secondary antibody ratios.

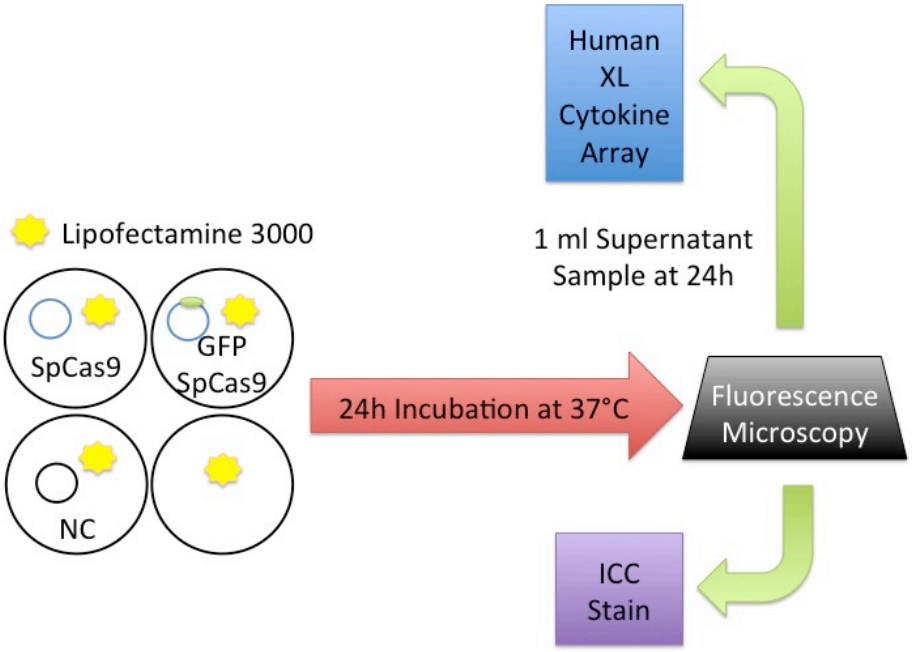

Figure 35: **Experimental Design for Transfection of IMhu with SpCas9 Plasmids using Lipofectamine 3000 and Supernatant Assessment with the Human XL Cytokine Array.** IMhu were transfected using 1.5 µl Lipofectamine 3000 and 1.5 µg of an SpCas9 plasmid, a GFP SpCas9 plasmid, a negative control plasmid, or only Lipofectamine 3000. The cells were incubated for 24 hours prior to supernatant sampling for analysis with the Human XL Cytokine Array and fluorescence microscopy and ICC analysis.
NC: Negative Control

This protocol was performed identically three times using separately thawed batches of IMhu to create biological triplicates. Fluorescence images of one batch of transfected and stained IMhu are shown below (Fig. 36). IMhu transfected with the GFP SpCas9 plasmid were transfected at a rate of 39%. 33% of cells transfected with the SpCas9 plasmid stained positively for SpCas9 with the Alexa Fluor 568 secondary antibody.

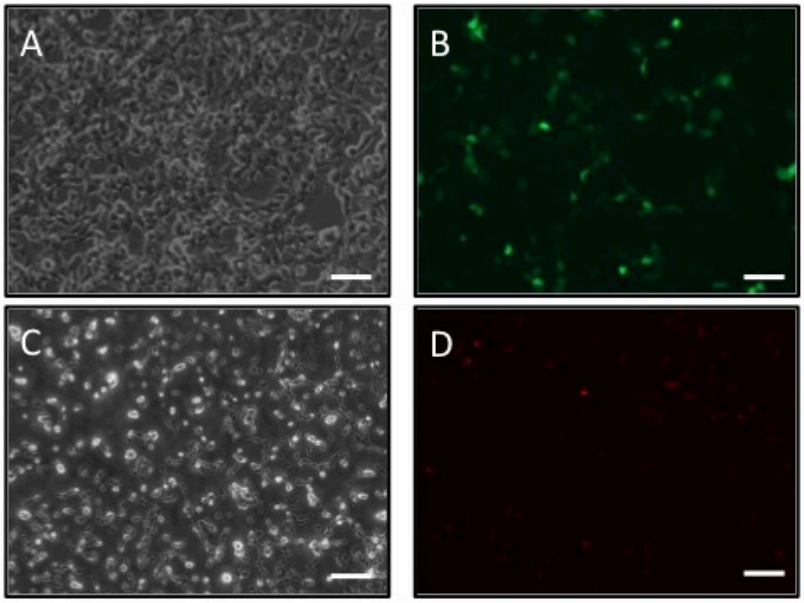

Figure 36: **IMhu Transfected with the GFP SpCas9 Plasmid or SpCas9 Plasmid and Fixed for SpCas9 Staining at 24 Hours Post-Transfection.** IMhu were transfected with 1.5 µg GFP SpCas9 (A, B) or SpCas9 plasmid (C, D) DNA and 1.5 µl Lipofectamine 3000 per well in a 24-well plate. GFP fluorescence images (A, B) were captured at 24 hours post-transfection, prior to fixation. IMhu are viewed under brightfield (A, C) and fluorescence microscopy GFP (B), and 568 nm (D) channels. Scale bars: 100 µm.

The sampled frozen supernatant was then assessed using the Human XL Cytokine Array as per manufacturer's protocol (Chapter 2.2.3.6). The results of all three repetitions were averaged for analysis (Fig. 37). Inter-group analysis of the NC, Spcas9, and Lipofectamine 3000 groups revealed no statistically significant differences in cytokine production between groups (all *p*s>0.05). Mann-Whitney tests were used to compare the cytokine concentrations between groups.

There was no statistically significant difference in cytokine values between SpCas9 and NC samples (U=4953, p=0.20), SpCas9 and Lipofectamine 3000 (U=4976, p=0.22), and NC and Lipofectamine 3000 (U=5479, p=0.94).

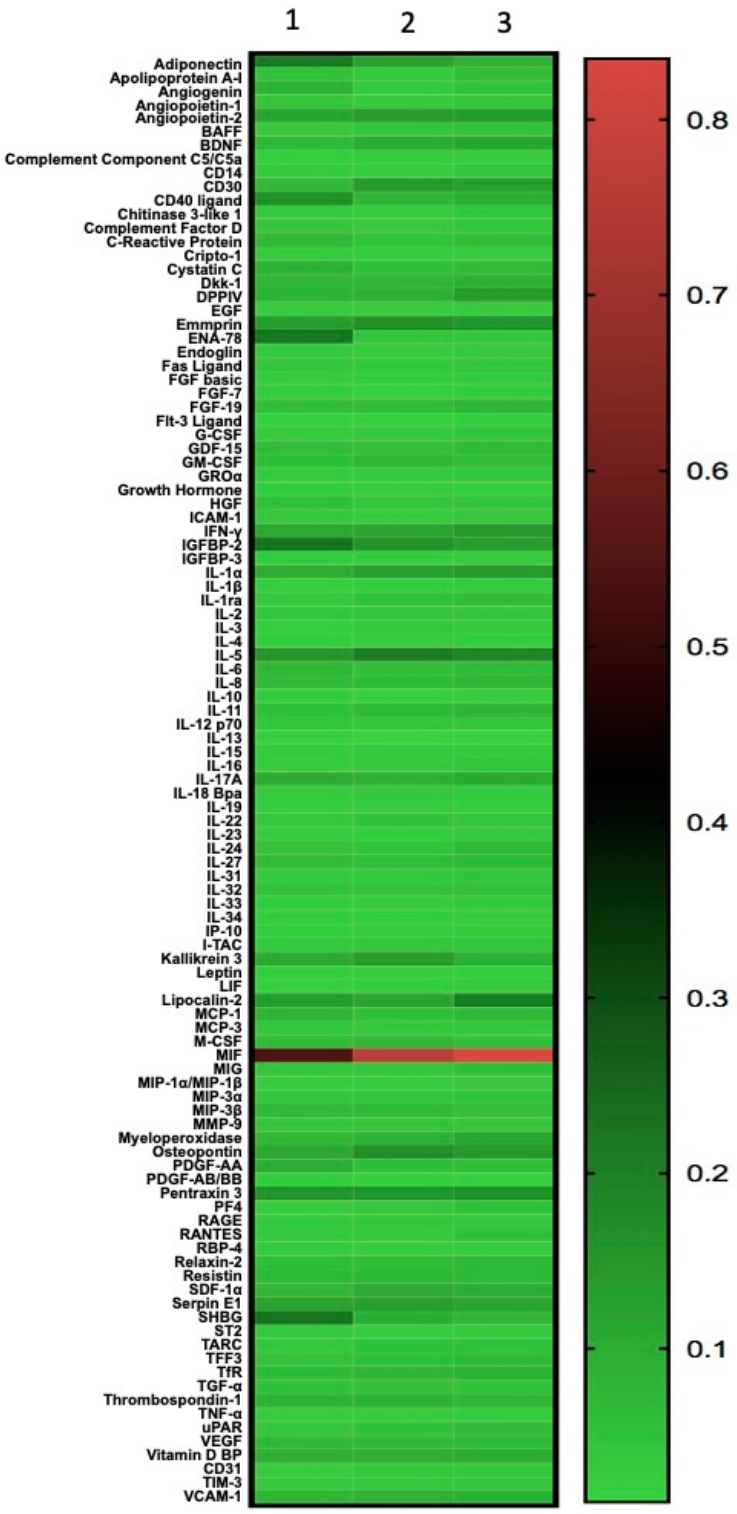

Figure 37**: Human XL Cytokine Array of Supernatant from Transfected IMhu.** Supernatant from IMhu transfected with the NC plasmid, the SpCas9 plasmid, or only exposed to Lipofectamine 3000 assessed via Human XL Cytokine Array. Pixel density of the dot-blot array was analyzed with Image J and the density was averaged (N=3). No significant difference in cytokine production was seen between any groups (Mann-Whitney tests all $p>0.05$).

1: Lipofectamine 3000 2: NC Plasmid 3: SpCas9 Plasmid

4. DISCUSSION

4.1 THP-1 CELLS

4.1.1 THP-1 CYTOKINE PRODUCTION

In contrast to reports of cytokine production in literature, a reduced capability to produce cytokines in response to immunostimulants was repeatedly measured in our THP-1 cell experiments.

It has been reported that THP-1 cells, with or without PMA differentiation to a macrophage-like phenotype, produce proinflammatory cytokines in response to stimulation with LPS. THP-1 cells differentiated with 20 μM PMA for 24 hours were shown to produce significant amounts of IL-6, IL-8, and TNFα at 6 to 48 hours post-stimulation with 1 or 2 μg/ml LPS [161]. THP-1 monocytes and macrophage-like cells (differentiated with 100 ng PMA for 48 hours) stimulated with 1 μg/ml LPS displayed a dramatic secretion of IL-6, IL-8, IL-10, TNFα, and IL-1β in a time-dependent manner, with cytokine concentrations increasing starting at one hour post-stimulation, continuing to 30 hours post-stimulation [162]. THP-1 cells have also been shown to express TLR9, and upregulate IL-8 mRNA in response to CpG ODN, indicating their capability to produce proinflammatory cytokines in response to stimulation with CpG ODNs [163]. Additionally, stimulation with LPS and ATP has been shown to activate caspase-1 and subsequent IL-1β production in PMA-differentiated THP-1 cells [164].

Our results showed that THP-1 cells differentiated with 500ng/ml PMA did not produce IL-1β in response to stimulation with 100ng/ml LPS with or without ATP stimulation (Chapter 3.2.2), contrasting the published reports of cytokine production in THP-1 cells following LPS stimulation. Additionally, THP-1 cells stimulated with CpG ODN, a TLR9 receptor antagonist, did not produce significant levels of Type I IFNs as expected (Chapter 3.2.1). These results may be contributed to many factors, including possible over-passaging, PMA concentrations of 500 ng/ml, instead of gentler PMA differentiation with lower concentrations, faulty cytokine measurement via HEK-Blue cells, or suboptimal concentrations of stimulants.

Cells which are over-passaged are subject to issues including genetic drift or selective culture pressures leading to altered function and are ultimately unreliable when compared to their low-passage counterparts [165]. While our protocols dictated that cells not be passaged excessively, it is possible that cell culture conditions played a part in the lacking cytokine production seen in our THP-1 cells, possibly due to phenotypic drift. Additionally, it has been shown that PMA concentrations used to differentiate THP-1 cells to a macrophage-like phenotype can alter the sensitivity of THP-1 cells to immunostimulants; reduction of the PMA concentration under 100 ng/ml (with concentrations as low as 5 ng/ml shown to induce stable differentiation) was shown to increase the immune reactivity of THP-1 cells, with up-regulation of TNFα production increased from 70- to 951-fold [96,97]. Ergo, our PMA concentrations of 500 ng/ml may have suppressed the immune reactivity of the THP-1 cells. Due to the lack of reliable protocols for THP-1 stimulation with CpG ODN, the manufacturer's recommendations were followed, though these concentrations may have been inefficient for THP-1 stimulation. Finally, in all experiments the HEK-Blue controls functioned as intended, indicating that the HEK-Blue cytokine measurements seen can be presumed to be accurate.

As results seen in THP-1 Dual cells were in line with what is expected for the cell line [NF-κB and IRF upregulation in response to CpG ODN and dsDNA, respectively (Chapter 3.3.1) as well as IL-1β production in response to LPS and ATP stimulation (Chapter 3.3.2)], it was concluded that the lack of a cytokine response measured in THP-1 cells was most likely due to suboptimal cell culture conditions, cell line degradation, or suboptimal immunostimulation protocols. The capability to directly analyze THP-1 Dual supernatant eliminated the need for HEK-Blue cytokine analysis and removed a potential source of contamination or errors. However, the up-regulation of the NF-κB and IRF pathways indicates pro-inflammatory activation, but it is not directly comparable to cytokine measurements in supernatant; these results do not indicate with certainty whether cytokines were ultimately excreted. Additionally, THP-1 Dual cells were stimulated in a monocytic state, whereas the THP-1 cells were stimulated as PMA-differentiated macrophages, which has been shown to affect cytokine production and inflammatory gene activation [162]. The results seen indicated a non-standard immune response of THP-1 cells to immunostimulants, the inability to effectively transfect the

cell line, however, meant that further investigation and troubleshooting were rendered irrelevant for the purposes of the current investigation.

4.1.2 THP-1 TRANSFECTION IS DEPENDENT ON PLASMID SIZE

To assess the innate immune responses to Cas9 expressed by THP-1 cells, said cells were to be transfected with plasmids containing Cas9. THP-1 cells were transfected using a wide variety of transfection reagents and methods, however, transfection in macrophage-like differentiated THP-1 cells has been described as very challenging, with high rates of cell death, and attempts made to overcome this effect have shown varying effectivity [159,166,167]

Liposomal transfection was initially attempted using a variety of cationic lipid transfection reagents (Chapter 3.4.1.1, Chapter 3.4.1.2, Chapter 3.4.1.3) with a final transfection efficacy of 1%. Electroporation (Chapter 3.4.2), showed initial rates of cell mortality near 100% with 0% of cells transfected, which could be improved to cell mortality of 20% and 1% transfected. Chemical transfection (Chapter 3.4.3.1, Chapter 3.4.3.2) yielded transfection rates of 1%. Lentiviral transduction (Chapter 3.4.5) led to no visible GFP signal at any time point post-transduction.

Finally, Nucleofection was used to transfect THP-1 Dual cells (Chapter 3.4.4). A transfection rate of 65% was reached, when transfecting THP-1 Dual cells with the Lonza GFP plasmid (4700 bp). To assess the efficacy of nucleofection, THP-1 Dual cells were also electroporated with the Lonza GFP plasmid, which led to a transfection rate of 2%, higher than previous electroporations performed using the same protocol at around 1%, indicating that the plasmid used was the deciding factor in the higher transfection rate seen (though monumentally lower than the 65% seen via nucleofection, confirming the efficacy of the transfection method). Nucleofection with larger plasmids (mKate: 6000 bp, mCherryCas9: 7400 bp) led to transfection rates of <1%.

Nucleofection and electroporation were shown to be effective in transfecting small plasmids (<5000 bp) in THP-1 cells, with recorded transfection rates over 80% via nucleofection. Transfection efficiency rapidly decreased in a manner dependent on plasmid size. The Lonza GFP positive control plasmid (4700 bp) was transfected at a rate of over 80%. Transfection with the mKate plasmid (6000 bp), mCherryCas9 plasmid

(7400 bp), and the GFP SpCas9 (9300 bp) resulted in transfection rates of <1%. Therefore, future experiments involving transfecting THP-1 cells with plasmids should be performed using electroporation or nucleofection, and would be advisable only if the plasmids were of a relatively small size (<5000 bp)- vital information, as published nucleofection protocols do not clearly describe this plasmid size-dependent transfection efficacy [166,168].

4.1.3 RAPID CAS9 PROTEIN DEGRADATION

To assess the immune responses of THP-1 cells to Cas9, THP-1 cells were to be transfected with Cas9 in protein form (Chapter 3.5). Due to initial difficulties with Cas9 protein transfection in THP-1 cells (Chapter 3.5.2), HEK cells were used as a substitute to establish transfection protocols.

HEK Blue cells electroporated with Cas9 protein and stained at one hour post-electroporation were 1% positive for a Cas9 signal; 0% of HEK cells stained at 3 hours post-electroporation expressed a Cas9 signal. This indicated that the time frame for intracellular Cas9 expression and staining in HEK cells might be well under an hour.

In the vein of this successful attempt, THP-1 Dual cells were electroporated with Cas9 protein and fixed for staining at 30 minutes, 45 minutes, 1 hour, and 1.5 hours post-electroporation. <1% of cells stained at 30 minutes post-electroporation expressed a Cas9 signal, all time points after 30 minutes showed no Cas9 signal-indicating a rapid degradation of Cas9 protein in THP-1 cells (Chapter 3.5.2.4). However, the repeated failure to transfect THP-1 cells with Cas9 protein considering previous successes, indicated that the previous Cas9 signals seen may have been due to an extraneous factor affecting all cells of the 30-minute samples, ubiquitous antibody uptake, or a high fluorescent background signal, rather than an intracellular Cas9 signal.

Cas9 delivery in its protein form is an exciting prospect for future therapeutic applications, and we have shown that Cas9 protein in THP-1 cells may be degraded within an hour of transfection, a testament to its transiency in target cells. This may make Cas9 proteins attractive for future gene editing therapies, as foreign DNA, for example Cas9 plasmids, may initiate longer lasting or stronger immune responses. Cas9 proteins, which are degraded quickly, may be able to avoid triggering these long-lasting responses by

quickly modifying the host genome in tandem with a gRNA, before being degraded by host cell defenses. The ultra-rapid degradation seen in our experiments may be unique to THP-1 cells, as macrophages have evolved to efficiently degrade intracellular proteins; it has been shown that macrophages degrade intracellular proteins so efficiently that these are not always able to be presented via MHC II [169]. This indicates that possible future Cas9 therapies may be challenging to effect in macrophages and macrophage-like cells. The benefits and drawbacks of Cas9 protein transfection versus Cas9 plasmid transfection are discussed below (Chapter 4.4.4.2)

4.2 IMHU CYTOKINE RELEASE CHARACTERIZATION

As the IMhu cell line is relatively unstudied, it was considered vital to establish baseline cytokine production in response to commercially available immunostimulants. As it stands, the cell line has already been characterized morphologically, its mortality in response to cytotoxic stimuli has been assessed, and cytokine-/chemokine-triggered cytokine production classified. The IMhu cell line has been shown to express typical leukocyte-derived cell type markers like P2RY12, TGFβR, and CD11b, physiologically seen on natural killer cells, monocytes, and macrophages, including primary microglia [104,105,170]. IMhu have been proven to react to proinflammatory cytokines including a mixture of TNFα, IL-1β, and IFNγ without increased toxicity, as well as displaying single-celled network morphology typical for microglia [105,171]. Primary and immortalized microglial cultures were also shown to display the same microglia-typical phenotype [104] Additionally, IMhu were shown to migrate over culture plates at rates similar to migration rates recorded in primary rabbit microglia, or approximately 20 to 27 μm/h, [104,172,173].

The characterization of IMhu cytokine production has shown that pro-inflammatory activation triggers the activation of the M1 phenotype in IMhu, inducing upregulation of the chemokines Vcam-1 and IL-8, and cytokines IL-32, IP-10, lipocalin-2, and IFNγ, a response similar to that characterized in primary human microglia [105,174]. IMhu respond to LPS stimulation similarly to primary microglial cells, with upregulated gene expression for IL-1β, IL-6, and TNFα, [104,175]. It has been shown that primary human microglia participate in inflammatory processes by secreting proinflammatory cytokines including TNF-α, IL-1β, IL-6, and IL-18 [176]. However, IMhu have not yet been fully assessed in terms of their cytokine responses to PRR ligands, a gap which this work aimed to fill.

To establish the baseline immune responses able to be produced by IMhu, cells were stimulated with a wide array of commercially available immunostimulants, and the resulting cytokine production was assessed (Chapter 3.7). The statistically significant (p<0.05) production of cytokines in response to stimulation with immunostimulants is summarized in the table below (Table. 4.7).

Stimulant	Pathway	IFN I/II	TNFα	IL-6	IL-1β	IL-18
dsDNA	CDS TLR9	-	-	+	-	-
CPG ODN	TLR9	-	-	-	-	-
Poly I:C	TLR3	+	+	+	-	+
Imiquimod	TLR7	+	-	+	-	-
LPS+ATP	Inflammasome	-	-	-	+	-

Table 4.2: **Cytokine Production in Stimulated IMhu Measured using HEK-Blue Cells or ELISA.**

CDS: Cytosolic DNA Sensors

The cytokine production seen in response to Poly I:C, LPS+ATP, and Imiquimod demonstrates that IMhu are immunocompetent and capable of producing innate immune responses in response to PAMPs and DAMPs via TLR3, TLR4, TLR7, and the NLRP3 inflammasome. This demonstrates morphological similarity to primary human microglia, which express all TLRs [177,178]. These results indicate the viability of the IMhu cell line as a model of human microglia like for the investigation of immune responses to Cas9 plasmids, though the lack of cytokine output seen to TLR9 and CDS stimulants poses additional questions.

The only response seen to an immunostimulant triggering TLR9 or CDS in IMhu was minimal IL-6 production in response to dsDNA transfection (Chapter 3.7.4). No other stimulatory trial in IMhu was able to induce cytokine production, in the cytokines measured, in response to a TLR9 or CDS stimulant or plasmid DNA. As there have been no investigations undergone as to whether the IMhu cell line expresses TLR9 or CDS, the cause of this lacking immune response remains to be seen. Primary murine and human

microglia, however, have been demonstrated to express TLR9 [177–180], indicating that a lack of TLR9 expression in IMhu would differentiate the cell line from primary microglia. One possible explanation for the lack of TLR9 response seen in IMhu in our experiments is that some studies have shown that additional cell stressors including Poly I:C, intermittent hypoxia, or LPS may increase or facilitate the expression of TLRs which may not always be constitutively expressed by primary microglia [181–183]. Further investigation of TLR9 expression in IMhu could include stimulation trials with additional cell stressors, or flow cytometry assessing for TLR9 expression, for example.

When investigating cytokine production in response to transfection Cas9 plasmids, a variety of PRRs must be brought into consideration as being potential effectors, as plasmid transfection leads to the production of mRNA and Cas9 protein, each component able to trigger various PRRs intra- and extracellularly. This means that though IMhu did not display typical responses to TLR9, their capability to respond to TLR3, TLR4, TLR7, and the NLRP3 inflammasome stimulants indicated their appropriateness for the assessment of the immunogenicity of many components of Cas9 plasmid-mediated gene therapies.

4.3 IMHU PLASMID TRANSFECTION DOES NOT UP-REGULATE CYTOKINE PRODUCTION

To assess the immunomodulatory effects of intracellular Cas9 and Cas9 plasmid expression in IMhu, IMhu first had to be efficiently transfected with plasmids. Initial transfection protocols with Lipofectamine 3000 were optimized through manipulation of the transfection reagent ratios, to increase the transfection efficiency of IMhu transfected with the GFP SpCas9 plasmid to 33% (Chapter 3.8.1).

IMhu were transfected with the GFP SpCas9 plasmid, the SpCas9 plasmid, the NC plasmid, or only exposed to Lipofectamine 3000 (Chapter 3.8.2). Poly I:C and Imiquimod served as positive controls for IMhu cytokine production. Supernatant samples were assessed using HEK-Blue cells for IL-6, TNFα, IL-1β, and IL-18. 20% of IMhu transfected with the SpCas9 plasmid were positively stained for Cas9 when fixed for staining at 24 hours post-transfection, indicating that the cytokine production seen could be assessed as being affected by cells expressing the SpCas9 plasmid. There was a significant production of IL-18 seen in response to stimulation with Poly I:C when

compared to cells exposed to SpCas9 (Dunn's test p=0.033). Significant production of IL-6 was seen in response to stimulation with Poly I:C when compared to cells exposed to SpCas9 (Dunn's test p=0.027). No other significant cytokine responses were measured in any cytokine in response to any transfection sample (all ps>0.05).

The Human XL Cytokine Array was used to assess the relative amount of production of 105 human cytokines in supernatant sampled from IMhu transfected with the SpCas9 and NC plasmids (Chapter 3.9). The lack of cytokine production of the selected cytokines evaluated above indicated that a broad net should be cast to assess if there was any up- or down-regulation in cytokine production in response to transfection with plasmid DNA. IMhu were transfected with GFP SpCas9 + Lipofectamine 3000, SpCas9 + Lipofectamine 3000, NC plasmid + Lipofectamine 3000, or only Lipofectamine 3000. Supernatant was sampled and the GFP signal was identified using fluorescence microscopy at 24 hours post-transfection. The cells were additionally fixed for ICC staining at this time point, which allowed for confirmation of an intracellular SpCas9 signal in the cells transfected with the SpCas9 plasmid.

Sampled supernatant was analyzed using the Human XL Cytokine Array. Analysis revealed that there was no significant up- or down-regulation of cytokine production in any of the 105 human cytokines evaluated when comparing the Cytokine Profiler results of cells transfected with the SpCas9 or NC plasmids to cells only exposed to Lipofectamine 3000 (Mann-Whitney tests, all ps>0.05). In addition, cells transfected with the SpCas9 plasmid did not significantly up- or down-regulate cytokine production in comparison to the cells transfected with the NC plasmid (U=4953, p=0.20). This lack of up- or down-regulation of cytokine production in response to plasmid transfection reinforced the results of the previous experiment: IMhu cells do not up-regulate cytokine production in response to transfection with SpCas9 plasmids and SpCas9 expression. IMhu also do not up-regulate cytokine production in cells transfected with non-Cas9 plasmids.

This lack of cytokine production in response to transfection with any plasmid: SpCas9, GFP SpCas9, or NC, mirrors the previously seen lack of cytokine production in IMhu in response to plasmid DNA. This also correlates with the above-mentioned lack of robust TLR9 or CDS-mediated cytokine production, indicating that IMhu may not

respond to dsDNA with the production of cytokines, which may minimize the significance of the lack of recorded cytokine production in IMhu post-transfection, as the cells may lack the rudimentary capability to mount robust immune responses to dsDNA, unlike their primary counterparts. Alternatively, the result might be interpreted as being reassuring, indicating that primary microglia may not be effectors of innate immune responses when transfected with Cas9 plasmids. However, as primary microglia have been shown to produce cytokines including TNFα, IL-1β, IL-6, and IL-12 in response to CpG ODN stimulation [179,184], the lack of cytokine production in IMhu in response to Cas9 plasmid transfection may indicate a deficiency of the cell line as a microglial model, rather than being a positive indicator of the successes of future ophthalmological gene editing therapies.

4.4 Limitations of the Study

4.4.1 The IMhu Cell Line as a Model of CNS Macrophages

Our investigations were performed using IMhu; in addition to the characterization of the IMhu cell line discussed above, cell lines designed as microglia-like cells have been assessed for their similarity to primary microglia.

Parenchymal microglia have been found to express the surface markers CD11b+ and CD45low, which distinguishes them from other CNS macrophages [185]. Immortalized human microglia have been shown to express the markers CD11b+, CD68, and CD86 (B7-2) [186], indicating their phenotypical similarity to primary microglia. Immortalized microglia have been shown to produce a similar cytokine response to immune stimuli as that of primary microglia, however their response is muted and the excreted cytokines are not as varied as in primary microglia [103]. Therefore, while immortalized microglial cell lines including IMhu display microglia-typical surface markers and can produce cytokines in response to immune stimuli, they may lack certain microglia-typical capabilities. This is a widely acknowledged shortcoming of using immortalized cell lines and limits the range of applicability of results gained when analyzing cell lines.

Immortalized cell lines offer advantages in ease of use, ease of procurement, and providing a stable population of cells developed under controlled circumstances. However, cell lines may display altered phenotypical traits or cell function due to genetic

manipulations during immortalization or serial passaging, as well as contamination with mycoplasma or other cell lines [187]. In addition, culture protocols differing between labs or gradual genomic drift of the cell line may lead to inconsistent results in experiments within one cell line.

The nature of cell culture- isolation of a specific cell type, dictates that the physiological interactions between microglia and the surrounding CNS milieu cannot be assessed when using IMhu. CNS exposure may mold microglia, making the attractivity of primary cells even more prominent. Efficient methods of microglia production from induced pluripotent stem cells have been developed [188], however, these cell lines also lack exposure to the CNS milieu and there is a lack of consensus on production methods as the field is new and rapidly expanding. Primary human microglia may be obtained from fetal abort tissue or post-mortem specimens [189], though acquiring such tissue is challenging, acquiring healthy CNS tissue even more so, and one has little to no control over the ante-mortem conditions. This limits the availability of primary human microglia; though primary animal microglia are more readily available, with post- and ante-mortem conditions being more easily controlled, there have been demonstrated differences seen between human and animal primary microglial cells.

Human microglia have been demonstrated to share a conserved core gene program of orthologous genes between rodents and humans as well as similar phenotypical states; however, human microglia typically demonstrate a heterogenous transcriptional state, whereas most animal microglia display a single dominant transcriptional state [190]. Additionally when compared to primate microglia, rodent microglia showed discrepancies in the presence of complement, phagocytic, and neurodegeneration susceptibility genes [190]. Human microglia have also been shown to react differently to Amyloid than murine microglia, with human microglia from AD brains showing an increased a transcriptional program steered by regulatory factor 8 in response to amyloid exposure, a reaction which was downregulated in murine AD model microglia [191]. Murine microglia also age differently than human microglia, with global gene expression from postmortem human samples displaying distinguishing gene expression between samples from donors of different ages, with minimal overlap seen in the gene expression development between humans and mice; ultimately though, the expression profiles

between human and murine microglia measured remained extensively overlapping, reassuring that murine microglia may remain adequate models for disease processes not directly related to aging or neurodegeneration [192].

In general, one may conclude that while the IMhu cell line does not behave identically to primary human microglia, its convenience in culturing and acquisition and its microglial markers and characteristics make it a suitable model for initially investigating microglial immune responses in vivo, prior to advancement to more complex methodological models.

4.4.2 Immune Responses of Cells in Isolation

The immune response triggered by individual cells is tied to their environment and the extracellular milieu. For example, it has been shown that murine microglia require the presence of LRRC33 to express TGF-β [193]. Additionally, microglial priming with inflammatory cytokines molds the microglial cytokine response [175], which indicates that cytokine production from other ocular cells during inflammatory processes including IRD might modify the microglial immune response to Cas9 transfection.

It has been shown that degenerative disorders of the retina including IRD lead to an accumulation of macrophages in the vitreous as well as increased concentrations of proinflammatory cytokines including TNFα, IL-1, IL-8, and IL-6, with the retinal microglia and RPE proposed as being the main sources of immunomodulatory factors [194]. Specific disease states have been described to display various inflammatory profiles, with increased microglial and macrophage activation as well as increased cyto-/ and chemokine concentrations found in human RP patients[195]. This inflammatory state may either be a consequence of or the cause of the RP disease process, with microglial activation seen as a response to photoreceptor cell death, an effect which has been shown to be lacking in NLRP3-deficient murine strains, indicating a link to the NLRP3 inflammasome in the phagocytosis of PR in RP and the importance of the inflammasome in mediating microglial activation in IRD [195]. The evidence of the modification of cytokine production in microglia in response to extracellular factors, and the presence of abnormal ocular states in IRD, indicates that an assessment of cytokine production of IMhu in isolation may not accurately represent the behavior of primary microglia in the optic milieu, especially in IRD. These facts may limit the impact of the results measured

by this investigation, especially when planning future gene therapies, which will most likely be applied in the diseased retina which often displays inflammation-induced modifications to the cytokine milieu.

Additionally, activated microglia have long been considered to be able to differentiate into M1 and M2 phenotypes, producing either pro-inflammatory or anti-inflammatory cytokines and immune responses [196]. However, in a diseased model the distinction between M1 and M2 is often blurred, with macrophages present in heterogeneous activation patterns [197,198]. The effects of differentiation into the M1 or M2 phenotype was not assessed in our experiments, and the impact of possible heterogenous M1/M2 expression in diseased models, including IRDs, was also not able to be assessed. The CNS milieu in degenerative diseases may alter the cellular immune response in microglia, including cytokine production and M1/M2 differentiation, and these relationships should be further elucidated to develop targeted ophthalmological gene therapy.

4.4.3 Cytokine Production Assessment

We investigated the innate immune response to SpCas9 by assessing cytokine production in samples of supernatant at various time points post-transfection. One limitation of our investigation was that cytokine production could not be measured continuously but only at various time points post stimulation. These time points were chosen based upon prior literature describing cytokine production in macrophages [100], but are still a limiting factor in interpreting the results as the minute dynamics of cytokine production could not be assessed. Additionally, supernatant sampling at various time points led to lower absolute amounts of supernatant during later sampling time points, which may have created additional cellular stress.

Moreover, cells were kept in culture for 24 to 48 hours without supernatant refreshment, and for some experiments, cultured in OptiMEM, a reduced serum medium which may have served as an additional cellular stressor. Reduced serum medium has been demonstrated to stress cells, for example: human lung epithelial cells cultured in reduced-serum OptiMEM medium were shown to display decreased cell viability when compared to cells cultured in DMEM from 24 hours of culture onwards, as well as displaying dysregulated levels of heat shock 70kDa protein 5, intracellular channel protein 1, and proteasome subunit alpha Type 2, indicating cellular stress and

destabilization [199]. Due to the experimental design, though, these factors were non-mitigatable, as reduced serum medium has been described as providing optimal conditions for transfection [200]. However, all experimental groups were cultured under the same conditions, indicating that the possible additional stressors became irrelevant when comparing differences in cytokine production between experimental groups, as all groups were cultured identically.

In addition to potential challenges posed by experimental design, one must consider the significance of cytokine measurements as a measure of cellular immune responses. Immune responses consist of cytokine production, activation of the complement cascade, activation of the adaptive immune system through antigen presentation, and phagocytosis of foreign substances by macrophages, among other things. By investigating only cytokine production, the other portions of the innate immune response to Cas9 were not quantified, and the adaptive immune response and its effects on the universal immune response were also not considered. The limited nature of this study means that the results necessitate further, broader assessments to investigate ocular immune responses to Cas9 more completely, though some work has already been undertaken.

Assessments of adaptive immunity in humans against Cas9 showed pre-existing systemic antibodies against SpCas9 and SaCas9 with accompanying anti-Sp- or anti-SaCas9 T cells evident in human donors [143,144]. In a non-human primate (NHP) trial, Systemic AAV-neutralizing antibodies (NAB) correlated to NAB concentration in the vitreous fluid, with NAB presence correlating with reduced or deficient transgene expression after intravitreal AAV application [201]. These results may indicate that Cas9 therapies applied intraocularly might lead to the production of intraocular and systemic antibodies against Cas9, which may act in combination with pre-existing Sp- or SaCas9 antibodies to threaten the efficiency and longevity of retinal gene therapies utilizing Cas9. The evidence of possible adaptive immune responses to Cas9 increases the import of assessing the holistic immune response to Cas9, in addition to the assessment of cytokine production in microglia in response to plasmid transfection, to fully assess the immunogenic potential of Cas9 plasmids.

4.4.4 PLASMID CAS9

4.4.4.1 The Choice of Cas9 Orthologue

We investigated the immunogenicity of Cas9 isolated from *Streptococcus pyogenes*. SpCas9 is the most widely adopted and utilized Cas9 orthologue, due in part to the fact that it was the first Cas9 used to cleave a targeted region of the human genome [202]. In addition, SpCas9 is considered attractive due to its protospacer adjacent motif (3' NGG), which allows for a wide variety of target sequences. However it has been shown that SpCas9 can also bind to 3'NAG and NGA, which may lead to off-target cleavage [203]. The size of the SpCas9 sequence (4.2kb) may also hinder transport and packaging in therapeutic applications.

Other smaller orthologues may become therapeutically relevant, including SaCas9 (1,053 bp) and CjCas9 (984 bp), as they may prove easier to package for transport to target cells due to their significantly smaller size when compared to SpCas9 plasmids [204]. SaCas9 has been shown to display comparative levels of gene targeting in comparison to SpCas9, can effect genome editing with specificity, and is small enough to be delivered via a single AAV vector [205]. However, when compared to SpCas9, SaCas9 requires a longer PAM sequence, potentially limiting the targets modifiable by SaCas9 [204]. SaCas9 has already been applied to murine trials, generating knock-in modifications efficiently, with similar efficiencies as seen in SpCas9-modified targets [204,206]. CjCas9 has also been successfully implemented to edit mammalian cells in vitro and in vivo, displaying efficient indel mutagenesis in both RPE and muscle cells when delivered via AAV [207]. Additionally, CjCas9 displays similar cleavage efficiency and off-target mutagenesis to SpCas9 and SaCas9 [204].

Initially, a CjCas9 plasmid was designed and modified with the intention of assessing innate immune responses to CjCas9, a goal hindered by the lack of available antibodies to CjCas9, and therefore the inability to confirm plasmid expression post-transfection. However, the immune responses to CjCas9 and SaCas9, among other Cas9 orthologues remain highly relevant to the future implementation of Cas9 orthologues for in vivo gene editing and should therefore be further elucidated, as the challenges facing SpCas9 plasmid utilization (plasmid size) may lead to the more widespread adoption of other Cas9 orthologues for gene editing therapies.

4.4.4.2 Isolated Plasmid Cas9 Assessment

This investigation primarily aimed to assess innate immune responses to Cas9 plasmids. This meant that the immunogenicity of other aspects of potential gene therapies were not evaluated, including gRNAs. Delivering Cas9 in plasmid form necessitated the creation of a "negative control" plasmid, and it was endeavored to create a plasmid as similar to the Cas9 experimental plasmid as possible; a plasmid which was identical except for the fact that it lacked the Cas9 sequence. This plasmid was created, but due to the missing Cas9 sequence, was smaller in size than the experimental Cas9 plasmid. Plasmid size was proven to be key in effecting THP-1 transfection rates, and the role it might play in effecting an innate immune response must be considered.

Electroporation with large plasmids, when compared to their smaller counterparts, was shown to decrease cell viability in a manner not related to transgene expression [208]. Additionally, smaller plasmids have been demonstrated to have higher transfection efficacy and intracellular persistence [209] which might facilitate an increased immune response to smaller plasmid transfection, due to higher total concentrations of plasmids transfected and present intracellularly. To overcome the size discrepancy, the creation of a plasmid with a nonsense stuffer sequence in the place of the Cas9 sequence was considered, but ultimately not performed, as the immunogenicity of the stuffer sequence was a potential concern and unable to be controlled for.

Additionally, Cas9 application in protein form is another possible method of Cas9 gene editing, which may be applied to future therapies. Cas9 proteins were utilized in THP-1 and HEK transfection trials, but their immunogenicity could not be accurately assessed due to the challenges faced during transfection and validation of intracellular

proteins. Ultimately, however, successful expression of the Cas9 transgene implies the presence of intracellular Cas9 plasmid DNA, RNA, and proteins. In this way, an indirect analysis of the immunogenicity of Cas9 proteins in IMhu cells was performed.

In clinical applications involving Cas9 proteins, a Cas9 protein, and therefore an immune stimulus, may be present intracellularly for a shorter period than during Cas9 plasmid trials, due to the high level of transience of transfected Cas9 proteins in cells. Cas9 ribonucleoproteins (RNPs) are generally present in cells for under than 24 hours, with the majority of indels seen at 3 hours post-transfection, whereas plasmid DNA is generally present intracellularly for up to 72 hours post-transfection [210,211]. The disparity in intracellular Cas9 presence and expression between proteins and plasmids implies the possible stimulation and activation of varying immunological processes. Additionally, in PBMCs, the STING-STAT6 pathway has been implicated in the production of immune responses to Cas9 proteins [147]. The release of the proinflammatory mediators MPO, CD40L, and MIP3α was inhibited via STING-STAT6 inhibition [147]. These results are relevant to the investigation of microglial immune responses, due to the functional similarities of systemic mononuclear cells and microglia when pertaining to the expression of the cGAS-STING pathway, indicating that microglia may also be susceptible to STING-STAT6-induced immune responses to Cas9 proteins [212].

gRNAs have also been shown to induce a type I IFN response in human cell lines and primary hematopoietic cells, when containing 5'-triphosphate, effecting increased cell death [142]. Ultimately, all functional parts of CRISPR/Cas therapies, including Cas9-plasmids, -proteins, -gRNA, and -delivery modalities may induce an immune response which may lead to cellular damage, the loss of tissue function, and other detrimental effects, and their immunogenicity must be further elucidated to increase the safety of CRISPR/Cas therapies.

4.5 FUTURE WORK

4.5.1 IMHU ASSESSMENT

The lack of a microglia-typical response to TLR9 and CDS stimuli raised the question of IMhu suitability as a model of human microglia regarding immune responses to DNA. To assess whether IMhu display the typical microglial TLR9 receptor, anti-TLR9

antibodies could be utilized to validate the presence or lack of TLR9 receptors on IMhu cells, via IHC or flow cytometry, for example. The presence of CDS could be assessed via evaluation of cGAS or STING presence, also per antibody-mediated signaling utilizing IHC or flow cytometry.

4.5.2 CAS9 PROTEINS

The highly transient nature of Cas9 proteins transduced directly into target cells makes them exciting for prospective gene therapy applications. If, as our findings suggest, Cas9 protein is present intracellularly at 30 minutes post-transfection and then rapidly degraded in THP-1 cells, this is highly relevant to future therapies involving Cas9 proteins. Our findings correlate to the description that Cas9 RNPs were active in HeLa cells for up to 3 hours post-transfection, with targeted cleavage beginning at 5 minutes post Cas9 RNP transfection [213].

Our findings indicate that RNPs may be active for an even shorter amount of time in macrophage-like cells. Further assessment the dynamics of cells transfected with Cas9 proteins may aid in the development of highly targeted and time-limited therapies. The dynamics of Cas9 protein transfection could, for example, be assessed using a variety of macrophage-like cell lines (THP-1, IMhu) and primary macrophages (PBMCs) modified by active fluorescent-tagged Cas9 RNPs. Fluorescent-tagged Cas9 RNP presence could then be assessed via fluorescence microscopy or flow cytometry, thus eliminating cell staining as a possible source of experimental error. RNP-mediated cleavage could be assessed over time via PCR amplification of target sequences isolated from modified cells, for example.

The apparent rapid degradation of DNA or Cas9 proteins in THP-1 cells may make systemic macrophages less attractive targets for future plasmid-based gene therapies, though protein-based approaches may potentially be more effective than plasmid-based approaches, as they potentially require shorter amounts of time to effect gene modification. The further assessment of Cas9 protein dynamics in macrophage-like cell lines and PBMCs would aid in designing macrophage-targeted gene therapies.

4.5.3 In Vivo Assessments/Adaptive Immune System

The results of our study may play a small part in the holistic assessment of Cas9 immune responses, providing one part of the larger immunological puzzle posed by potential gene editing strategies. For reference, reports of long-term sustained CRISPR/Cas mediated gene editing have been made in animal models for DMD, demonstrating sustained gene editing for one year post-editing [148], CRISPR/Cas9 correction was sustained for over 200 days in murine models of hemophilia B [2]. In addition to these trials, ocular CRISPR/Cas therapies and their immune responses and longevity should also be assessed in vivo.

To continue identifying which individual components of CRISPR/Cas9 gene editing may instigate an immune response, in vivo assessment, initially in murine models, which have been shown to contain microglia similar to human microglia, of ocular Cas9 plasmid transfection should be attempted. This would facilitate the assessment of the innate as well as the adaptive immune responses. One method of application might include AAV-mediated Cas9 transport, either with coupled AAV vectors to carry SpCas9 or single AAV vectors transporting a smaller Cas9 orthologue, like Sa- or CjCas9. Systemic and ocular cytokine production, and proinflammatory mRNA upregulation could be measured, for example, along with flow cytometric assessment of MCH I/II upregulation and antibody production assessment to evaluate the adaptive immune responses in systemic and ocular samples. The dynamics of possible immune responses could also be assessed with various samples taken from animals at multiple time points post-Cas9 application, or with ocular samples taken from various subjects at differing time points. These in vivo assessments would facilitate the assessment of immune responses in relation to the CNS milieu, which plays a key role in the modification of immune responses in the CNS, painting a more complete picture of microglial and ocular and CNS immune responses to Cas9.

4.5.4 Assessing Modified Cells

Ultimately, once the immunogenicity of individual components of gene therapy has been elucidated, one must assess the longevity and lasting modifications made to cells which have been modified by CRISPR/Cas systems to assess the effectivity of the gene therapy. The CRISPR/Cas-mediated modification of these cells must be quantifiable and the modification able to be assessed over time to quantify the final benefit gained or treatment effected. Ideally this analysis would take place in an in vivo study capable of accurately representing the human CNS milieu, initially murine models, over a period of time long enough to assess the longevity of the Cas9-induced modifications, with measurements of CRISPR/Cas modification and cell viability at various time points during the study, facilitating the assessment of the dynamics of Cas9-mediated modifications in vivo.

4.6 Take Home Message

Ultimately, valuable insights were gained into cellular macrophage models and cytokine production in response to Cas9. We were able to describe a direct relationship between transfection efficacy and plasmid size in THP-1 cells, which may limit their effective use in further investigations involving the transfection of larger (>4kb) plasmids. IMhu cells were shown to produce typical cytokines in response to PAMPs and DAMPs via TLR3, TLR4, TLR7, and the NLRP3 inflammasome, an indicator of their suitability as a cellular model of human microglia. However, IMhu were demonstrated to lack a microglia-typical response to TLR9 and CDS stimuli, indicating a possible significant dissimilarity of the cell line to primary human microglia. Finally, IMhu were shown to be unresponsive to Cas9 plasmid transfection, showing neither up- nor downregulation of cytokine production. This result may be interpreted a positive predictive factor for the successes of future microglial gene editing therapies. Alternatively, the predictiveness of this result may be limited by the IMhu cell line's lack of responses to CDS and TLR9 stimuli, indicating a possible microglia-non-typical inability to react to plasmid DNA. All in all, further investigations of Cas9 plasmid-mediated immune responses in microglial cells are required, to continue the process of assessing threats to future Cas9-mediated ocular gene editing therapies.

5. ABSTRACT

5.1 ABSTRACT

Aims

Inherited retinal diseases (IRD) lead to over 2 million cases of blindness worldwide. Targeted gene therapies utilizing CRISPR/Cas9 aim to treat IRD through the repair of underlying mutations. To improve the safety and efficacy of Cas9 therapies, innate immune responses to Cas9 must be assessed. This thesis aims to evaluate the immune response to Cas9 plasmids in models of central nervous system (CNS) macrophages, to improve the safety of ocular Cas9 gene therapies.

Methods

THP-1 cells and Immortalized human microglia SV40 (IMhu) served as models of systemic and CNS based macrophages, respectively. Model cells were stimulated with plasmids, Cas9 in protein form, or commercial immunostimulants, and cytokine production was measured in the supernatant using HEK-Blue reporter cells, ELISA, or the Human XL Cytokine Array. Statistical analyses were performed using One-way ANOVA or Kruskal-Wallis tests with post hoc testing using Tukey's or Dunn's tests.

Results

THP-1 cells nucleofected with a Lonza GFP plasmid (4700 bp) showed a 65% rate of transfection. Plasmids over 5000 bp were nucleofected at rates below 1%. IMhu stimulated with: dsDNA produced IL-6 ($p<0.05$), Poly I:C produced IFN I/II, TNFα, IL-6, and IL-18 (all $p<0.05$), Imiquimod produced IFN I/II and IL-6 (all $p<0.05$), and LPS+ATP produced IL-1β ($p= 0.046$). There was no up- or down-regulation seen in cytokines produced by IMhu transfected with Cas9, or negative control (NC) plasmids when compared to IMhu only exposed to Lipofectamine 3000 or when comparing Cas9 plasmid-transfected cells to NC-transfected cells when analyzed using the Human XL Cytokine Array for 102 human cyto- and chemokines (all $p>0.05$).

Conclusions

THP-1 cells can be effectively transfected using nucleofection and plasmids under 5000 bp. IMhu produced significant amounts of cytokines in response to immunostimulants, establishing their immune competence. IMhu showed no up- or down-regulation of 102 assessed human cyto- or chemokines in response to Cas9 or NC plasmid transfection. This lack of a cytokine response to Cas9 indicates that human microglia may be appropriate targets for gene therapy via Cas9. It also indicates that microglia may not be the effectors of an innate immune response to gene therapies in other cells. Further analysis of the CNS immune response, including the adaptive immune response, to Cas9 gene therapies will help to assess the safety and longevity of CRISPR/Cas9 therapies more thoroughly.

5.2 ZUSAMMENFASSUNG

Fragestellung

Vererbte Netzhauterkrankungen (IRD) verursachen weltweit über 2 Millionen Blindheitsfälle. Gezielte Gentherapien mit CRISPR/Cas9 zielen darauf ab, IRD durch gezielte Reparatur zugrunde liegender Mutationen zu behandeln. Um die Sicherheit und Wirksamkeit von Gentherapien mit CRIPSPR/Cas9 zu verbessern, müssen Immunantworten auf Cas9 evaluiert werden. Das Ziel dieser Arbeit ist die angeborene Immunantwort auf Cas9-Plasmide in zellulären Modellen von Makrophagen des Zentralnervensystems (ZNS) zu bewerten, um die Sicherheit von okulären Cas9-Gentherapien zu verbessern.

Methodik

THP-1-Zellen und immortalisierte menschliche Mikroglia SV40 (IMhu) dienten jeweils als Modelle für systemische Makrophagen und CNS Makrophagen. THP-1-Zellen oder IMHu wurden mit Plasmiden, Cas9 in Proteinform oder kommerziell erhältliche Immunostimulanzien stimuliert und die Zytokinproduktion im Überstand unter Verwendung von HEK Blue-Reporterzellen, ELISA oder des Human XL Cytokine Array bewertet. Statistische Analysen wurden mittels One-way-ANOVA- oder Kruskal-Wallis-Tests mit post-hoc Tukey- oder Dunn-Tests durchgeführt.

Zusammenfassung der Ergebnisse

THP-1-Zellen, die mit Plasmiden oder Cas9-Protein unter Verwendung mehrerer Transfektionsmethoden transfiziert wurden, erzielten Transfektionsraten unter 2%. Die Nukleofektion mit einem Lonza GFP-Plasmid (4700 bp) ergab eine Transfektionsrate von 65%. Plasmide über 5000 bp wurden mit Raten unter 1% nukleofiziert. Mit dsDNA stimulierte IMhu produzierten IL-6 (p<0,05). Mit Poly I: C stimulierte IMhu produzierten IFN I / II, TNFα, IL-6 und IL-18 (alle p <0,05). Mit Imiquimod stimulierte IMhu produzierten IFN I / II und IL-6 (alle p <0,05). Die Stimulation mit LPS + ATP führte dazu, dass IMhu eine signifikante Menge an IL-1β produzierten (p=0.046). Es wurde keine Auf- oder Abregulierung von Cyto- und Chemokinproduktion bei mit Cas9 transfizierten IMhu oder bei mit dem negativen Kontrollplasmid (NC) transfizierten IMhu festgestellt, im Vergleich zu IMhu die nur Lipofectamin 3000 ausgesetzt waren

(alle p>0.05). Es wurde auch keine Auf- oder Abregulierung der Cyto- und Chemokinproduktion beim Vergleich von mit Cas9-Plasmiden transfizierten Zellen und mit NC-transfizierten Zellen bei der Analyse unter Verwendung des Human XL Cytokine Array für 102 humane Cyto- und Chemokine (alle p> 0,05) beobachtet.

Schlussfolgerung

THP-1-Zellen können unter Verwendung von Nukleofektion und Plasmiden unter 5000 bp effektiv transfiziert werden. IMhu produzierten signifikante Mengen an Zytokinen als Reaktion auf etablierte Immunstimulanzien. IMhu zeigten keine Auf- oder Abregulierung der Produktion von 102 humane Cyto- oder Chemokine als Reaktion auf Cas9- oder Plasmidtransfektion. Das Fehlen einer Zytokinantwort auf Cas9 weist darauf hin, dass menschliche Mikroglia geeignete Ziele für die Gentherapie über Cas9 sein können. Es zeigt auch, dass Mikroglia möglicherweise nicht die Effektoren einer angeborenen Immunantwort auf Gentherapien in anderen Zellen sind. Es bedarf eine weitere Analyse der ZNS-Immunantwort, einschließlich der adaptiven Immunantwort auf Cas9-Gentherapien, um die Sicherheit und Langlebigkeit von CRISPR/Cas9-Therapien gründlicher beurteilen zu können.

6. REFERENCES

1. University of Pennsylvania. Phase I trial of NY-ESO-1 redirected CRISPR edited T cells (NYCE cells) engineered to express NY-ESO-1 TCR and gene edited to eliminate endogenous TCR and PD-1. NIH OBA RAC Public Review 2016. https://osp.od.nih.gov/wp-content/uploads/2016/08/1524_RAC_Briefing_Slides.pdf. Published 2018. Accessed September 19, 2020.
2. Stephens CJ, Lauron EJ, Kashentseva E, Lu ZH, Yokoyama WM, Curiel DT. Long-term correction of hemophilia B using adenoviral delivery of CRISPR/Cas9. *J Control Release*. 2019;298:128-141. doi:10.1016/j.jconrel.2019.02.009
3. Rodrigues GA, Shalaev E, Karami TK, Cunningham J, Slater NKH, Rivers HM. Pharmaceutical development of AAV-Based gene therapy products for the eye. *Pharm Res*. 2018;36(2):1-20. doi:10.1007/S11095-018-2554-7
4. Hori J, Niederkorn JY. Immunogenicity and immune privilege of corneal allografts. *Chem Immunol Allergy*. 2007;92:290-299. doi:10.1159/000099279
5. Savulescu J. Harm, ethics committees and the gene therapy death. *J Med Ethics*. 2001;27(3):148-150. doi:10.1136/jme.27.3.148
6. Machitani M, Sakurai F, Wakabayashi K, et al. Inhibition of CRISPR/Cas9-mediated genome engineering by a Type I interferon-induced reduction in guide RNA expression. *Biol Pharm Bull*. 2017;40(3):272-277. doi:10.1248/bpb.b16-00700
7. Haapaniemi E, Botla S, Persson J, Schmierer B, Taipale J. CRISPR-Cas9 genome editing induces a p53-mediated DNA damage response. *Nat Med*. 2018;24(7):927-930. doi:10.1038/s41591-018-0049-z
8. Perry VH, Teeling J. Microglia and macrophages of the central nervous system: The contribution of microglia priming and systemic inflammation to chronic neurodegeneration. *Semin Immunopathol*. 2013;35(5):601-612. doi:10.1007/s00281-013-0382-8
9. Bourne RRA, Flaxman SR, Braithwaite T, et al. Magnitude, temporal trends, and projections of the global prevalence of blindness and distance and near vision impairment: a systematic review and meta-analysis. *Lancet Glob Heal*. 2017;5(9):e888-e897. doi:10.1016/S2214-109X(17)30293-0
10. Chuvarayan Y, Finger RP, Köberlein-Neu J. Economic burden of blindness and visual impairment in Germany from a societal perspective: a cost-of-illness study. *Eur J Heal Econ*. 2020;21(1):115-127. doi:10.1007/s10198-019-01115-5
11. Flaxman SR, Bourne RRA, Resnikoff S, et al. Global causes of blindness and distance vision impairment 1990–2020: A systematic review and meta-analysis. *Lancet Glob Heal*. 2017;5(12):e1221-e1234. doi:10.1016/S2214-109X(17)30393-5
12. Broadgate S, Yu J, Downes SM, Halford S. Unravelling the genetics of inherited retinal dystrophies: Past, present and future. *Prog Retin Eye Res*. 2017;59:53-96. doi:10.1016/j.preteyeres.2017.03.003
13. Cremers FPM, Boon CJF, Bujakowska K, Zeitz C. Special issue introduction: Inherited retinal disease: Novel candidate genes, genotype-phenotype correlations, and inheritance models. *Genes (Basel)*. 2018;9(4):215. doi:10.3390/genes9040215
14. Daiger SP, Sullivan LS, Bowne SJ. RetNet. https://sph.uth.edu/retnet/sum-dis.htm#A-genes. Published 2019. Accessed September 19, 2020.
15. Chao DL, Burr A, Pennesi M. *RPE65-Related Leber Congenital Amaurosis / Early-Onset Severe Retinal Dystrophy*. University of Washington, Seattle; 1993. https://www.ncbi.nlm.nih.gov/books/NBK549574/. Accessed September 19, 2020.
16. Vázquez-Domínguez I, Garanto A, Collin RWJ. Molecular therapies for inherited retinal diseases—current standing, opportunities and challenges. *Genes (Basel)*. 2019;10(9):654. doi:10.3390/genes10090654
17. Ziccardi L, Cordeddu V, Gaddini L, et al. Gene therapy in retinal dystrophies. *Int J Mol Sci*. 2019;20(22):5722. doi:10.3390/ijms20225722

18. Turvey SE, Broide DH. Innate immunity. *J Allergy Clin Immunol*. 2010;125(2 Suppl 2):S24-S32. doi:10.1016/j.jaci.2009.07.016
19. Akira S, Uematsu S, Takeuchi O. Pathogen recognition and innate immunity. *Cell*. 2006;124(4):783-801. doi:10.1016/j.cell.2006.02.015
20. Aristizábal B, González Á. Innate Immunity. *J Allergy Clin Immunol*. 2010;125(2). doi:10.1016/j.jaci.2009.08.001
21. Mogensen TH. Pathogen recognition and inflammatory signaling in innate immune defenses. *Clin Microbiol Rev*. 2009;22(2):240-273. doi:10.1128/CMR.00046-08
22. Roh JS, Sohn DH. Damage-associated molecular patterns in inflammatory diseases. *Immune Netw*. 2018;18(4). doi:10.4110/in.2018.18.e27
23. Kawai T, Akira S. The roles of TLRs, RLRs and NLRs in pathogen recognition. *Int Immunol*. 2009;21(4):317-337. doi:10.1093/intimm/dxp017
24. Gay NJ, Symmons MF, Gangloff M, Bryant CE. Assembly and localization of Toll-like receptor signalling complexes. *Nat Rev Immunol*. 2014;14(8):546-558. doi:10.1038/nri3713
25. Kawai T, Akira S. The role of pattern-recognition receptors in innate immunity: update on Toll-like receptors. *Nat Immunol*. 2010;11(5):373-384. doi:10.1038/ni.1863
26. Sellge G, Kufer TA. PRR-signaling pathways: Learning from microbial tactics. *Semin Immunol*. 2015;27(2):75-84. doi:10.1016/j.smim.2015.03.009
27. Gao W, Xiong Y, Li Q, Yang H. Inhibition of toll-like receptor signaling as a promising therapy for inflammatory diseases: A journey from molecular to nano therapeutics. *Front Physiol*. 2017;8:508. doi:10.3389/fphys.2017.00508
28. Kawasaki T, Kawai T. Toll-like receptor signaling pathways. *Front Immunol*. 2014;5(SEP):461. doi:10.3389/fimmu.2014.00461
29. Poltorak A, He X, Smirnova I, et al. Defective LPS signaling in C3H/HeJ and C57BL/10ScCr mice: Mutations in Tlr4 gene. *Science (80-)*. 1998;282(5396):2085-2088. doi:10.1126/science.282.5396.2085
30. Alexopoulou L, Holt AC, Medzhitov R, Flavell RA. Recognition of double-stranded RNA and activation of NF-κB by Toll-like receptor 3. *Nature*. 2001;413(6857):732-738. doi:10.1038/35099560
31. Hayashi F, Smith KD, Ozinsky A, et al. The innate immune response to bacterial flagellin is mediated by Toll-like receptor 5. *Nature*. 2001;410(6832):1099-1103. doi:10.1038/35074106
32. Hemmi H, Takeuchi O, Kawai T, et al. A Toll-like receptor recognizes bacterial DNA. *Nature*. 2000;408(6813):740-745. doi:10.1038/35047123
33. Hemmi H, Kaisho T, Takeuchi O, et al. Small-antiviral compounds activate immune cells via the TLR7 MyD88-dependent signaling pathway. *Nat Immunol*. 2002;3(2):196-200. doi:10.1038/ni758
34. Ohashi K, Burkart V, Flohé S, Kolb H. Cutting edge: Heat shock protein 60 Is a putative endogenous ligand of the Toll-Like receptor-4 complex. *J Immunol*. 2000;164(2):558-561. doi:10.4049/jimmunol.164.2.558
35. Jones BW, Heldwein KA, Means TK, Saukkonen JJ, Fenton MJ. Differential roles of Toll-like receptors in the elicitation of proinflammatory responses by macrophages. *Ann Rheum Dis*. 2001;60(Suppl. 3). doi:10.1136/ard.60.90003.iii6
36. Wong SW, Kwon MJ, Choi AMK, Kim HP, Nakahira K, Hwang DH. Fatty acids modulate toll-like receptor 4 activation through regulation of receptor dimerization and recruitment into lipid rafts in a reactive oxygen species-dependent manner. *J Biol Chem*. 2009;284(40):27384-27392. doi:10.1074/jbc.M109.044065
37. Yamamoto M, Sato S, Mori K, et al. Cutting edge: A novel Toll/IL-1 receptor domain-containing adapter that preferentially activates the IFN-β promoter in the Toll-like receptor signaling. *J Immunol*. 2002;169(12):6668-6672. doi:10.4049/jimmunol.169.12.6668
38. Subramanian S, Tus K, Li QZ, et al. A Tlr7 translocation accelerates systemic

autoimmunity in murine lupus. *Proc Natl Acad Sci U S A*. 2006;103(26):9970-9975. doi:10.1073/pnas.0603912103
39. So EY, Ouchi T. The application of toll like receptors for cancer therapy. *Int J Biol Sci*. 2010;6(7):675-681. doi:10.7150/ijbs.6.675
40. Jialal I, Kaur H, Devaraj S. Toll-like receptor status in obesity and metabolic syndrome: A translational perspective. *J Clin Endocrinol Metab*. 2014;99(1):39-48. doi:10.1210/jc.2013-3092
41. Pope RM, Huang QQ. The role of Toll-like receptors in rheumatoid arthritis. *Curr Rheumatol Rep*. 2009;11(5):357-364. doi:10.1007/s11926-009-0051-z
42. Shaw MH, Reimer T, Kim YG, Nuñez G. NOD-like receptors (NLRs): bona fide intracellular microbial sensors. *Curr Opin Immunol*. 2008;20(4):377-382. doi:10.1016/j.coi.2008.06.001
43. Inohara N, Chamaillard M, McDonald C, Nuñez G. NOD-LRR proteins: Role in host-microbial interactions and inflammatory disease. *Annu Rev Biochem*. 2005;74:355-383. doi:10.1146/annurev.biochem.74.082803.133347
44. Inohara N, Ogura Y, Chen FF, Muto A, Nuñez G. Human Nod1 confers responsiveness to bacterial lipopolysaccharides. *J Biol Chem*. 2001;276(4):2551-2554. doi:10.1074/jbc.M009728200
45. Pauleau A, Murray PJ. Role of Nod2 in the response of macrophages to Toll-Like receptor agonists. *Mol Cell Biol*. 2003;23(21):7531-7539. doi:10.1128/mcb.23.21.7531-7539.2003
46. Chamaillard M, Hashimoto M, Horie Y, et al. An essential role for NOD1 in host recognition of bacterial peptidoglycan containing diaminopimelic acid. *Nat Immunol*. 2003;4(7):702-707. doi:10.1038/ni945
47. Girardin SE, Boneca IG, Viala J, et al. Nod2 is a general sensor of peptidoglycan through muramyl dipeptide (MDP) detection. *J Biol Chem*. 2003;278(11):8869-8872. doi:10.1074/jbc.C200651200
48. Martinon F, Burns K, Tschopp J. The Inflammasome: A molecular platform triggering activation of inflammatory caspases and processing of proIL-β. *Mol Cell*. 2002;10(2):417-426. doi:10.1016/S1097-2765(02)00599-3
49. Franchi L, Amer A, Body-Malapel M, et al. Cytosolic flagellin requires Ipaf for activation of caspase-1 and interleukin 1β in salmonella-infected macrophages. *Nat Immunol*. 2006;7(6):576-582. doi:10.1038/ni1346
50. Boyden ED, Dietrich WF. Nalp1b controls mouse macrophage susceptibility to anthrax lethal toxin. *Nat Genet*. 2006;38(2):240-244. doi:10.1038/ng1724
51. Mariathasan S, Weiss DS, Newton K, et al. Cryopyrin activates the inflammasome in response to toxins and ATP. *Nature*. 2006;440(7081):228-232. doi:10.1038/nature04515
52. Amores-Iniesta J, Barberà-Cremades M, Martínez CM, et al. Extracellular ATP Activates the NLRP3 Inflammasome and Is an Early Danger Signal of Skin Allograft Rejection. *Cell Rep*. 2017;21(12):3414-3426. doi:10.1016/j.celrep.2017.11.079
53. Gray EE, Winship D, Snyder JM, Child SJ, Geballe AP, Stetson DB. The AIM2-like receptors are dispensable for the interferon response to intracellular DNA. *Immunity*. 2016;45(2):255-266. doi:10.1016/j.immuni.2016.06.015
54. Chiffoleau E. C-type lectin-like receptors as emerging orchestrators of sterile inflammation represent potential therapeutic targets. *Front Immunol*. 2018;9:15. doi:10.3389/fimmu.2018.00227
55. Geijtenbeek TBH, Torensma R, Van Vliet SJ, et al. Identification of DC-SIGN, a novel dendritic cell-specific ICAM-3 receptor that supports primary immune responses. *Cell*. 2000;100(5):575-585. doi:10.1016/S0092-8674(00)80693-5
56. Bezbradica JS, Rosenstein RK, Demarco RA, Brodsky I, Medzhitov R. A role for the ITAM signaling module in specifying cytokine-receptor functions. *Nat Immunol*. 2014;15(4):333-342. doi:10.1038/ni.2845
57. Kingeter LM, Lin X. C-type lectin receptor-induced NF-κB activation in innate immune

and inflammatory responses. *Cell Mol Immunol*. 2012;9(2):105-112. doi:10.1038/cmi.2011.58
58. Loo YM, Gale M. Immune signaling by RIG-I-like receptors. *Immunity*. 2011;34(5):680-692. doi:10.1016/j.immuni.2011.05.003
59. Yoneyama M, Kikuchi M, Natsukawa T, et al. The RNA helicase RIG-I has an essential function in double-stranded RNA-induced innate antiviral responses. *Nat Immunol*. 2004;5(7):730-737. doi:10.1038/ni1087
60. Vance RE. Cytosolic DNA sensing: The field narrows. *Immunity*. 2016;45(2):227-228. doi:10.1016/j.immuni.2016.08.006
61. Hopfner KP, Hornung V. Molecular mechanisms and cellular functions of cGAS–STING signalling. *Nat Rev Mol Cell Biol*. 2020;21(9):501-521. doi:10.1038/s41580-020-0244-x
62. Ray A, Gulati K, Joshi J, Sreemanti G, Nishant R. Cytokines and their role in health and disease: A brief overview. *MOJ Immunol*. 2016;4(2). doi:10.15406/moji.2016.04.00121
63. Dinarello CA. Historical insights into cytokines. *Eur J Immunol*. 2007;37(Suppl. 1):S34. doi:10.1002/eji.200737772
64. Meurs E, Chong K, Galabru J, et al. Molecular cloning and characterization of the human double-stranded RNA-activated protein kinase induced by interferon. *Cell*. 1990;62(2):379-390. doi:10.1016/0092-8674(90)90374-N
65. Vivier E, Tomasello E, Baratin M, Walzer T, Ugolini S. Functions of natural killer cells. *Nat Immunol*. 2008;9(5):503-510. doi:10.1038/ni1582
66. Lee AJ, Chen B, Chew MV, et al. Inflammatory monocytes require type I interferon receptor signaling to activate NK cells via IL-18 during a mucosal viral infection. *J Exp Med*. 2017;214(4):1153-1167. doi:10.1084/jem.20160880
67. Chi X, Li Y, Qiu X. V(D)J recombination, somatic hypermutation and class switch recombination of immunoglobulins: Mechanism and regulation. *Immunology*. 2020;160(3):233-247. doi:10.1111/imm.13176
68. Janeway CA, Travers P, Walport M, Shlomchik MJ. T Cell-mediated immunity. In: *Immunobiologs: The Immune System in Health and Disease*. 5th ed. New York City: Garland Science; 2001. https://www.ncbi.nlm.nih.gov/books/NBK10762/. Accessed October 27, 2020.
69. Ota M, Tsujikawa A, Ojima Y, et al. Retinal sensitivity after resolution of the macular edema associated with retinal vein occlusion. *Graefe's Arch Clin Exp Ophthalmol*. 2012;250(5):635-644. doi:10.1007/s00417-011-1860-0
70. Zhou R, Caspi RR. Ocular immune privilege. *F1000 Biol Rep*. 2010;2(1):3. doi:10.3410/B2-3
71. Cunha-Vaz J, Bernardes R, Lobo C. Blood-retinal barrier. *Eur J Ophthalmol*. 2011;21(Suppl. 6):3-9. doi:10.5301/EJO.2010.6049
72. Stein-Streilein J. Immune regulation and the eye. *Trends Immunol*. 2008;29(11):548-554. doi:10.1016/j.it.2008.08.002
73. Taylor AW. Ocular immunosuppressive microenvironment. *Chem Immunol Allergy*. 2007;92:71-85. doi:10.1159/000099255
74. Vendomèle J, Khebizi Q, Fisson S. Cellular and molecular mechanisms of anterior chamber-associated immune deviation (ACAID): What we have learned from knockout mice. *Front Immunol*. 2017;8:1686. doi:10.3389/fimmu.2017.01686
75. Isaacson P, Wright DH. Extranodal malignant lymphoma arising from mucosa-associated lymphoid tissue. *Cancer*. 1984;53(11):2515-2524. doi:10.1002/1097-0142(19840601)53:11<2515::aid-cncr2820531125>3.0.co;2-c.
76. Detrick B, Hooks JJ. Immune regulation in the retina. *Immunol Res*. 2010;47(1-3):153-161. doi:10.1007/s12026-009-8146-1
77. Vecino E, Rodriguez FD, Ruzafa N, Pereiro X, Sharma SC. Glia-neuron interactions in the mammalian retina. *Prog Retin Eye Res*. 2016;51:1-40. doi:10.1016/j.preteyeres.2015.06.003

78. Rashid K, Akhtar-Schaefer I, Langmann T. Microglia in Retinal Degeneration. *Front Immunol*. 2019;10:1975. doi:10.3389/FIMMU.2019.01975
79. Chen M, Xu H. Parainflammation, chronic inflammation, and age-related macular degeneration. *J Leukoc Biol*. 2015;98(5):713-725. doi:10.1189/jlb.3RI0615-239R
80. Karlstetter M, Scholz R, Rutar M, Wong WT, Provis JM, Langmann T. Retinal microglia: Just bystander or target for therapy? *Prog Retin Eye Res*. 2015;45:30-57. doi:10.1016/j.preteyeres.2014.11.004
81. Wang N, Lai C, Liu C, et al. Origin of fundus hyperautofluorescent spots and their role in retinal degeneration in a mouse model of Goldmann-Favre syndrome. *Dis Model Mech*. 2013;6(5):1113-1122. doi:10.1242/dmm.012112
82. Silverman SM, Wong WT. Microglia in the retina: Roles in development, maturity, and disease. *Annu Rev Vis Sci*. 2018;4:45-77. doi:10.1146/annurev-vision-091517-034425
83. Langmann T. Microglia activation in retinal degeneration. *J Leukoc Biol*. 2007;81(6):1345-1351. doi:10.1189/jlb.0207114
84. Zhao L, Zabel MK, Wang X, et al. Microglial phagocytosis of living photoreceptors contributes to inherited retinal degeneration. *EMBO Mol Med*. 2015;7(9):1179-1197. doi:10.15252/emmm.201505298
85. Cousins SW, Espinosa-Heidmann DG, Csaky KG. Monocyte activation in patients with age-related macular degeneration: A biomarker of risk for choroidal neovascularization? *Arch Ophthalmol*. 2004;122(7):1013-1018. doi:10.1001/archopht.122.7.1013
86. Okunuki Y, Mukai R, Nakao T, et al. Retinal microglia initiate neuroinflammation in ocular autoimmunity. *Proc Natl Acad Sci U S A*. 2019;116(20):9989-9998. doi:10.1073/pnas.1820387116
87. Ramirez AI, de Hoz R, Salobrar-Garcia E, et al. The role of microglia in retinal neurodegeneration: Alzheimer's disease, Parkinson, and glaucoma. *Front Aging Neurosci*. 2017;9:214. doi:10.3389/fnagi.2017.00214
88. Griffiths L, Binley K, Iqball S, et al. The macrophage - A novel system to deliver gene therapy to pathological hypoxia. *Gene Ther*. 2000;7(3):255-262. doi:10.1038/sj.gt.3301058
89. Liao HK, Gu Y, Diaz A, et al. Use of the CRISPR/Cas9 system as an intracellular defense against HIV-1 infection in human cells. *Nat Commun*. 2015;6(1):1-10. doi:10.1038/ncomms7413
90. Biju KC, Santacruz RA, Chen CC, Robert A, Senlin L. Microglia as an attractive cellular vehicle for gene therapy of Parkinson's disease. *Mol Ther*. 2011;19:S79. doi:10.1016/s1525-0016(16)36774-0
91. Raikwar SP, Thangavel R, Dubova I, et al. Targeted gene editing of glia maturation factor in microglia: A novel Alzheimer's disease therapeutic target. *Mol Neurobiol*. 2019;56(1):378-393. doi:10.1007/s12035-018-1068-y
92. Dauletbekov D, Bartz-Schmidt KU, Fischer MD. Subretinal and intravitreal retinal injections in monkeys. In: *Methods in Molecular Biology*. Vol 1715. Humana Press Inc.; 2018:251-257. doi:10.1007/978-1-4939-7522-8_18
93. Zhan L, Krabbe G, Du F, et al. Proximal recolonization by self-renewing microglia re-establishes microglial homeostasis in the adult mouse brain. *PLoS Biol*. 2019;17(2):e3000134. doi:10.1371/journal.pbio.3000134
94. Priller J, Prinz M. Targeting microglia in brain disorders. *Science (80-)*. 2019;364(6448):32-33. doi:10.1126/science.aau9100
95. Tsuchiya S, Yamabe M, Yamaguchi Y, Kobayashi Y, Konno T, Tada K. Establishment and characterization of a human acute monocytic leukemia cell line (THP-1). *Int J Cancer*. 1980;26(2):171-176. doi:10.1002/ijc.2910260208
96. Park EK, Jung HS, Yang HI, Yoo MC, Kim C, Kim KS. Optimized THP-1 differentiation is required for the detection of responses to weak stimuli. *Inflamm Res*. 2007;56(1):45-50. doi:10.1007/s00011-007-6115-5
97. Maeß MB, Wittig B, Cignarella A, Lorkowski S. Reduced PMA enhances the

responsiveness of transfected THP-1 macrophages to polarizing stimuli. *J Immunol Methods*. 2014;402(1-2):76-81. doi:10.1016/j.jim.2013.11.006
98. Jin C, Wu L, Li J, Fang M, Cheng L, Wu N. Multiple signaling pathways are involved in the interleukine-4 regulated expression of DC-SIGN in THP-1 cell line. *J Biomed Biotechnol*. 2012:357060. doi:10.1155/2012/357060
99. Madhvi A, Mishra H, Leisching GR, Mahlobo PZ, Baker B. Comparison of human monocyte derived macrophages and THP1-like macrophages as in vitro models for M. tuberculosis infection. *Comp Immunol Microbiol Infect Dis*. 2019;67:101355. doi:10.1016/j.cimid.2019.101355
100. da Sousa-Vasconcelos PS, Da Seguins WS, De Souza Luz E, De Pinho RT. Pattern of cytokine and chemokine production by THP-1 derived macrophages in response to live or heat-killed mycobacterium bovis bacillus calmette-guérin moreau strain. *Mem Inst Oswaldo Cruz*. 2015;110(6):809-813. doi:10.1590/0074-02760140420
101. Rio-Hortega P. El "tercer elemento" de los centros nerviosos. *Nat probable la microglia Bol Soc Esp Biol*. 1919;3:108–115.
102. Ginhoux F, Lim S, Hoeffel G, Low D, Huber T. Origin and differentiation of microglia. *Front Cell Neurosci*. 2013;7:45. doi:10.3389/fncel.2013.00045
103. Nagai A, Nakagawa E, Hatori K, et al. Generation and characterization of immortalized human microglial cell lines: Expression of cytokines and chemokines. *Neurobiol Dis*. 2001;8(6):1057-1068. doi:https://doi.org/10.1006/nbdi.2001.0437
104. Garcia-Mesa Y, Jay TR, Checkley MA, et al. Immortalization of primary microglia: a new platform to study HIV regulation in the central nervous system. *J Neurovirol*. 2017;23(1):47-66. doi:10.1007/s13365-016-0499-3
105. Chiavari M, Ciotti GMP, Navarra P, Lisi L. Pro-inflammatory activation of a new immortalized human microglia cell line. *Brain Sci*. 2019;9(5). doi:10.3390/brainsci9050111
106. van Rees GF, Lago SG, Cox DA, et al. Evidence of microglial activation following exposure to serum from first-onset drug-naïve schizophrenia patients. *Brain Behav Immun*. 2018;67:364-373. doi:10.1016/j.bbi.2017.10.003
107. Aldana BI. Microglia-Specific Metabolic Changes in Neurodegeneration. *J Mol Biol*. 2019;431(9):1830-1842. doi:10.1016/j.jmb.2019.03.006
108. Harris AR, Yuan JX, Munson JM. Assessing multiparametric drug response in tissue engineered tumor microenvironment models. *Methods*. 2018;134-135:20-31. doi:10.1016/j.ymeth.2017.12.010
109. Kraus LM. Formation of different hæmoglobins in tissue culture of human bone marrow treated with human deoxyribonucleic acid. *Nature*. 1961;192(4807):1055-1057. doi:10.1038/1921055a0
110. Rogers S, Pfuderer P. Use of viruses as carriers of added genetic information. *Nature*. 1968;219(5155):749-751. doi:10.1038/219749a0
111. Friedmann T, Roblin R. Gene therapy for human genetic disease? *Science (80-)*. 1972;175(4025):949-955. doi:10.1126/science.175.4025.949
112. Sun M. Cline loses two NIH grants. *Science (80-)*. 1981;214(4526):1220. doi:10.1126/science.7302590
113. Beutler E. The Cline affair. *Mol Ther*. 2001;4(5):396-397. doi:10.1006/mthe.2001.0486
114. Blaese R., Culver KW, Miller AD, et al. T lymphocyte-directed gene therapy for ADA-SCID: Initial trial results after 4 years. *Science (80-)*. 1995;270(5235):475-480. doi:10.1126/science.270.5235.475
115. U.S. Food and Drug Administration. Drug approval package Elelyso (Taliglucerase alfa) injection. Accessdata FDA. http://www.accessdata.fda.gov/drugsatfda_docs/nda/2012/022458Orig1s000TOC.cfm. Published 2012. Accessed October 27, 2020.
116. The Royal Swedish Academy of Sciences. Press release: The Nobel Prize in Chemistry 2020. https://www.nobelprize.org/prizes/chemistry/2020/press-release/. Published 2020.

Accessed October 24, 2020.
117. Silva G, Poirot L, Galetto R, et al. Meganucleases and other tools for targeted genome engineering: Perspectives and challenges for gene therapy. *Curr Gene Ther*. 2011;11(1):11-27. doi:10.2174/156652311794520111
118. Belfort M, Roberts RJ. Homing endonucleases: Keeping the house in order. Presented at the: 1997. doi:10.1093/nar/25.17.3379
119. Grosse S, Huot N, Mahiet C, et al. Meganuclease-mediated inhibition of HSV1 infection in cultured cells. *Mol Ther*. 2011;19(4):694-702. doi:10.1038/mt.2010.302
120. Li L, Wu LP, Chandrasegaran S. Functional domains in Fok I restriction endonuclease. *Proc Natl Acad Sci U S A*. 1992;89(10):4275-4279. doi:10.1073/pnas.89.10.4275
121. Alwin S, Gere MB, Guhl E, et al. Custom zinc-finger nucleases for use in human cells. *Mol Ther*. 2005;12(4):610-617. doi:10.1016/j.ymthe.2005.06.094
122. Isalan M. Zinc-finger nucleases: How to play two good hands. *Nat Methods*. 2012;9(1):32-34. doi:10.1038/nmeth.1805
123. Joung JK, Sander JD. TALENs: A widely applicable technology for targeted genome editing. *Nat Rev Mol Cell Biol*. 2013;14(1):49-55. doi:10.1038/nrm3486
124. Gaj T, Gersbach CA, Barbas CF. ZFN, TALEN, and CRISPR/Cas-based methods for genome engineering. *Trends Biotechnol*. 2013;31(7):397-405. doi:10.1016/j.tibtech.2013.04.004
125. Jinek M, Chylinski K, Fonfara I, Hauer M, Doudna JA, Charpentier E. A programmable dual-RNA-guided DNA endonuclease in adaptive bacterial immunity. *Science (80-)*. 2012;337(6096):816-821. doi:10.1126/science.1225829
126. Hille F, Charpentier E. CRISPR-cas: Biology, mechanisms and relevance. *Philos Trans R Soc B Biol Sci*. 2016;371(1707):20150496. doi:10.1098/rstb.2015.0496
127. Cong L, Ran FA, Cox D, et al. Multiplex genome engineering using CRISPR/Cas systems. *Science (80-)*. 2013;339(6121):819-823. doi:10.1126/science.1231143
128. Savić N, Schwank G. Advances in therapeutic CRISPR/Cas9 genome editing. *Transl Res*. 2016;168:15-21. doi:10.1016/j.trsl.2015.09.008
129. Ran FA, Hsu PD, Wright J, Agarwala V, Scott DA, Zhang F. Genome engineering using the CRISPR-Cas9 system. *Nat Protoc*. 2013;8(11):2281-2308. doi:10.1038/nprot.2013.143
130. Nelson CE, Hakim CH, Ousterout DG, et al. In vivo genome editing improves muscle function in a mouse model of Duchenne muscular dystrophy. *Science (80-)*. 2016;351(6271):403-407. doi:10.1126/science.aad5143
131. Xiao Q, Guo D, Chen S. Application of CRISPR/Cas9-based gene editing in HIV-1/AIDS therapy. *Front Cell Infect Microbiol*. 2019;9(March):69. doi:10.3389/fcimb.2019.00069
132. Vertex Pharmaceuticals Incorporated. A safety and efficacy study evaluating CTX001 in subjects with severe sickle cell disease. ClinicalTrials.gov. https://clinicaltrials.gov/ct2/show/NCT03745287. Published 2018. Accessed September 19, 2020.
133. Research to Prevent Blindness. Groundbreaking Gene Therapy for Retinal Disease. https://www.rpbusa.org/rpb/news-and-publications/news/latest/groundbreaking-gene-therapy-for/. Accessed October 24, 2020.
134. Ruan GX, Barry E, Yu D, Lukason M, Cheng SH, Scaria A. CRISPR/Cas9-Mediated genome editing as a therapeutic approach for Leber Congenital Amaurosis. *Mol Ther*. 2017;25(2):331-341. doi:10.1016/j.ymthe.2016.12.006
135. Ledford H. CRISPR treatment inserted directly into the body for first time. *Nature*. 2020;579(7798):185. doi:10.1038/d41586-020-00655-8
136. Kolata G, Wee S, Belluck P. Chinese scientist claims to use Crispr to make first genetically edited babies. *New York Times*. https://www.nytimes.com/2018/11/26/health/gene-editing-babies-china.html. Published November 27, 2018.

137. WHO. Statement on governance and oversight of human genome editing. https://www.who.int/news-room/detail/26-07-2019-statement-on-governance-and-oversight-of-human-genome-editing. Published 2019. Accessed August 7, 2020.
138. Wee S. Chinese scientist who genetically edited babies gets 3 years in prison. *New York Times*. https://www.nytimes.com/2019/12/30/business/china-scientist-genetic-baby-prison.html. Published December 30, 2019.
139. Marshall E. Gene therapy death prompts review of adenovirus vector. *Science (80-)*. 1999;286(5448):2244-2245. doi:10.1126/science.286.5448.2244
140. Zhu J, Huang X, Yang Y. The TLR9-MyD88 pathway is critical for adaptive immune responses to adeno-associated virus gene therapy vectors in mice. *J Clin Invest*. 2009;119(8):2388-2398. doi:10.1172/JCI37607
141. Bucher K, Rodríguez-Bocanegra E, Dauletbekov D, Fischer MD. Immune responses to retinal gene therapy using adeno-associated viral vectors – Implications for treatment success and safety. *Prog Retin Eye Res*. 2021;83. doi:10.1016/j.preteyeres.2020.100915
142. Wienert B, Shin J, Zelin E, Pestal K, Corn JE. In vitro–transcribed guide RNAs trigger an innate immune response via the RIG-I pathway. *PLoS Biol*. 2018;16(7):e2005840. doi:10.1371/journal.pbio.2005840
143. Charlesworth CT, Deshpande PS, Dever DP, et al. Identification of preexisting adaptive immunity to Cas9 proteins in humans. *Nat Med*. 2019;25(2):249-254. doi:10.1038/s41591-018-0326-x
144. Wagner DL, Amini L, Wendering DJ, et al. High prevalence of Streptococcus pyogenes Cas9-reactive T cells within the adult human population. *Nat Med*. 2019;25(2):242-248. doi:10.1038/s41591-018-0204-6
145. Mehta A, Merkel OM. Immunogenicity of Cas9 Protein. *J Pharm Sci*. 2020;109(1):62-67. doi:10.1016/j.xphs.2019.10.003
146. Simhadri VL, McGill J, McMahon S, Wang J, Jiang H, Sauna ZE. Prevalence of Pre-existing Antibodies to CRISPR-Associated Nuclease Cas9 in the USA Population. *Mol Ther - Methods Clin Dev*. 2018;10:105-112. doi:10.1016/j.omtm.2018.06.006
147. Kang R, Zhu S, Zeh H, Tang D. The STING-STAT6 pathway drives Cas9-induced host response in human monocytes. *Biochem Biophys Res Commun*. 2018;506(1):278-283. doi:10.1016/j.bbrc.2018.10.080
148. Nelson CE, Wu Y, Gemberling MP, et al. Long-term evaluation of AAV-CRISPR genome editing for Duchenne muscular dystrophy. *Nat Med*. 2019;25(3):427-432. doi:10.1038/s41591-019-0344-3
149. Gardiner KL, Cideciyan AV, Swider M, et al. Long-term structural outcomes of late-stage RPE65 gene therapy. *Mol Ther*. 2019;28(1):266-278. doi:10.1016/j.ymthe.2019.08.013
150. Spark Therapeutics. Three-year follow-up phase 3 data provide additional information on efficacy, durability and safety of investigational LUXTURNA™ (voretigene neparvovec) in patients with biallelic RPE65-mediated inherited retinal disease. https://sparktx.com/press_releases/three-year-follow-up-phase-3-data-provide-additional-information-on-efficacy-durability-and-safety-of-investigational-luxturna-voretigene-neparvovec-in-patients-with-biallelic-rpe65-mediat/. Accessed September 20, 2020.
151. Jacobson SG, Cideciyan AV, Roman AJ, et al. Improvement and decline in vision with gene therapy in childhood blindness. *N Engl J Med*. 2015;372(20):1920-1926. doi:10.1056/NEJMoa1412965
152. Bainbridge JWB, Mehat MS, Sundaram V, et al. Long-Term effect of gene therapy on Leber's Congenital Amaurosis. *N Engl J Med*. 2015;372(20):1887-1897. doi:10.1056/nejmoa1414221
153. Herzog RW. Encouraging and unsettling findings in long-term follow-up of AAV gene transfer. *Mol Ther*. 2020;28(2):341-342. doi:10.1016/j.ymthe.2020.01.007
154. Addgene. What is Polymerase Chain Reaction (PCR).

https://www.addgene.org/protocols/pcr/. Accessed August 27, 2020.
155. Addgene. Molecular biology protocol - Restriction digest of plasmid DNA. https://www.addgene.org/protocols/restriction-digest/. Published 2016. Accessed August 27, 2020.
156. NEB. Protocol for Dephosphorylation of 5´-ends of DNA using rSAP. Ipswich, Massachusetts, USA. https://international.neb.com/protocols/0001/01/01/protocol-for-dephosphorylating-with-cip. Published 2016. Accessed August 27, 2020.
157. Addgene. Protocol - How to Ligate Plasmid DNA. https://www.addgene.org/protocols/dna-ligation/. Accessed August 27, 2020.
158. Thermofisher Scientific. Useful Numbers for Cell Culture. https://www.thermofisher.com/nl/en/home/references/gibco-cell-culture-basics/cell-culture-protocols/cell-culture-useful-numbers.html. Accessed December 30, 2020.
159. Maeß MB, Buers I, Robenek H, Lorkowski S. Improved protocol for efficient nonviral transfection of premature THP-1 macrophages. *Cold Spring Harb Protoc*. 2011;6(5). doi:10.1101/pdb.prot5612
160. ATCC. Transfection protocol for THP-1 cells. Center for Open Science. https://osf.io/kwqms/download. Published 2011. Accessed October 10, 2020.
161. Liu X, Yin S, Chen Y, et al. LPS-induced proinflammatory cytokine expression in human airway epithelial cells and macrophages via NF-κB, STAT3 or AP-1 activation. *Mol Med Rep*. 2018;17(4):5484-5491. doi:10.3892/mmr.2018.8542
162. Chanput W, Mes J, Vreeburg RAM, Savelkoul HFJ, Wichers HJ. Transcription profiles of LPS-stimulated THP-1 monocytes and macrophages: A tool to study inflammation modulating effects of food-derived compounds. *Food Funct*. 2010;1(3):254-261. doi:10.1039/c0fo00113a
163. Akhtar M, Watson JL, Nazli A, McKay DM. Bacterial DNA evokes epithelial IL-8 production by a MAPK-dependent, NF-kappaB-independent pathway. *FASEB J*. 2003;17(10):1319-1321. doi:10.1096/fj.02-0950fje
164. Netea MG, Nold-Petry CA, Nold MF, et al. Differential requirement for the activation of the inflammasome for processing and release of IL-1β in monocytes and macrophages. *Blood*. 2009;113(10):2324-2335. doi:10.1182/blood-2008-03-146720
165. Hughes P, Marshall D, Reid Y, Parkes H, Gelber C. The costs of using unauthenticated, over-passaged cell lines: How much more data do we need? *Biotechniques*. 2007;43(5):575-586. doi:10.2144/000112598
166. Maeß MB, Wittig B, Lorkowski S. Highly efficient transfection of human THP-1 macrophages by nucleofection. *J Vis Exp*. 2014;(91):51960. doi:10.3791/51960
167. Tang X, Aljahdali B, Alasiri M, et al. A method for high transfection efficiency in THP-1 suspension cells without PMA treatment. *Anal Biochem*. 2018;544:93-97. doi:10.1016/j.ab.2017.12.032
168. Robenek H, Buers I, Hofnagel O, Lorkowski S, Severs NJ. GFP-tagged proteins visualized by freeze-fracture immuno-electron microscopy: A new tool in cellular and molecular medicine. *J Cell Mol Med*. 2009;13(7):1381-1390. doi:10.1111/j.1582-4934.2008.00407.x
169. Brazil MI, Weiß S, Stockinger B. Excessive degradation of intracellular protein in macrophages prevents presentation in the context of major histocompatibility complex class II molecules. *Eur J Immunol*. 1997;27(6):1506-1514. doi:10.1002/eji.1830270629
170. Butovsky O, Jedrychowski MP, Moore CS, et al. Identification of a unique TGF-β-dependent molecular and functional signature in microglia. *Nat Neurosci*. 2014;17(1):131-143. doi:10.1038/nn.3599
171. Lisi L, Stigliano E, Lauriola L, Navarra P, Dello Russo C. Proinflammatory-activated glioma cells induce a switch in microglial polarization and activation status, from a predominant M2b phenotype to a mixture of M1 and M2a/B polarized cells. *ASN Neuro*. 2014;6(3):171-183. doi:10.1042/AN20130045
172. Rawat P, Spector SA. Development and characterization of a human microglia cell

model of HIV-1 infection. *J Neurovirol*. 2017;23(1):33-46. doi:10.1007/s13365-016-0472-1
173. Wires ES, Alvarez D, Dobrowolski C, et al. Methamphetamine activates nuclear factor kappa-light-chain-enhancer of activated B cells (NF-κB) and induces human immunodeficiency virus (HIV) transcription in human microglial cells. *J Neurovirol*. 2012;18(5):400-410. doi:10.1007/s13365-012-0103-4
174. Orihuela R, McPherson CA, Harry GJ. Microglial M1/M2 polarization and metabolic states. *Br J Pharmacol*. 2016;173(4):649-665. doi:10.1111/bph.13139
175. Lively S, Schlichter LC. Microglia responses to pro-inflammatory stimuli (LPS, IFNγ+TNFα) and reprogramming by resolving cytokines (IL-4, IL-10). *Front Cell Neurosci*. 2018;12. doi:10.3389/fncel.2018.00215
176. Wang WY, Tan MS, Yu JT, Tan L. Role of pro-inflammatory cytokines released from microglia in Alzheimer's disease. *Ann Transl Med*. 2015;3(10):136. doi:10.3978/j.issn.2305-5839.2015.03.49
177. Centre BE, Institutet K. Expression of Toll-like receptors in the nervous system A survey of the literature and some additional experiments Andrea Björkman. 2007.
178. Olson JK, Miller SD. Microglia Initiate Central Nervous System Innate and Adaptive Immune Responses through Multiple TLRs. *J Immunol*. 2004;173(6):3916-3924. doi:10.4049/jimmunol.173.6.3916
179. Dalpke A, Frank J, Peter M, Heeg K. Activation of toll-like receptor 9 by DNA from different bacterial species. *Infect Immun*. 2006;74(2):940-946. doi:10.1128/IAI.74.2.940-946.2006
180. Dalpke AH, Schäfer MK-H, Frey M, et al. Immunostimulatory CpG-DNA Activates Murine Microglia. *J Immunol*. 2002;168(10):4854-4863. doi:10.4049/jimmunol.168.10.4854
181. Yousif NM, de Oliveira ACP, Brioschi S, Huell M, Biber K, Fiebich BL. Activation of EP2 receptor suppresses poly(I: C) and LPS-mediated inflammation in primary microglia and organotypic hippocampal slice cultures: Contributing role for MAPKs. *Glia*. 2018;66(4):708-724. doi:10.1002/glia.23276
182. Kielian T, Esen N, Bearden ED. Toll-like receptor 2 (TLR2) is pivotal for recognition of S. aureus peptidoglycan but not intact bacteria by microglia. *Glia*. 2005;49(4):567-576. doi:10.1002/glia.20144
183. Smith SMC, Friedle SA, Watters JJ. Chronic intermittent hypoxia exerts CNS region-specific effects on rat microglial inflammatory and TLR4 gene expression. *PLoS One*. 2013;8(12):e81584. doi:10.1371/journal.pone.0081584
184. Takeshita S, Takeshita F, Haddad DE, Janabi N, Klinman DM. Activation of microglia and astrocytes by CpG oligodeoxynucleotides. *Neuroreport*. 2001;12(14):3029-3032. doi:10.1097/00001756-200110080-00010
185. Sedgwick JD, Schwender S, Imrich H, Dorries R, Butcher GW, Ter Meulen V. Isolation and direct characterization of resident microglial cells from the normal and inflamed central nervous system. *Proc Natl Acad Sci U S A*. 1991;88(16):7438-7442. doi:10.1073/pnas.88.16.7438
186. Nagai A, Mishima S, Ishida Y, et al. Immortalized human microglial cell line: Phenotypic expression. *J Neurosci Res*. 2005;81(3):342-348. doi:10.1002/jnr.20478
187. Kaur G, Dufour JM. Cell lines. *Spermatogenesis*. 2012;2(1):1-5. doi:10.4161/spmg.19885
188. Haenseler W, Sansom SN, Buchrieser J, et al. A highly efficient human pluripotent stem cell microglia model displays a neuronal-co-culture-specific expression profile and inflammatory response. *Stem Cell Reports*. 2017;8(6):1727-1742. doi:10.1016/j.stemcr.2017.05.017
189. Durafourt BA, Moore CS, Blain M, Antel JP. Isolating, culturing, and polarizing primary human adult and fetal microglia. *Methods Mol Biol*. 2013;1041:199-211. doi:10.1007/978-1-62703-520-0_19

190. Geirsdottir L, David E, Keren-Shaul H, et al. Cross-Species Single-Cell Analysis Reveals Divergence of the Primate Microglia Program. *Cell*. 2019;179(7):1609-1622.e16. doi:10.1016/j.cell.2019.11.010
191. Zhou Y, Song WM, Andhey PS, et al. Human and mouse single-nucleus transcriptomics reveal TREM2-dependent and TREM2-independent cellular responses in Alzheimer's disease. *Nat Med*. 2020;26(1):131-142. doi:10.1038/s41591-019-0695-9
192. Galatro TF, Holtman IR, Lerario AM, et al. Transcriptomic analysis of purified human cortical microglia reveals age-associated changes. *Nat Neurosci*. 2017;20(8):1162-1171. doi:10.1038/nn.4597
193. Qin Y, Garrison BS, Ma W, et al. A milieu molecule for TGF-β required for microglia function in the nervous system. *Cell*. 2018;174(1):156-171.e16. doi:https://doi.org/10.1016/j.cell.2018.05.027
194. Holan V, Hermankova B, Krulova M, Zajicova A. Cytokine interplay among the diseased retina, inflammatory cells and mesenchymal stem cells - a clue to stem cell-based therapy. *World J Stem Cells*. 2019;11(11):957-967. doi:10.4252/wjsc.v11.i11.957
195. Wooff Y, Man SM, Aggio-Bruce R, Natoli R, Fernando N. IL-1 family members mediate cell death, inflammation and angiogenesis in retinal degenerative diseases. *Front Immunol*. 2019;10(JULY):1618. doi:10.3389/fimmu.2019.01618
196. Mills CD, Kincaid K, Alt JM, Heilman MJ, Hill AM. M-1/M-2 macrophages and the Th1/Th2 paradigm. *J Immunol*. 2000;164(12):6166-6173. doi:10.4049/jimmunol.164.12.6166
197. Pettersen JS, Fuentes-Duculan J, Suárez-Fariñas M, et al. Tumor-associated macrophages in the cutaneous SCC microenvironment are heterogeneously activated. *J Invest Dermatol*. 2011;131(6):1322-1330. doi:10.103/jid.2011.9
198. Vogel DYS, Vereyken EJF, Glim JE, et al. Macrophages in inflammatory multiple sclerosis lesions have an intermediate activation status. *J Neuroinflammation*. 2013;10:35. doi:10.1186/1742-2094-10-35
199. Rashid M ur, Coombs KM. Serum-reduced media impacts on cell viability and protein expression in human lung epithelial cells. *J Cell Physiol*. 2019;234(6):7718-7724. doi:10.1002/jcp.27890
200. Young ATL, Moore RB, Murray AG, Mullen JC, Lakey JRT. Assessment of Different Transfection Parameters in Efficiency Optimization. *Cell Transplant*. 2004;13(2):179-185. doi:10.3727/000000004773301861
201. Kotterman MA, Yin L, Strazzeri JM, Flannery JG, Merigan WH, Schaffer D V. Antibody neutralization poses a barrier to intravitreal adeno-associated viral vector gene delivery to non-human primates. *Gene Ther*. 2015;22(2):116-126. doi:10.1038/gt.2014.115
202. Cho SW, Kim S, Kim JM, Kim JS. Targeted genome engineering in human cells with the Cas9 RNA-guided endonuclease. *Nat Biotechnol*. 2013;31(3):230-232. doi:10.1038/nbt.2507
203. Kleinstiver BP, Prew MS, Tsai SQ, et al. Engineered CRISPR-Cas9 nucleases with altered PAM specificities. *Nature*. 2015;523(7561):481-485. doi:10.1038/nature14592
204. Cebrian-Serrano A, Davies B. CRISPR-Cas orthologues and variants: optimizing the repertoire, specificity and delivery of genome engineering tools. *Mamm Genome*. 2017;28(7-8):247-261. doi:10.1007/s00335-017-9697-4
205. Ran FA, Cong L, Yan WX, et al. In vivo genome editing using Staphylococcus aureus Cas9. *Nature*. 2015;520(7546):186-191. doi:10.1038/nature14299
206. Zhang X, Liang P, Ding C, et al. Efficient Production of Gene-Modified Mice using Staphylococcus aureus Cas9. *Sci Rep*. 2016;6. doi:10.1038/srep32565
207. Kim E, Koo T, Park SW, et al. In vivo genome editing with a small Cas9 orthologue derived from Campylobacter jejuni. *Nat Commun*. 2017;8. doi:10.1038/ncomms14500
208. Lesueur LL, Mir LM, André FM. Overcoming the Specific Toxicity of Large Plasmids Electrotransfer in Primary Cells In Vitro. *Mol Ther - Nucleic Acids*. 2016;5:e291.

doi:10.1038/mtna.2016.4
209. Kreiss P, Cameron B, Rangara R, et al. Plasmid DNA size does not affect the physicochemical properties of lipoplexes but modulates gene transfer efficiency. *Nucleic Acids Res*. 1999;27(19):3792-3798. doi:10.1093/nar/27.19.3792
210. Kim S, Kim D, Cho SW, Kim J, Kim JS. Highly efficient RNA-guided genome editing in human cells via delivery of purified Cas9 ribonucleoproteins. *Genome Res*. 2014;24(6):1012-1019. doi:10.1101/gr.171322.113
211. DeWitt MA, Corn JE, Carroll D. Genome editing via delivery of Cas9 ribonucleoprotein. *Methods*. 2017;121-122:9-15. doi:10.1016/j.ymeth.2017.04.003
212. Jeffries AM, Marriott I. Human microglia and astrocytes express cGAS-STING viral sensing components. *Neurosci Lett*. 2017;658:53-56. doi:10.1016/j.neulet.2017.08.039
213. Yu X, Liang X, Xie H, et al. Improved delivery of Cas9 protein/gRNA complexes using lipofectamine CRISPRMAX. *Biotechnol Lett*. 2016;38(6):919-929. doi:10.1007/s10529-016-2064-9

7. APPENDICES

7.1 APPENDIX A: PLASMID MAPS

7.1.1 SPCAS9 PLASMID

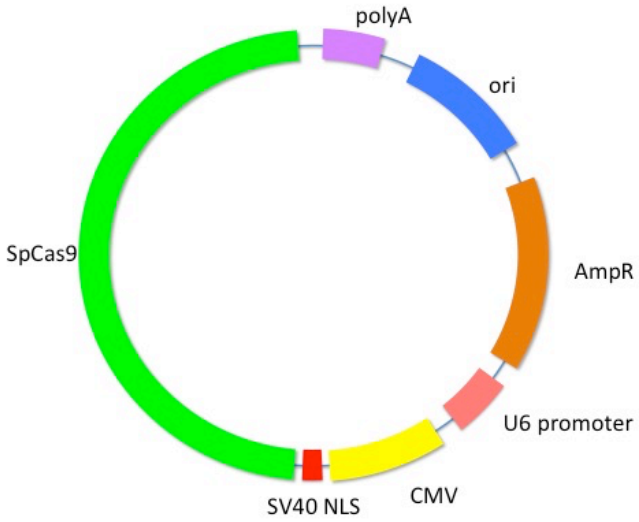

Figure 38: **SpCas9 Plasmid Map**. SpCas9: SpCas9 sequence, ori: Origin of replication, AmpR: Ampicillin resistance gene and promoter, CMV: CMV enhancer and promoter, polyA: polyA signal.

7.1.2 NC PLASMID

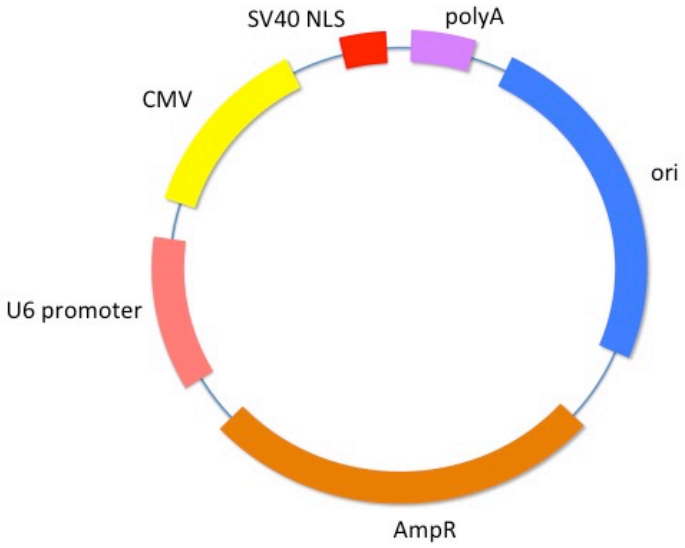

Figure 39: **NC Plasmid Map**. ori: Origin of replication, AmpR: Ampicillin resistance gene and promoter, CMV: CMV enhancer and promoter, polyA: polyA signal.

7.2 APPENDIX B: LIPOFECTAMINE 3000 AND DNA CONCENTRATIONS

0.5 µg DNA 1 µl L3K	0.5 µg DNA 1 µl L3K	0.5 µg DNA 1 µl L3K	0.5 µg DNA 1.5 µl L3K	0.5 µg DNA 1.5 µl L3K	0.5 µg DNA 1.5 µl L3K
0.5 µg DNA 2 µl L3K	0.5 µg DNA 2 µl L3K	0.5 µg DNA 2 µl L3K	0.5 µg DNA 2.5 µl L3K	0.5 µg DNA 2.5 µl L3K	0.5 µg DNA 2.5 µl L3K
0.5 µg DNA 0.5 µl L3K	0.5 µg DNA 0.5 µl L3K	0.5 µg DNA 0.5 µl L3K	0.5 µg DNA 0.25 µl L3K	0.5 µg DNA 0.25 µl L3K	0.5 µg DNA 0.25 µl L3K
No L3K No DNA	No L3K No DNA	No L3K No DNA	No L3K No DNA	No L3K No DNA	No L3K No DNA

Table 7.2: **Lipofectamine 3000 and DNA concentrations.**
DNA: Plasmid DNA
L3K: Lipofectamine 3000

7.3 APPENDIX C: ELECTROPORATION SETTINGS

7.3.1 CHAPTER 3.4.2.1

Voltage	Pulse Time (ms)	Pulse Number
1900	30	1
1720	10	2
1680	20	1
1500	30	1
1300	30	1
1050	50	1
1400	10	3
1350	35	1
1800	20	1
1600	30	1

Table 7.3.1: **Electroporation Settings for Chapter 3.4.2.1.**

7.3.2 CHAPTER 3.4.2.2

Voltage	Pulse Time (ms)	Pulse Number
1300	30	1
1250	40	1
1600	10	3
1400	10	3
1400	20	2

Table 7.3.2: **Electroporation Settings for Chapter 3.4.2.2.**

7.3.3 CHAPTER 3.4.2.2.1

Voltage	Pulse Time (ms)	Pulse Number
500	10	1
700	10	1
700	20	1
800	10	1
800	20	1

800	20	2
800	30	2
1000	10	1
1000	20	1
1000	20	2
1000	40	1
1100	40	1
1100	20	2
1200	20	1
1200	20	2
1300	30	1

Table 7.3.3: **Electroporation Settings for Chapter 3.4.2.2.1.**

7.3.4 CHAPTER 3.4.2.3

Voltage	Pulse Time (ms)	Pulse Number
500	20	1
700	20	1
800	20	1
1250	30	1
1400	20	2
1600	10	3

Table 7.3.4: **Electroporation Settings for Chapter 3.4.2.3.**

7.4 APPENDIX D: GENEJUICE AND PLASMID DNA CONCENTRATIONS

	0.5 µl	**1 µl**	**1.5 µl**	**2 µl**	**2.5 µl**	**3 µl**	**GeneJuice (GJ)**
0.2 µg	0.5 µl GJ 0.2 µg DNA	1 µl GJ 0.2 µg DNA	1.5 µl GJ 0.2 µg DNA	2 µl GJ 0.2 µg DNA	2.5 µl GJ 0.2 µg DNA	3 µl GJ 0.2 µg DNA	
0.4 µg	0.5 µl GJ 0.4 µg DNA	1 µl GJ 0.4 µg DNA	1.5 µl GJ 0.4 µg DNA	2 µl GJ 0.4 µg DNA	2.5 µl GJ 0.4 µg DNA	3 µl GJ 0.4 µg DNA	
0.6 µg	0.5 µl GJ 0.6 µg DNA	1 µl GJ 0.6 µg DNA	1.5 µl GJ 0.6 µg DNA	2 µl GJ 0.6 µg DNA	2.5 µl GJ 0.6 µg DNA	3 µl GJ 0.6 µg DNA	
0.8 µg	0.5 µl GJ 0.8 µg DNA	1 µl GJ 0.8 µg DNA	1.5 µl GJ 0.8 µg DNA	2 µl GJ 0.8 µg DNA	2.5 µl GJ 0.8 µg DNA	3 µl GJ 0.8 µg DNA	
Plasmid DNA (DNA)							

Table 7.4: **GeneJuice and DNA Concentrations.**

7.5 APPENDIX E: NUCLEOFECTION SETTINGS

	Voltage	Pulse Time (ms)	Pulse Number	Plasmid DNA (Y/N)
Trial 1	1250	30	1	Yes
Trial 2	1400	20	2	Yes
Control 1	1250	30	1	No
Control 2	1400	20	2	No
Control 3	-	-	-	Yes

Table 7.5: **Nucleofection Settings.**

7.6 APPENDIX F: TRANSFECTION OF IMHU WITH GFP SPCAS9 USING LIPOFECTAMINE 3000

	0.15 µl	**0.2 µl**	**0.4 µl**	**Lipofectamine 3000 (L3K)**
50 ng	0.15 µl L3K 50 ng DNA	0.2 µl L3K 50 ng DNA	0.4 µl L3K 50 ng DNA	
100 ng	0.15 µl L3K 100 ng DNA	0.2 µl L3K 100 ng DNA	0.4 µl L3K 100 ng DNA	
200 ng	0.15 µl L3K 200 ng DNA	0.2 µl L3K 200 ng DNA	0.4 µl L3K 200 ng DNA	
300 ng	0.15 µl L3K 300 ng DNA	0.2 µl L3K 300 ng DNA	0.4 µl L3K 300 ng DNA	
400 ng	0.15 µl L3K 400 ng DNA	0.2 µl L3K 400 ng DNA	0.4 µl L3K 400 ng DNA	
GFP SpCas9 DNA (DNA)				

Table 7.6: **Concentration of Lipofectamine 3000 and GFP SpCas9 for IMhu Transfection.**

Declaration of Authorship

The work for this thesis took place in the Institute for Ophthalmic Research, Eye Clinic Tübingen, under the supervision of Dominik Fischer, Daniyar Dauletbekov, and Kirsten Bucher.

The study was conceived in collaboration with Dominik Fischer and Daniyar Dauletbekov.

I performed all experiments independently, after initial training by Daniyar Dauletbekov. Helen Pan performed the lentiviral transduction (Chapter 3.4.5). Mario Bonillo produced the NC and SpCas9 plasmids (Appendix A).

I performed all statistical analyses.

I assure you that I wrote this manuscript independently and have not used any other sources other than those listed in the reference section.

Tübingen, February 3rd, 2022

PUBLICATIONS

Pfromm JK, Bonillo M, Dauletbekov D, Bucher K, Fischer MD. Plasmid-mediated gene transfer of Cas9 induces vector-related but not SpCas9-related immune responses in human retinal pigment epithelial cells. Sci Rep. 2022 Aug 1;12(1):13202. doi: 10.1038/s41598-022-17269-x. PMID: 35915300; PMCID: PMC9343442.

M. Bonillo*, J.K. Pfromm*, M.D. Fischer. (2022) Challenges to gene-editing approaches in the retina. Herausforderungen für Gene-Editing-Ansätze in der Netzhaut. *Klinische Monatsblatter fur Augenheilkunde,* 239(3), 275–283. https://doi.org/10.1055/a-1757-9810

Dauletbekov D.L., Pfromm J.K., Fritz A.K., Fischer M.D. (2019) Innate Immune Response Following AAV Administration. In: Bowes Rickman C., Grimm C., Anderson R., Ash J., LaVail M., Hollyfield J. (eds) Retinal Degenerative Diseases. Advances in Experimental Medicine and Biology, vol 1185. Springer, Cham

ACKNOWLEDGEMENTS

Firstly, I would like to thank Dominik Fischer for his support and guidance throughout this process. I am immensely grateful for the learning opportunities my time in the lab provided. I appreciate the insights into translational work and clinical studies I was able to gain, as well as the opportunity to design my own experiments and experience the trials and elations of lab work first-hand.

Thank you to my wonderful colleagues at the Institute for Ophthalmic research in Tübingen. Daniyar Dauletbekov, who guided me through my very first experiments, and was ever supportive in the days and months thereafter. Oksana Faul, for her patience and good humor, and for teaching me everything from how to turn on the hood to how to use the autoclave. Mario Bonillo, who shared many of my tribulations, and was ever ready to search for solutions. Thank you for your continuing collaboration and for all of the brainstorming sessions. Kirsten Bucher, for helping me put the finishing touches on my work, and all the other members of the group, who made every day in the lab fun. The members of the Schnichels lab for their kind assistance in various projects, and Yamel Cardona and the Weber lab, for the generous use of their Nucleofector.

My tremendous friends: Sophia, Stina, Lisa, Ingrid, Kathrin, Till, Phil, Astrid, and Madeleine, for their never-ending solidarity and encouragement.

Volker and Dani, for unfailingly putting up with me. I don't know how you do it.

My brother Lukas, for all of the laughs and for always keeping me grounded.

To my Tante Doris and Opa and Oma, for supporting me during my first months in Germany and for countless rounds of Kaffee and Kuchen. I couldn't have done any of this without you.

Grandma, for her love, and the reminders that there's no use getting worked up about things; it is what it is.

Finally, I would like to thank my parents. These past years have been hard, and often a little scary, and I am endlessly grateful for the knowledge that no matter what, I've got you in my corner. That if all else fails I can always come home. Thank you for proofreading this thesis and offering your invaluable support and opinions. Thank you for giving me the opportunity to do anything I could possibly dream of and fostering my abilities to realize those opportunities. I love you.